Nonlinear properties of phase-sensitive fiber-optic parametric amplifiers for signal processing

Weilin Xie

université PARIS-SACLAY

NNT : 2018SACLS108

Thèse de doctorat

UNIVERSITÉ PARIS SUD
Comprendre le monde, construire l'avenir

Nonlinear Properties of Phase-Sensitive Fiber-Optic Parametric Amplifiers for Signal Processing

Thèse de doctorat de l'Université Paris-Saclay
Préparée à l'Université Paris-Sud

École doctorale n°572 Ondes et Matière (EDOM)
Spécialité de doctorat: Optique et Photonique

Thèse présentée et soutenue à Orsay, le 7 mai 2018, par

M. Weilin XIE

Composition du Jury :

M. Nicolas TREPS Professeur, Université Pierre et Marie Curie, Laboratoire Kastler Brossel (LKB)	Président
M. Thomas SCHNEIDER Professeur, Technische Universität Braunschweig, Institut für Hochfrequenztechnik (IHF)	Rapporteur
M. Thierry CHARTIER Professeur, Université de Rennes 1, Fonctions Optiques pour les Technologies de l'information (FOTON)	Rapporteur
M. Philippe DELAYE Directeur de Recherche, CNRS Université Paris Saclay, Laboratoire Charles Fabry (LCF)	Examinateur
M. Ihsan FSAIFES Ingenieur de Recherche, École Polytechnique	Examinateur
M. Fabien BRETENAKER Directeur de Recherche, CNRS Université Paris Saclay, Laboratoire Aimé Cotton (LAC)	Directeur de thèse
M. Yi DONG Professeur, Shanghai Jiao Tong University, State Key Laboratory of Advanced Optical Communication Systems and Networks (SKL)	Co-Directeur de thèse

Université Paris-Saclay
Espace Technologique / Immeuble Discovery
Route de l'Orme aux Merisiers RD 128 / 91190 Saint-Aubin, France

ABSTRACT

The capability and the performance of the widely deployed optic and photonic systems and subsystems strongly depend on the performance of the optical amplifiers such as the noise properties and the nonlinearities. In this context, phase-sensitive fiber-optic parametric amplifiers (PS-FOPAs), relying on four-wave mixing (FWM) in silica optical fibers, outperform conventional phase-insensitive amplifiers thanks to their unique phase squeezing property. They can be exploited for many advanced applications such as noiseless amplification and mitigation of the nonlinear impairments. Together with the vast gain spectrum and other functionality such as wavelength conversion and phase conjugation, they have been regarded as a promising candidate for the next generation of optical amplifiers towards all-optical communication and signal processing.

The PS-FOPA can be conventionally described by the fundamental coupled wave equations which can be derived from the nonlinear Schrödinger equation. The general form of the coupled wave equations governing the FOPAs contains only three or four interacting waves according to the FWM mechanism. However, for a more general case, the high-order waves emerged from the cascaded FWM processes will inevitably impact the characteristics of the amplifiers such as the gain properties and the phase-sensitivity.

The objective of this thesis is to thoroughly study the nonlinear properties in terms of the gain properties and the phase sensitivities with respect to different configurations of a dual-pump signal-idler degenerate PS-FOPA. A more accurate numerical analysis is obtained by using the so-called 7-wave model that incorporates the first order high-order signals and pumps stemming from the cascaded FWM processes. This model permits to assess a more precise physical interpretation of the multi-wave interactions based on phase matching conditions and interaction strength, revealing the underlying relations between the dispersion, phase-sensitivity, and gain properties. Moreover, the simultaneous phase and amplitude regenerative capability of a fundamental PS-FOPA is evaluated for the sake of the overall optimization of the regeneration process. It allows fully exploiting the potential regenerative ability of a basic PS-FOPA configuration

acting as a fundamental building block of the future all-optical functionalities. The analysis approach based on this model permits application-oriented optimization and is of particular guiding significance for design and optimization of PS-FOPA, and can be steadily applied in various application scenarios.

Keywords: Four-wave mixing, fiber-optic parametric amplifier, phase-sensitive amplifier, microwave photonics, multi-wave model, regeneration.

Acknowledgment

It is indeed my great fortune and honor to have the opportunity to pursue my Ph.D. degree at the Laboratoire Aimé Cotton at CNRS/Universite Paris Saclay/Universite Paris Sud and at Shanghai Jiao Tong University. I am very grateful to everyone that has made this possible and rewarding.

Foremost I would like to appreciate my two great Ph.D. directors: supervisor Prof. Fabien Bretenaker and co-supervisor Prof. Yi Dong for accepting me as their Ph.D. student and making all this possible. They do not only share their knowledge and expertise in scientific researches but also helping me growing up as a mature Ph.D. student and even an independent researcher. Their insightful vision, guidance, and great personalities have been an excellent academic and life role model that is a life-long benefit to me. I am also grateful for the working atmosphere during my study, the knowledge in food and wine should lead to another Ph.D. program. Dr. Ihsan Fsaifes also deserves my gratitude for the time he devoted to help me with the discussions and experiment works.

A special thank goes to Prof. Fabienne Goldfarb for her helps for the administrations, without whom it could be extremely tough to get through all these difficult administration procedures.

Prof. Alfredo De Rossi and Prof. Sylvain Combrié are particularly acknowledged for leading me into the new horizon of integrated nonlinear photonics, stimulating discussions, and the very close collaboration.

I want so much to thank Prof. Nicolas Treps for the fruitful discussions regarding the noise things, which maybe hated by the others and for the guiding lessons for the quantum photonics.

I express my deep gratitude to all the jury members. I am particularly honored for your coming. I also thank the scholarship that funded my Ph.D. study.

I express my gratitude to the technical services and the administration of LAC. Thanks in general to all the people in LAC. I am grateful to all the people that I have

been collaborated with, Rupamanjari Ghosh, Amrita and Hema Ramachandran from New Delhi and Bangalore in India who kindly welcomed me.

Many thanks go to the group members in LAC, the partners in TRT, and all the members from SJTU and BIT. I will never forget the wonderful memories with you, Mr. Labidi, Syamsundar, Professor Aliou, Jasleen, Mélanie, Chitram, Oriane, Alexia, and the others.

Finally, I would be remiss in not saving my greatest thanks for my parents, my family, my friends, for anyone who loves me and for all the people I love!

Table of contents

Table of figures

Chapter I

Introduction

Fiber-optic communication systems and networks, lying in the center of the globalized information and communication technology industries, have facilitated the information revolution all over the world and have thus drastically changed our daily lives. One of the most important and essential enabling technologies for the fiber-optic communication systems and networks is the optical amplifiers, which generally pose severe limitations on the performance and capability of not only the fiber-optic communication systems and networks but also other optical and photonic systems and subsystems. Therefore, future progress and advances in the area of optical amplifiers will lead to a profound evolution to the whole information society.

This thesis focuses on a particular kind of emerging optical amplifiers known as the phase-sensitive amplifiers (PSA), especially its implementation in fiber, the phase-sensitive fiber-optic parametric amplifier (PS-FOPA). Such kind of optical amplifiers has received considerable attention due to its unique phase squeezing property that brings about the capabilities such as noiseless amplification. This outperforms conventional optical amplifiers and is regarded as a promising candidate for the future optical amplifiers in next-generation optical and photonic systems and subsystems. Therefore, this thesis is dedicated to the study and the future development in the field of PS-FOPA.

1.1 Background

After the birth of highly integrated semiconductor laser and the low loss silica optical fiber, optical and photonic technologies have emerged with the hope of taking the place of conventional electrical technologies, paving the way towards the ultimate all-optical communication and processing. The extensive implementation and thorough deployment

of optical and photonic based processing systems and transmission networks are believed to be the next stage of the long-term information revolution. Amongst all the representative technologies, fiber-optic communication is one of the most appealing and successful realizations that has already revolutionized the entire modern telecommunication systems and networks. It has also played a non-substitutable role in establishing the infrastructure of the information communication technology (ICT) based information society. It is also worth mentioning that the photonic based processing exploited either in the optical domain or in the electrical domain is capable of offering a large bandwidth and rapid processing speed that has received considerable attention from both industry and academic communities. The former is usually regarded as all-optical processing while the latter is generally called microwave photonics, respectively.

In fiber-optic communication systems and networks, even though the propagation losses of the optical fiber are almost negligible compared with the conventional electrical cables, other processing stages may also degrade the signal power and the signal-to-noise ratio (SNR) as well, not to mention the losses due to the modulation and detection processes. Similarly, in optical and photonic processing, inescapable processing losses also pose stringent limits on the overall processing capability and performance.

As a consequence, optical amplifiers have become one of the most essential parts that determine the capabilities, characteristics, and performances of the optical and photonic systems and subsystems as well as their limitations. Conventional optical amplifiers, such as erbium-doped fiber amplifiers (EDFAs), semiconductor amplifiers (SOA), and Raman amplifiers, have already been widely deployed in today's fiber-optic communication systems and networks. Their development has facilitated the progress and evolution of the optical and photonic technologies, not only in telecommunication community but also in optical signal processing and microwave photonics.

The explosive growth of novel applications resulting from the ever-increasing social demands has inspired the endless pursuit of transmission capacity and processing speed and capability. These requirements have been translated into the need for larger bandwidth and higher spectral efficiency in fiber-optic communication.

On one hand, along with the advent of wavelength-division multiplexing (WDM) technique, the exploitation of more optical bandwidth in terms of more WDM channels has become feasible, giving rise to a substantial progress in link capacity through increasing the optical spectral bandwidth that can be utilized for data transmission. With

such a motivation, a great number of WDM channels have been untapped beyond the conventional band (C-band), such as long band (L-band) and short band (S-band). In view of this, the effective optical spectral bandwidth of those conventional optical amplifiers, especially the extensively implemented EDFAs, was mainly restricted within the C-band. Therefore, they have begun to show weakness in a sense.

On the other hand, for the sake of higher spectral efficiency, all the parameters of the complex optical field were made use of through the development of advanced high-order modulation formats, together with the progress in coherent communication technologies. Beyond the amplitude of the optical field, phase, frequency and even polarization are extensively exploited. However, the linear and nonlinear effects in fiber deteriorate the phase noise of the transmitted signals, resulting in severe impairment in the SNR. This effect is more significant for advanced high-order modulation formats as they utilize the phase to carry information. In this case, the functionality of amplifiers should be further upgraded from straightforward amplification to the regeneration, reshaping, and retiming (3R-regeneration) of the signals. It is also worth mentioning that although the optical amplifiers were initially invented for compensating the loss in either propagation or other sections, they also introduce extra noise during amplification, thus further degrading the SNR. Consequently, in transmission links, these extra noises accumulate, thus further reducing the potential transmission distance.

In light of this, advances in all these aspects involving the increased optical bandwidth and spectral efficiency as well as the optimized noise performance, have led to brand new technical challenges and intricate requirements on optical amplifiers.

In this context, fiber-optic parametric amplifier (FOPA), exploiting nonlinear four-wave mixing (FWM) in optical fibers, has stepped into the horizon. It has long been regarded as a promising candidate for the next generation optical amplifier because it is capable of providing a considerable optical gain over a vast optical spectral range limited by the pumping configurations and the phase-matching conditions. Compared with the state-of-the-art EDFAs, the underlying tremendously broad gain spectrum can potentially provide considerable gains from S-band to L-band, or within an even wider optical spectral bandwidth and is quite beneficial for increasing the channel number thus the capacity of the WDM based modern fiber-optic communication systems.

Considering the noise performances, quite particularly, FOPA is capable of operating in a unique phase-sensitive mode, for which the gain and noise properties of

the amplifier depending on the relative phase between the signal to be amplified and the pumping sources. In regard to this unique phase dependence property, this kind of amplifiers is thus named phase-sensitive amplifier (PSA). More precisely, in the context of the FOPA, it is called PS-FOPA. On the contrary, conventional amplifiers, owing to the fact that their gain and noise properties are independent of the initial phase of the signal to be amplified, are so-called phase-insensitive amplifiers (PIAs). Such phase-sensitivity can be exploited to realize the noiseless amplification with a theoretical 0 dB noise figure (NF). Thanks to the squeezing effect as a result of the phase-sensitivity, it has also been utilized to mitigate the nonlinear impairment in transmission links using high-order modulation formats, as well as the regeneration of such complex signals.

Owing to the outstanding noise properties and the particular functionalities of the PSAs, optical and photonic systems utilizing PSAs exhibit superior capabilities and excellent performances, outperforming those adopting conventional PIAs. Therefore, the investigation and analysis of the unique phase-sensitive property, as well as the other gain characteristics of the PSA, can accelerate the comprehension of the operation, leading to the realization of more efficient and versatile PSAs based systems in practice.

1.2 Motivation

From the practical point of view, the PSA is able to exhibit a quantum-limited 0 dB NF as well as other superior properties such as the broad gain spectrum, ultra-fast response, and nonlinear impairment mitigation. Such PSAs can thus potentially play a critical role as an excellent regenerator in fiber-optic communication systems and networks and they have also become beneficial or even mandatory in any other optical and photonic systems and subsystems where ultra-low noise amplification is urgently demanded.

In this context, the thorough investigation and analysis of the characteristics of the PSA, especially the linear and nonlinear properties of the PS-FOPA, can fundamentally assist to comprehend the underlying physical mechanisms that lead to the quadrature squeezing and thus the phase-sensitivity and the resulting noiseless amplification nature as well. On top of this, the insightful understanding can not only facilitate the design but also enable the overall optimization of the PSA based optical and photonic systems and subsystems. Therefore, it would offer great opportunities to fully exploit the untapped potential, improving the capability and performance of PSA based systems.

1.3 This thesis

1.3.1 Scope

The main topic of this thesis aims at proposing approaches to facilitate the design and the optimization of the PS-FOPA. To this end, the thorough investigation and analysis of the properties of the PS-FOPA are of critical significance. Therefore, a precise description of the underlying nonlinear FWM processing of the PS-FOPA is of great importance and is hence highly desired.

In this thesis, in order to obtain a more precise physical picture, the improvement in the conventional theoretical model is sought for. On this basis, it would allow for a more accurate interpretation of the phase-sensitive processes, giving rise to the exploitation of the potential capabilities of the PS-FOPA. It would also help to establish a versatile approach for the design and optimization of the PS-FOPA for more general application scenarios rather than simply in fiber-optic communications.

1.3.2 Contribution

In this thesis, in order to unfold and optimize the untapped potential of the PSAs, full understanding of the underlying physical mechanisms of the phase-sensitive parametric processes is thus aimed. To this end, rather than the conventional 3-wave or 4-wave model, a more precise 7-wave model, which takes into account the first order high-order signals and pumps in addition to the fundamental waves in an FWM process, is derived from the nonlinear Schrödinger equation.

Such model allows more accurate numerical investigation and analysis of the sophisticated nonlinear interaction amongst all the involved waves. It further permits to assess the underlying phase matching conditions and the interaction strength that govern the efficiency of the FWM processes. This way, the interpretation in terms of the phase matching can be explored to elaborate the phase-sensitive processes.

With the help of such model, we first analyze the dependence of the gain properties on the configurations of the allocations of the pumps and signal in terms of pump-pump separation and the wavelength offset with respect to the zero dispersion wavelength. This

also unveils the relations between the FWM efficiency and the phase-matching condition and interaction strength. In turn, this dependence facilitates the optimization of the gain properties, for example, the maximum gain that can be achieved in a fundamental dual-pump PS-FOPA. In addition to the gain properties, the dependence on the dispersion characteristics is likewise established.

From a practical standpoint, the phase squeezing capability of the PSAs can be utilized for simultaneous phase and amplitude regeneration of the complex modulation formats towards future all-optical functionalities. In order to take full advantage of the regenerative ability of a fundamental PSA configuration, the optimization in terms of the wavelength allocation of the pumps and signal, the pump power, and the degree of saturation is proposed and numerically demonstrated. This optimization and also the optimization approach based on the 7-wave model is of particular guiding significance for the design and implementation of the PSA system.

1.3.3 Outlines

The overall architecture of this thesis is organized as follows:

To explicitly introduce and emphasize the importance of this work, in chapter I, the background, motivation, and the introduction of this thesis is presented.

In chapter II, starting from the historical evolution of fiber-optic communication systems, the development of optical amplifiers are highlighted. The performance metrics of optical amplifiers are briefed for the ease of further discussion.

Based on the nonlinear light-matter interaction, the linear and nonlinear effects for wave propagation in optical fibers is discussed in chapter III. The fundamentals of FOPA is presented and extended to the concept of FOPA-based PSA. The theoretical multi-wave model is derived and presented.

In chapter IV, investigation on the phase sensitivity and the gain properties of a dual-pump degenerate PS-FOPA is presented. An optimization method regarding the phase sensitive gain is proposed and numerically verified.

The regenerative capability is numerically assessed with a systematic optimization approach in chapter V. Applicable regeneration is theoretically evaluated.

The overall conclusions and perspectives of the thesis are presented in chapter VI.

Chapter II

Optical amplifiers and their properties

2.1 Modern optical and photonic technologies

Information communication technology (ICT), including very large scale integration (VLSI), semiconductor technologies, communication technologies, and electronic engineering, has long been regarded as the essence and fundamentals of the modern information society. Ever since the worldwide blooming of the electronic engineering and information technologies in the last few decades, they have extensively stretched and rapidly spread their applications over every single corner around the world, and have to date become indispensable in every single aspect of our daily lives.

Along with the rapid growth of social demands due of the explosive development in both science and technology and as well as the global economy in the last few decades of the last century, the emergence of numerous fancy applications led to an endless pursuit of technologies for information processing in terms of broad bandwidth and high speed. However, the conventional electronic based information and communication technologies were quickly approaching the physical limit and soon have encountered their bottlenecks. Though some novel technologies such as Fin field-effect transistor (FET) based tri-gate transistor and multi-core multi-thread processors were invented to deal with these physical challenges, electronic technologies based ICTs began to show signs of weakness.

At the same time, laser-based optical and photonic technologies, along with the invention of the laser in the early 1960s, have manifested themselves as cutting-edge technologies[1]. Their key advantages over conventional electronic technologies, including low and constant attenuation, radio-resistance, immunity to electromagnetic interference, anti-corrosion, low dispersion, small volume, reduced weight and cost, broad bandwidth,

and ultra large potential transmission capacity, have prepared laser as a brand new opportunity for information processing and transmission. Especially, with the maturity of optoelectronic devices, silica optical fiber based optical and photonics industry, VLSI and semiconductor technologies, and the other relevant fields and industries, laser technologies have become more and more practical and applicable. Furthermore, this has, in turn, started to revolutionize the conventional ICT societies relying on their particularly advanced systems and architectures established on the basis of optical and photonic technologies[2].

Several supporting techniques have been considered as the underlying fundamentals of the so-called optical and photonic revolution. On top of that, amplifiers have long been regarded as one essential aspect for almost all the photonic and optical technologies. As such, they have to date played a major and critical role in the emergence, development, implementation, deployment, and evolution of optical and photonic systems and subsystems.

The fundamental of modern photonic technology, the laser itself, is the acronym of “lightwave amplification by stimulated emission of radiation”. No doubt that the amplification process is an inevitable procedure in the generation of laser. Besides, although optical devices embody less loss than conventional electronic devices and components, a variety of causes that lead to losses such as insertion loss are still unavoidable. Not to mention the losses experienced in fiber-optical communications, and free space optical transmissions for instance. Therefore, optical amplifiers, analogous to their electrical counterpart, have been extensively adopted and deployed in all kinds of optical and photonic systems and subsystems. As a consequence, their features and properties will significantly impact the overall system performance. Particularly, in some systems, the performance almost relies on the properties and parameters of the optical amplifiers.

For instance, in optical communication systems and networks, various kinds of amplifiers have become indispensable parts. They have been preliminarily utilized to compensate the propagation loss in optical communication systems, permitting long-haul transmissions over hundreds and even thousands of kilometers across the continents and through the oceans[3]. Recently, along with the emerging of the advanced complex modulation formats, a unique kind of amplifier, PSA, has entered researchers’ awareness. In addition to the fundamental amplificative functionality, PSA permits to offer an opportunity for nearly noiseless amplification and for mitigating the nonlinear effects in long-haul transmission. Therefore, this unique kind of amplifiers has soon taken the stage on the historical arena and has been considered as a promising ultimate solution for the

future all-optical and photonic systems and subsystems.

2.2 Optical amplifiers: background and applications

2.2.1 Demand for advanced optical amplifiers

One of the most important issues that cannot be ignored for any kind of system is the losses. From a signal system point of view, it is also often regarded as attenuation. In general, it describes the decrease of the flux or the intensity when a signal is propagating through a medium. In regard to the optical and photonic context, losses for lightwave signals propagating in media are inevitable and harmful in most of the cases. In any kind of optical system, the loss will degrade the signals of interests, decreasing the signal-to-noise ratio as a result. For instance, in a resonant optical cavity, the loss will reduce the photon number, which is related to the cavity lifetime. This loss is usually compensated by the gain medium in order to maintain the laser oscillation.

The loss effect is particularly detrimental in fiber-optical communication systems and networks. Ideally, any communication system should not deteriorate the quality of the signals propagating within it. In reality, silica optical fiber, though benefiting greatly from its unique properties, is, however, not an ideal medium as it usually introduces several kinds of other impairments besides the general considerations concerning the transmission losses to any kinds of signals launched into it. These transmission impairments can be mainly divided into two categories: linear impairments and nonlinear impairments. The former includes chromatic dispersion (CD), polarization-mode dispersion (PMD), timing offset, and optical filtering. And the latter is an effect from the Kerr-induced fiber nonlinearity, which contains self-phase modulation (SPM), cross-phase modulation (XPM), four-wave mixing (FWM), and nonlinear phase noises. Obviously, the modulated lightwave signals propagating in fibers always undergo not only linear impairments but also other nonlinear degradations during the transmission. Consequently, it is almost impossible to recover the original information without error after a certain distance of transmission.

Modern optical fibers[4], [5] exhibit about 0.2 dB/km loss, enabling ultra-long-haul transmission over tens of kilometers without deploying components for amplifying the signal. The invention of silica glass optical fiber and its introduction in fiber-optical

communication systems[6] have incented the thorough-going reform of the data transmission techniques. Together with the advent of semiconductor lasers[7], [8] that are capable of operating at room temperatures[9] and photon detection with high speed[10] and high quantum efficiency[11]. It has consequently brought about the drastic revolution of the entire information society, enabling access, processing, and transferring enormous information and data all through every corner of the world[12].

For the conventional IM/DD[13], [14], [15], [17] system, especially when the data rate was not that high, the most significant influence came from the linear impairments, such as the propagation loss, fundamental fiber thermal noise at room temperature, and the presence of shot noise. Conventional optical amplifiers including EDFA[21] and GaAlAs based semiconductor amplifiers (SOA)[22] have allowed efficient optical amplification. With the advent of WDM[20], those technologies have eventually given rise to an explosive growth of the link capacity, leading to a worldwide tendency on the development of large capacity and long-haul transmission systems. Commercial transmission systems are potentially able to support intercontinental[24], transatlantic[25], and transpacific[26] transmissions over tens of thousands of kilometers[27].

By far, only the linear impairments remain the dominant source of noise due to the relatively simple system architecture. The side effects can be efficiently dealt with by using the above conventional amplifiers. Issues happen in the pursuit of higher capacities.

Driven by the fundamental concept of WDM, straightforwardly increasing the number of channels was clearly an effective approach to increase the transmission capacity. However, the bandwidth of the conventional EDFA was unable to cover all the potential WDM channels, hurdling the practical deployment of WDM channels towards other sub-bands rather than conventional C-band around 1550 nm. This urgent demand was quickly addressed by the new kinds of amplification schemes such as Raman amplification[28], extending the WDM coverage from C-band towards long-wavelength L-band and short-wavelength S-band with appropriate pumping configuration[29].

Besides, scientists have also been attempting to increase the spectral efficiency in order to enlarge the capacity within one single channel. This was achieved through the introduction of advanced high-order modulation formats that exploit information from the complex optical field. In these systems, the influences of linear impairment involving chromatic dispersion and differential group delay induced polarization-mode dispersion become important and sensitive, demanding for effective dispersion management. Except

for the deployment-level management using dispersion compensated fiber, optical soliton has also attracted considerable attention owing to its interesting features that could be used to manipulate the dispersion in a dynamic fashion[30]. The last decade has still witnessed the tremendous advancing of spectral efficient modulation formats underlying the rapid progress in lightwave communication systems. In this period of time, the baud rate has increased leading to the shorter pulse width. Since silica optical fiber is a dispersive element resulting from all the modal, material, and waveguide dispersions, it indistinctively broadens signals propagating through it, leading to the spreading intersymbol interference that severely contaminates the signal quality. On top of this, another limiting factor is the contribution from the nonlinear Kerr effect. Commonly, since the power of the lightwave signal is generally kept within a relatively low level, the weak intensity-dependent refractive index fluctuation is weaker. However, in long-haul transmissions, the nonlinear impairments accumulated after a series of cascaded amplifiers may become remarkably critical and detrimental especially for the advanced complex modulation formats that make use of both phase and amplitude of the lightwave signal.

Similar to all the other components as well as their electrical counterpart, optical subsystems and optical amplifiers including EDFA and SOA will inevitably induce extra noises accompanying the amplification processes[31]. Moreover, when a series of optical amplifiers are deployed in tandem, which is almost the case in the practical fiber-optic communication systems, their extra noises will sum up together, accumulating to a dominant noise source over thermal noise or shot noise. Obviously, the characteristics of these optical amplifiers, especially their noise properties will pose an ultimate performance limit on the overall transmission system, highlighting their particular significance.

In this context, the requirement of all-optical repeaters, namely, optical amplifiers, has progressed towards the phase that concentrates not only simply on the transitional performance metrics such as gain and power efficiency, but also other aspects including gain spectrum coverage, signal-to-noise ratio (SNR), i.e., noise factor, and the regenerative ability. Meanwhile, in allusion to the complex high-order modulation formats that are quite sensitive to the nonlinear impairments, the capability to alleviate the nonlinear effect was becoming popular and critical.

2.2.2 Phase-sensitive fiber optical parametric amplifiers

Optical parametric amplifiers (OPAs)[32], based on nonlinear interactions, is capable of transferring energy from the pump to designated signals or idlers according to phase matching and relative phase conditions. Hence, they are able to provide a discrete or lumped gain, acting as a typical amplifier. According to the phase matching condition, the potential operating bandwidth of the OPA gain spectrum could be extended to several tens or even over one hundred nanometers[33] at telecom wavelengths[34]. Their gain spectrum can potentially cover the entire S-band, C-band, and L-band or even a broader spectral range. Meanwhile, OPA is also able to mitigate the fiber introduced degradations such as dispersion and Kerr nonlinearities that may eventually deteriorate the phase noise and thus the bit error rate (BER) performance. Besides, it is worth mentioning that the unique phase-sensitive operation might ultimately lead to ideal noiseless amplification without degrading the noise factor. This intriguing feature has become the focus as a candidate enabler for the next generation optical amplifiers.

In general, OPA can be realized by exploiting either $\chi^{(2)}$ or $\chi^{(3)}$ nonlinear media[35]. The underlying parametric process, which is generally instantaneous and does not store any energy inside the medium, is based on the energy interchange between the involved waves subjected to the phase matching and relative phase conditions. In order to maintain the single-mode operation and the compatibility with fiber optical communication systems, the so-called FOPA relying on the FWM process on the basis of the 3rd-order nonlinear susceptibility of silica fiber[36] has received increasing attention. The invention of highly nonlinear fibers (HNLFs) that exhibit a 5-10 times higher nonlinear coefficient[37] than traditional silica optical fibers in the late 1990s has further boosted the practical progress of FOPA[38]. The broadband gain spectrum in combination with the inherent compatibility, has allowed for the efficient amplification beyond the optical spectral range of EDFAs[39], showing new opportunities for optical communication society.

In principle, one or two strong pumps accompanying the signal will co-propagate through the nonlinear medium, stimulating the nonlinear interaction with the materials. In particular, within the context of silica optical fiber, this interaction exploits nonlinear Kerr effect resulting from the intensity induced refractive index changes[40]. This way, the efficiency of the energy transfer is strongly related to the phase matching condition that will

be carefully discussed later. Meanwhile, since the underlying process relies on the relative phase amongst the interacting waves, the FOPA is capable to operate in a unique phase-sensitive fashion[41], [42]. This way, only the desired in-phase component will be amplified while the quadrature component experiences de-amplification[43], opening up the possibilities towards the potential ideal noiseless amplification[44].

2.2.3 Potential applications of phase-sensitive amplifiers

Though the most important initial motivation for the development and evolution of such FOPA based PSA has been the demand for all-optical repeating rather than conventional optical-to-electrical conversion and electrical-to-optical conversion in fiber-optic communication systems and networks, the numerous requirements from the telecommunication society have inspired tremendous progress in investigation and exploitation of the unique squeezing properties of PSA[45]. Consequently, this has, in turn, established a series of solid and broad fundamentals for other application scenarios of PSA.

Generally speaking, those extensive application fields can be roughly categorized into two groups: amplification of signals for loss compensation and additional functionalities such as e.g., wavelength conversion and signal processing.

2.2.3.1 Wavelength conversion and signal broadcasting

In modern telecommunication systems and networks, optical amplifiers have expedited the elimination of optical-to-electrical conversion, reducing the repeater interval, hence leading to remarkable advances in transmission efficiency. To further increase the efficiency and capacity towards the ultimate all-optical communication networks, the implementation of all-optical functionalities, particularly the routing and switching, are of key importance.

In typical WDM systems, to achieve the routing functionality, e.g., the ability to convert signals in one certain wavelength into another wavelength without losing the contained information, this WDM channel was optical-to-electrical converted and modulated on to the optical carrier in other WDM channel. This process was, not only time-consuming but also increased the complexity of the router nodes. In addition, sometimes this information should be converted into a number of other channels for broadcasting.

Such wavelength conversion is required to be performed in the optical domain in future all-optical networks. Some special devices, for instance, the optical add-drop multiplexer

(OADM) as shown in Fig. 2.1, have been adopted to carry out functions such as adding, blocking, selective passing or redirecting different WDM channels all-optically.

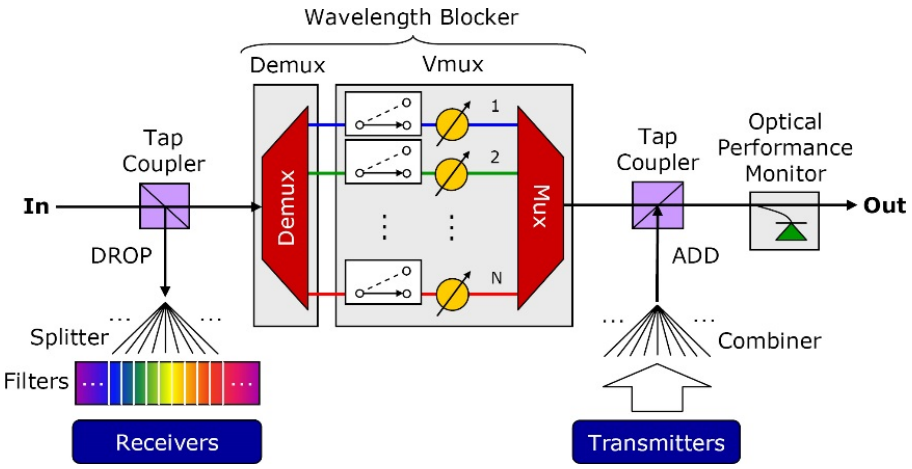

Fig. 2.1 Optical add/drop multiplexer (OADM) subsystem.

General architecture of a broadband optical add/drop multiplexer (OADM) subsystem[46], [47]. Demux: Demultiplexer; Mux: Multiplexer.

Since the PSA involves multiple waves simultaneously, its physical essence relies on the conversion of photons between different waves with different frequencies in a fully elastic manner, namely, the energy exchanges without storage inside the medium. According to their different roles played in a certain FWM process, by changing the relative phase between the initial waves, the direction of the energy flow will be modified correspondingly[48]. In this way, along with the energy exchange, the optically-carried information can likewise be transferred or copied on to the other wavelength, allowing the realization of wavelength conversion all-optically[49]. Similarly, when cascaded FWM is implemented, the original signal can be copied to a series of equally spaced wavelengths, naturally forming the multicasting without losing the information[50].

2.2.3.2 3R regeneration

Recently, the ever-increasing capacity of transmission systems is rapidly approaching and even exceeding the nonlinear Shannon limit[51]. Such a breakthrough has ceaselessly motivated the development of all-optical regeneration rather than simply amplification of the transmitting signals (see Fig. 2.2). This allows for easing the need for optical-to-electrical conversions as well as the accompanying digital signal processing at mid-range repeaters.

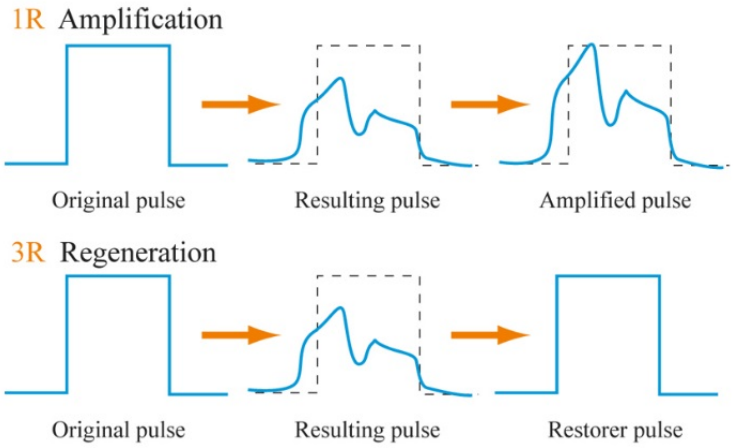

Fig. 2.2 1R amplification and 3R regeneration of optical pulses.
Comparison between conventional 1R amplification and 3R regeneration of optical pulses.

The vital drawback of conventional amplifiers such as EDFA and Raman optical amplifiers is the accumulation of linear and nonlinear deteriorations that occur in these relays in long-haul transmission. In view of this, conventional optical-to-electrical conversion seemed to be a suitable trade-off prior to the emergence of the so-called 3R regeneration, which has exhibited capability to re-amplify, re-time, and re-shape optical pulses with certain modulation formats[52]. This has indicated the possibility towards lossless and endless concatenation.

With the large-scale deployment of high-order modulation formats, for example, the highly spectrally efficient quadrature amplitude modulation (QAM), the investigation of modulation format transparent regeneration has become central with some additional requirements on simultaneous multi-channel regeneration[53], [54]. In this respect, some novel architectures regarding 3R regeneration have been proposed and experimentally demonstrated using other lumped nonlinear components such as nonlinear optical loop mirror (NOLM)[55], [56] and SOA[57], [58]. Among these, FOPA based PSA has received the largest attention not only due to its intrinsic compatibility to fiber systems but also because of the popular scalability[59] for transparent multi-level[60] and multi-channel[61] operation.

In order to sustain the continuous growth in capacity, the spectral density, namely the spectral efficiency should keep increasing. This is, however, ultimately limited by the nonlinear Shannon limit[62], [63], resulting in an upper limit of the channel density[64]. On the other side, the capacity can also be promoted for hosting more transmission channels in a broader optical spectral range. This strategy brings about more difficulties in practical

realization. For the effective routing and switching of optical communication systems with such complexity, precise narrowband regeneration with modulation format compatibility is highly desired. Therefore, the highly selective phase-sensitive property of the PSA is particularly intriguing for spectrally efficient advanced high-order modulation formats and high data rate[65].

2.2.3.3 Microwave photonics

Microwave photonics[66] (MWP) is an emerging interdisciplinary field that makes use of optical and photonic technologies to deal with conventional radio frequency (RF) and microwave (MW) issues[67], which might be quite difficult or even impossible to achieve with traditional electrical technologies. In addition, these MWP technologies can, in turn, facilitate photonic functionalities and enhance the performance of optical communication systems and networks.

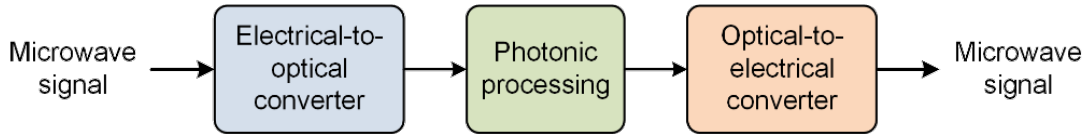

Fig. 2.3 A typical microwave photonic system.
The input microwave signal is converted into an optical signal before being processed using photonic technologies and then converted back into the electrical domain.

Compared with electrical signal processing, MWP technologies, benefiting from the broad bandwidth owing to the intrinsic high operating frequency of lightwave signal, small volume, ultra-low loss of silica fiber, immunity to electromagnetic interference, and potential capability of integration, provide impressive solutions in optical domain with unprecedented flexibility and capability. As a matter of fact, the development of MWP technologies evolves in parallel with optical telecommunication since they share common fundamentals including large bandwidth electro-optic modulators for generating optically-carried RF and MW signals and fast p-i-n photodetectors with high quantum efficiency as discussed in section 2.2.1 .

In the early days of MWP, since silica optical fiber had provided unprecedented advantages over electrical cables in terms of loss and dispersion, fibers have been extensively adopted to carry and transfer RF signals for remote radar antenna, satellite, and

astronomy scenarios. Soon after the emergence of integrated optical devices, the coverage of MWP has been rapidly stretched into cable videos, signal processing, and other applications[68].

One primary limiting factor lies in the fact that the optical-to-electrical and electrical-to-optical conversions always introduce huge insertion loss and thus restrict the SNR of the resulting RF and microwave signals. On one side, the efficiency of those modulation approaches, such as that of amplitude modulation utilizing Mach-Zehnder modulator (MZM), is insufficient, thereby inducing large losses. On the other side, the overall responsivity is restricted, leading to a limited conversion efficiency. Meanwhile, in analog photonics link, which is also usually called MWP-link, transmitting analog RF or MW signals instead of digital signals, the extremely weak signals collected from remote radar antenna will additionally suffer from the fiber induced transmission attenuation. This will ulteriorly degrade the SNR performance. Therefore, certain steps, particularly amplification processes, must be taken in order to compensate for all these losses.

Basically, amplification can be realized either in optical domain or in the electrical domain for the purpose of compensating the transmission and conversion losses. Besides the volume, size, and weight, the progress of electrical amplifiers has also encountered the electronic bottleneck, leading to the limited operating bandwidth and frequency. It is worth mentioning that, except for the limited noise figure stemming from the extra noises, electrical amplifiers also suffer from flicker noises that dominate over other noise sources at low Fourier frequencies. In addition, the nonlinearity of the electrical amplifiers degrades the spurious free dynamic range (SFDR)[72]. Similarly, amplification can also be accomplished in the optical domain using conventional optical amplifiers or state-of-the-art optical parametric amplifiers. According to the power law of PD, there exists a factor of two for the conversion from optical gain to electrical gain. Other advantages of these optical amplifiers include immunity to electromagnetic interference and relatively smaller extra noise, namely, low noise figure. Particularly, the latter feature manifests significantly in a special operation mode of parametric amplifier, i.e., phase-sensitive mode. Theoretically, in some certain configurations, PSA is capable to hold a 0-dB noise figure, showing great potential for signal amplification. Meanwhile, the highly phase-selective function resulting from the phase-sensitivity creates opportunities to mitigate the nonlinear phase noise thus improving the noise performance of the MWP-link. Particularly, the linearity of PSA in small signal regime could fundamentally improve the SFDR of fiber-based analog photonics

link (APL)[73], [74]. These unique features have drawn increasing attention and will be the topics of this thesis.

2.3 Properties of optical amplifiers

2.3.1 General properties

2.3.1.1 Gain

Gain is the most important and fundamental property of any optical or electrical amplifier. The general definition of gain is given by the ratio of output power to the input power. For the ease of practical engineering usage, the gain is usually expressed in logarithm form with the unit in decibel (dB).

2.3.1.2 Bandwidth and gain spectrum

In general, for a certain amplifier, the bandwidth is the frequency span in Fourier domain within which the signal will be amplified. In other words, bandwidth can also be regarded as the Fourier frequency range over which the amplifier is still effective.

One needs to clarify that the definitions of bandwidth for electrical and optical amplifiers are quite different. For a typical electrical amplifier, since its frequency response is band-limited, the conventional definition is always valid for different types of amplifiers including broadband amplifiers and narrow-band amplifiers. However, this is not the case for optical amplifiers. The frequency response of the optical amplifier is limited by the underlying physical characteristics, for example, for FOPA, the frequency response is limited by the ultra-fast Kerr effect and the bandwidth of the gain medium or pumping mechanism.

In common situations, the bandwidth of optical amplifiers is defined as the optical spectrum range or optical bandwidth coverage. Taking EDFA as a representative, usually, the bandwidth is operating in C-band. Therefore, this characteristic is usually alternatively regarded as the bandwidth or gain spectrum of the optical amplifier.

2.3.1.3 Saturation

Though the gain of an amplifier can be very high, however, the actual output power cannot

be infinite. There is a certain limit on the maximum output power, beyond which the amplification is no longer effective. In this regime, the gain relation becomes no longer linear, which is called saturation regime. Equivalently, the input signal power that brings the amplifier into saturation regime is usually called saturation input power. Interestingly, for optical amplifiers such as EDFA, the noise property in saturation regime will be modified compared with that in the small signal linear regime.

2.3.1.4 Noise

For a well-designed ideal amplifier, the signal and noise will be amplified in the same manner with the same gain since the amplifier cannot distinguish signal and noise. However, practically, a real amplifier usually introduces extra noises due to the underlying physical processes in the amplifier and possible pumping noises.

To describe the extra noise induced by the amplifier, a noise factor is introduced, which is defined as the ratio between SNR at the amplifier input SNR_i and the SNR at the amplifier output SNR_o.

$$F = \frac{SNR_i}{SNR_o} \tag{2-1}$$

From an engineering point of view, for the ease of calculations, the noise factor is often expressed in logarithm with the unit of dB.

$$\begin{aligned} NF &= 10\log_{10}(F) = 10\log_{10}\left(\frac{SNR_{\mathrm{i}}}{SNR_{\mathrm{o}}}\right) = SNR_{\mathrm{i,dB}} - SNR_{\mathrm{o,dB}} \\ &= \frac{P_{\mathrm{sig,i}}/P_{\mathrm{nis,i}}}{P_{\mathrm{sig,o}}/P_{\mathrm{nis,o}}} = \frac{P_{\mathrm{sig,i}}\cdot\left(GP_{\mathrm{nis,i}} + P_{\mathrm{nis,extra}}\right)}{P_{\mathrm{nis,i}}\cdot GP_{\mathrm{sig,i}}} \\ &= \frac{GP_{\mathrm{nis,i}} + P_{\mathrm{nis,extra}}}{GP_{\mathrm{nis,i}}} \end{aligned} \tag{2-2}$$

Provided that the input and output signal and noise power are denoted as $P_{\mathrm{sig,i}}$, $P_{\mathrm{sig,o}}$, and $P_{\mathrm{nis,i}}$, $P_{\mathrm{nis,o}}$, respectively, the noise figure (NF) can be calculated according to Eq. (2-2), where $P_{\mathrm{nis,extra}}$ is the extra noise induced during the amplification process. It is clear from the equation that for a typical amplifier, as it is usually unable to not distinguish signal and noise, thus both will be amplified in a same manner. Consequently, the finite NF is almost due to the extra noise induced by the amplifier itself.

Consider an optical amplifier based on stimulated emission, the origin of the extra noise is more often the amplified spontaneous emission (ASE). In an ideal case, the NF can be as low as 3 dB according to the coupling of vacuum noise coming from other modes[31], [75]. This typical value for a commercial EDFA is usually 4~6 dB.

2.3.1.5 Linearity and dynamic range

The amplifier can be not only noisy but also nonlinear. The nonlinearity of an amplifier can be intuitively understood when new frequency components are generated during the amplification process. The linearity is quantified as the extent to which the proportion between input and output amplitude is the same for high amplitude and low amplitude input. Even if most of the amplifiers are supposed to be perfectly linear, that is to say, the signal gain for any input level within the bandwidth is constant. However, due to the imperfections of the amplifier, not all the signals will be amplified in the same fashion and this is related to the dynamic range.

Basically, the dynamic range is defined as the ratio between the largest and the smallest available input or output levels. Owing to the nonlinearities, if more than one frequency component is launched into the amplifier, the nonlinear distortions may lead to the creation of new frequency components, therefore degrading the dynamic range. Even with only one frequency component, the nonlinearity may bring about new frequency component such as frequency doubled second-harmonic. Dynamic range can be assessed either at the input or at the output.

2.3.2 Concatenation

Modern industrialized silica optical fiber exhibits linear propagation loss as small as 0.2 dB/km for transmitting lightwave signals in C-band and the adjacent S- and L-band around 1500~1600 nm spectral range. Though the attenuation is quite negligible compared with electrical cables, for long-haul lightwave transmission systems, periodical compensation to boost the signal power is still inevitable. A typical fiber optical long-haul transmission system with optical amplifiers is illustrated below in Fig. 2.4.

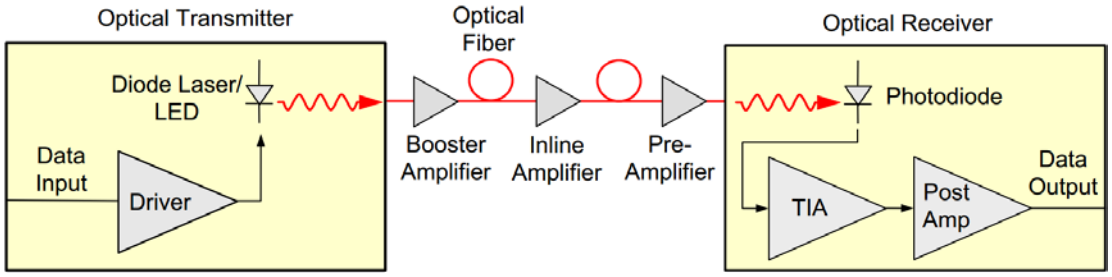

Fig. 2.4 Fiber optical long-haul transmission system based on cascaded optical amplifiers.

After the emission of the modulated lightwave signal, the booster amplifier is adopted to preliminarily amplify the lightwave signal when launched into the fiber. Similarly, pre-amplifier is also employed right before the detection for the purpose of increasing the sensitivity of the optical receiver. Besides, in general, a lot of inline amplifiers are deployed in tandem along the transmission fiber link. For the arrangement of the locations of all the inline optical amplifiers, losses and, sometimes, dispersion and nonlinear effects are all important effects that should be taken into consideration.

As aforementioned, not only the signal itself but also the noise will be amplified and eventually accumulated at the receiver end. Therefore, the noise performance of each of the inline amplifiers contributes to the final NF. This noise performance of the cascaded multistage system can be described and calculated by Friis formula.

The total noise factor of a series of cascaded stages (not only amplifiers but also lossy stages) is determined by the noise factor of each stage as:

$$F_{\text{tot}} = F_1 + \frac{F_2 - 1}{G_1} + \frac{F_3 - 1}{G_1 G_2} + \frac{F_4 - 1}{G_1 G_2 G_3} + \cdots \frac{F_n - 1}{G_1 G_2 \cdots G_{n-1}} \tag{2-3}$$

where F_i and G_i are the noise factor and available power gain of the i-th stage, repectively, while n is the total number of the stages. Note that all the values in Friis formula are expressed in ratios, not in decibels.

The most important conclusion drawn from Eq. (2-3) lies in the fact that the overall noise figure is primarily dominated by the noise figure of the first stage. This is reasonable, since the noise from the first stage Conversely, the other successive stages contribute diminishingly on the final SNR. Therefore, usually, the first stage plays the most critical role and is often designed with optimization towards low NF. This kind of amplifiers is consequently called low-noise amplifiers (LNAs)[76].

2.4 Conclusion

In this chapter, starting from the historical evolution of modern optical and photonic technologies, the optical amplifiers have been reviewed followed by the introduction of the general properties of the optical amplifiers.

Chapter III

Multi-wave model for phase-sensitive fiber-optic parametric amplifiers

The fundamental physical mechanism underlying PS-FOPA is the Kerr nonlinearity in silica optical fiber. Starting from the nonlinear phenomenon, the basics of nonlinear optics in optical fibers are introduced. The underlying linear and nonlinear properties, that the waves may experience during propagation in silica optical fibers, are of particular importance and will, therefore, be described in this chapter.

This chapter serves as an introduction to the theoretical model which will be used to analyze the characteristics of the PSA. As this work is focused on the FOPA based PSA, the unique operation exploiting the phase-sensitivity of the gain is introduced and compared with the general phase-insensitive operation in traditional amplifiers. Starting from the basic wave equation, a set of coupled-wave ordinary differential equations (CWODEs) describing the evolution of slow-varying amplitude propagating in the nonlinear medium is derived. Successively, the mathematical results of phase-sensitive and phase-insensitive processes are presented for the ease of intuitively understanding of the physical mechanism.

From the standpoint of a preliminary FWM experiment, a multi-wave model incorporating a set of CWODEs is established to precisely describe the actual nonlinear interaction that occurs during propagation.

3.1 Nonlinearity and nonlinear phenomenon

3.1.1 Nonlinear phenomenon

In the field of nonlinear optics, researches on light-matter interaction are the primary concern. It was not until the invention of the laser, the highly intense and highly coherent light source which can serve as an enabling tool for the investigation of light-matter interaction, that the substantial researches and progresses in nonlinear optics have been thereby activated. Soon after the invention of laser[77], [78], [79], [80] in the early 1960s, the observation of second-harmonic generation (SHG) was performed by P. A. Franken and colleagues in 1961[81], which was generally regarded as the dawn of nonlinear optics. In the following years, a great number of interests in the area of nonlinear optics have sprung up ranging from fundamental scientific research to practical applications. On this basis, enormous emerging fields such as fundamental physics, innovative materials, laser technologies, and optical communications have surged and been continuously advanced, ceaselessly achieving remarkable accomplishments.

An intuitive interpretation of the nonlinear phenomenon can be summarized as follows: during the light-matter interaction, the lightwave itself modifies the physical property of the material including the response to the incident light such as refractivity, reflectivity, and susceptibility. Consequently, this modification will in turn influence or even alter the characteristic of the interaction process, and the optical field itself, leading to the nonlinear response of the medium. Obviously, there is a certain requirement on the intensity of the incident light to reach the nonlinear regime. Therefore, the reason why the birth of laser was the milestone for the researches and advances of nonlinear interactions primarily lies in the fact that the ultra-high power, namely, the intense electric field of the laser, is a prerequisite to obtaining the nonlinear interaction. In addition, the high coherence and highly monochromatic property of lasers are also important conditions to facilitate nonlinear light-matter interaction.

Consider the dependence of the polarization $P(t)$ of a material system on the strength of the applied electrical field $E(t)$. We assume the output polarization depends only on the applied electric field. We also neglect the frequency dependence of the nonlinear susceptibilities and suppose that the material is transparent. Hereby, the output

polarization of the medium can be described as the combination of the power series of the susceptibilities $\chi^{(n)}$ $(n = 1, 2, 3 \ldots)$ by the relation expressed in the following:

$$\begin{aligned} P(t) &= \varepsilon_0 \left[\chi^{(1)} E(t) + \chi^{(2)} E^2(t) + \chi^{(3)} E^3(t) + \cdots \right] \\ &= P^{(1)}(t) + P^{(2)}(t) + P^{(3)}(t) + \cdots \end{aligned} \tag{3-1}$$

where ε_0 is the vacuum permittivity and $E(t)$ is the electric field of the input optical lightwave. For the sake of simplicity, the output polarization is written only in scalar form and we neglect the tensor nature of the nonlinear effect.

Let us first take care of the completely linear case where the output polarization only depends on the electric field of the incident lightwave in a completely linear manner:

$$P(t) = \varepsilon_0 \chi^{(1)} E(t) \tag{3-2}$$

where $\chi^{(1)}$ is known as the first order susceptibility or linear susceptibility.

In regard to the nonlinear case, high-order susceptibilities $\chi^{(2)}$ and $\chi^{(3)}$ are the second- and third-order nonlinear susceptibilities, respectively. Accordingly, the second and the third terms $P^{(2)}(t) = \varepsilon_0 \chi^{(2)} E^2(t)$ and $P^{(3)}(t) = \varepsilon_0 \chi^{(3)} E^3(t)$ are the second- and third-order nonlinear polarizations. As aforementioned, a vectorial form of Eq. (3-1) should be considered for a thorough description of the nonlinear interaction.

It is not surprising that with the action of these high-order nonlinear effects, the generation of new frequency components is the direct consequence of the light-matter interaction as can be seen from Eq. (3-1). On this basis, a great number of nonlinear effects such as three-wave mixing (TWM) in typical $\chi^{(2)}$ nonlinear media and four-wave mixing (FWM) in $\chi^{(3)}$ nonlinear media take place. As a consequence, they have become the fundamental physical phenomena for various applications of nonlinear optics including difference frequency generation (DFG), sum frequency generation (SFG), SHG, third-harmonic generation (THG), and optical rectification (OR), for instance. The underlying optical parametric process have further inspired the emergence of some profound research fields, to name a few, parametric oscillation and parametric amplification as representatively shown below in Fig. 3.1.

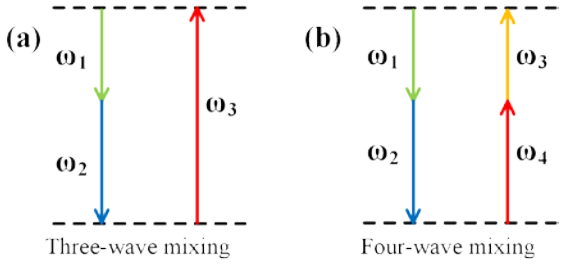

Fig. 3.1 High-order nonlinear interactions and energy-level descriptions.

The geometry of the high-order nonlinear interactions and their energy-level descriptions. (a) TWM based on $\chi^{(2)}$ media; (b) FWM occurs in $\chi^{(3)}$ media.

In order to obtain a more rigorous and detailed description regarding the nonlinear optical phenomena, the time-varying polarization should be taken into consideration. Usually, this can be accomplished by solving the nonlinear equation above to obtain a more general form and by expressing the second- and third-order susceptibilities in forms of fundamental physical constants. Here it is given without detailed derivation in Eq. (3-3)[82].

$$\nabla^2 E - \frac{n^2}{c^2}\frac{\partial^2 E}{\partial t^2} = \frac{1}{\varepsilon_0 c^2}\frac{\partial^2 P^{NL}}{\partial t^2}, \tag{3-3}$$

where n is the linear refractive index and c is the speed of light in vaccum. This equation can be interpreted as an inhomogeneous wave equation where the polarization P^{NL} associated with nonlinear response drives the electric field E.

It should be noted that by expanding the power series of the second- and third-order polarizations separately, one could steadily find that in third-order polarization the nonlinear effect will affect the polarization at the frequency of the incident optical fields. This indicates that for the optical wave incident on a $\chi^{(3)}$ medium, the third-order nonlinearity will modify the refractive index it undergoes. For such a circumstance, the refractive index can be represented as

$$n = n_0 + n_2 I\,, \tag{3-4}$$

where n_0 is the linear refractive index and I is the intensity of the incident optical wave which is written as

$$I = \frac{1}{2} n_0 \varepsilon_0 c A^2\,, \tag{3-5}$$

where A is the field amplitude of the applied wave. Therefore, n_2 can be generally used

to characterize the strength of the nonlinearity in this type of media as:

$$n_2 = \frac{3\chi^{(3)}}{2n_0^2\varepsilon_0 c}. \tag{3-6}$$

This intensity dependent nonlinear refractive index n_2 is also called Kerr nonlinear effect named after John Kerr, the physicist who discovered this effect in 1875.

3.1.2 Nonlinear media

The nonlinear property of the medium, especially the nonlinear susceptibility, is determined by the characteristics and geometric structures of the materials. In many cases, second- and third-order nonlinearities may occur simultaneously in the same medium.

However, for materials that exhibit inversion symmetry at the molecular level and for some optically isotropic media, the second-order nonlinearity does not exist and $\chi^{(2)}$ in these materials completely vanishes[83]. For these media in which the second-order nonlinear interaction is absent, the third-order nonlinearity thus dominates.

Though most of the first nonlinear discoveries and experiments were produced and conducted in $\chi^{(2)}$ nonlinear media[84] especially nonlinear crystals[85], the $\chi^{(3)}$ nonlinear effect in inversion symmetric medium has also attracted appreciable interests[86]. Though many crystal materials exhibit large $\chi^{(2)}$ nonlinearity, they also introduce considerable attenuation due to the large coupling loss which severely limits the total power that can be coupled into the crystal[87]. This eventually leads to the limits in the total nonlinear efficiency. In addition, since the processes stimulated by $\chi^{(2)}$ nonlinearity such as SHG and SFG involve waves with very large frequency interval, most of those crystal materials and waveguides are not able to maintain transparency and single-mode operation within a large optical bandwidth (quite often beyond one octave). Moreover, the difficulties in the compatibility with the nowadays widely deployed fiber-optic communication systems and networks have posed a lot of serious technical challenges on the practical prospect.

In opposition to $\chi^{(2)}$ nonlinearity, $\chi^{(3)}$ nonlinear materials, especially the silica optical fibers, are almost ideal candidates for a series of potential applications. Since silica is an inversion symmetric material, it only exhibits $\chi^{(3)}$ nonlinearities[88]. Though the THG still can not be fitted within a single optical band, hindering the single mode operation for all the interacting waves. The other resulting nonlinear phenomena such as

FWM can occur within a relatively narrow optical bandwidth, and more importantly, the silica optical fiber is able to keep single-mode operation within this bandwidth. The nonlinear medium, the fiber itself, shows an extremely low loss and high coupling efficiency. Additionally, it is intrinsically compatible with the existing telecommunication systems in a seamless manner. This has thus prepared optical fiber as the center of many relevant researches.

However, it has to be mentioned that the nonlinearity of silica optical fiber is relatively weak (by at least two orders of magnitude) compared with some $\chi^{(2)}$ materials. The nonlinear index coefficient n_2, which is used to characterize the strength of the nonlinearity, depends on core composition and structure for silica optical fiber. The typical value for optical fiber is around $2.2\sim3.4\times10^{-20}\,\mathrm{m}^2/\mathrm{W}$, also depending on the polarization changes when the waves propagate along the fiber. Fortunately, thanks to the efficient coupling between the fiber subsystems and the low loss nature of the silica optical fiber, the nonlinear effect can be observed at a relatively low power level. Indeed, the total induced nonlinearity can be assessed by the product of nonlinear coefficient, incident power, and total interaction length, which is also regarded as the figure of merit for the nonlinear efficiency[89]. The possibility to have high incident power and ultra-long interaction length reduces the requirement on the nonlinearity of the medium. It should be mentioned that if n_2 is increased, one may obtain significant nonlinearity without exciting Brillouin scattering.

In light of this, provided one has a sufficiently long optical fiber, the nonlinear efficiency can be significantly improved, allowing for the efficient generation and observation of different nonlinear effects in such a medium. From the application point of view, a long fiber is never an issue in fiber optical communication systems and networks. And the transfer from the lumped bulk nonlinear medium to the distributed nonlinear medium has also brought new opportunities for fiber optical parametric amplification.

However, for the sake of further integration, the length of the optical fiber cannot be immoderately increased. The relatively weak nonlinearity has asked to further improve the nonlinear coefficient. It is desirable to implement the nonlinear effect using a fiber as short as several hundreds of meters. By combining particularly designed core diameter, reduced core area and proper doping[90], the nonlinear coefficient and nonlinear

refractive index can be substantially improved. This way, more than ten times higher nonlinear coefficient can be achieved. This special sort of silica optical fiber is called highly nonlinear fiber (HNLF)[91]. The emergence of such HNLF has facilitated the implementation of nonlinear effect based FOPA for real practical scenarios[92]-[95].

3.1.3 Parametric nonlinear process

The nonlinear interaction can be either a parametric or a non-parametric process. As aforementioned, the parametric process is named “parametric” due the induced modulation of medium parameters, the refractive index for instance. The parametric process neither alters the quantum state of the medium nor stores any energy inside the medium. The latter indicates there is no energy exchange between the electric field and the dielectric medium during the interaction. In this sense, the parametric nonlinear interaction is a complete elastic process and responds instantaneously.

The non-parametric nonlinear processes are quite distinct in a fashion that the energy of the electromagnetic field is partly transferred to the nonlinear medium, the interaction is therefore inelastic. In a $\chi^{(3)}$ nonlinear medium, the resulting stimulated inelastic scattering is an important manifestation. When related to vibration excitation of silica, the stimulated Raman scattering (SRS)[96] and the stimulated Brillouin scattering (SBS)[97] induced by optical phonons and acoustic phonons, respectively, are the two most famous and well-studied stimulated inelastic phenomena in optical fibers[98]. Here, we will not focus on these non-parametric processes. However, it is worth noting that SRS and SBS all have a certain threshold indicating that only when the power of the electromagnetic field exceeds a certain level, significant conversion takes place. This threshold behavior leads to a critical limiting factor for parametric amplification when a large amount of incident power is imperative.

3.1.4 Nonlinearity in silica optical fiber

The further development of fiber optical communication systems and networks towards high speed, large capacity, and long distance is essentially based upon the research and development in the field of nonlinear optics. Especially, the fascinating evolutions in optical communications have in turn continuously motivated and also benefitted from

the drastic progress of the basic theory and the advanced technologies of nonlinear fiber optics. Since the rapid increase of the speed and capacity has started to approach and even exceed the nonlinear Shannon limit[51], the importance and significance of nonlinear fiber optics are becoming critical due to the fact that silica optical fiber has long been the perfect applicable platform for practical implementation of nonlinear optics. For this sake, the linear and nonlinear effects for wave propagating in fibers should be considered with extra care.

3.2 Wave propagation in fiber: linear effects

3.2.1 Loss and effective length

Loss or linear attenuation is the primary detrimental effect when a lightwave signal is propagating in silica optical fibers. Given the incident signal power P_0, then the optical power at distance L from the input end of the fiber can be expressed as

$$P_L = P_0 \exp(-\alpha L), \tag{3-7}$$

where α is the attenuation coefficient or attenuation constant. In general, α is usually expressed in units of $1/\mathrm{km}$. Alao it can be defined in units of $\mathrm{dB/km}$ as:

$$\alpha_{\mathrm{dB}} = -\frac{10}{L}\log\left(\frac{P_{\mathrm{L}}}{P_0}\right) = 4.343\,\alpha\,. \tag{3-8}$$

In general, the fiber losses are frequency dependent. The silica fibers fabricated by one of the most popular procedures called modified chemical vapor deposition (MCVD) exhibit small losses [about 0.22 dB/km for standard single-mode fiber (SMF)] over the whole C-band around 1550 nm.

The total fiber losses are the consequence of several factors involving material absorption and Rayleigh scattering. Among these sources, the most limiting flaw is the vibration absorption peak due to the OH-ion, which is regularly located at ~2.73 μm. Its harmonics at $1.4\,\mu\mathrm{m}$ and sub-overtones at $\sim 1.23\,\mu\mathrm{m}$ almost overlap with the telecommunication wavelength, thus dominating over other side effects. Just because of this, special precautions are imperative to rule out the OH-ion or at the least to minimize the level of it in the fabrication. On the other side, Rayleigh scattering is due to random refractive index fluctuations of silica.

Sometimes, in order to be concise while keeping sufficient physical meaning, the fiber losses can be taken into account as the effective length as defined by

$$L_{\text{eff}} = \frac{1-\exp(-\alpha L)}{\alpha}. \tag{3-9}$$

This way, the length is normalized to the loss, simplifying some intricate calculations of nonlinear interactions.

3.2.2 Chromatic dispersion

As aforementioned, silica is a highly dispersive medium: the refractive index $n(\omega)$ is frequency dependent. The origin of chromatic dispersion is due to the characteristic resonance frequencies at which the electromagnetic wave interacts with the bounded electrons of a dielectric of a medium in an absorption manner[100]. Several factors are responsible for the overall chromatic dispersion of the fiber.

- Modal dispersion

According to the large core size of the multimode fiber, different modes launched into the fiber correspond to different angles and travel along different paths. The propagation path differences lead to temporal pulse broadening. Obviously, modal dispersion only exists in multimode fibers.

- Material dispersion

Material dispersion stems from the characteristic dispersion of the material which strongly relates to the core constituents. In practice, the actual dispersion profile of the silica fibers deviates from the pure silica dispersion due to dopants such as GeO_2 and P_2O_5 in the core.

- Waveguide dispersion

In waveguides such as silica optical fiber, especially single-mode fiber, the dispersion is related to the fiber-design parameters, for example, the refractive index difference between core radius and core-cladding[101]. Thus it is a function of fiber refractive index profile and wavelength.

With finite linewidth of the lightwave and the chromatic dispersion dependent refractive index, different frequency components of the optical signals propagating in fiber travel with distinct phase velocities $c/n(\omega)$. The lightwave is thus spectrally and temporally spread out. This effect is especially critical for ultra-short lightwave pulses.

Since the propagation constant β is directly determined by the frequency dependent refractive index, the dispersion can often be described as a Taylor expansion of β about the center frequency ω_0 of the lightwave pulse

$$\beta(\omega) = n(\omega)\frac{\omega}{c} = \beta_0 + \beta_1(\omega-\omega_0) + \frac{\beta_2}{2!}(\omega-\omega_0)^2 + \frac{\beta_3}{3!}(\omega-\omega_0)^3 + \frac{\beta_4}{4!}(\omega-\omega_0)^4 + \ldots \tag{3-10}$$

where β_{m} is the high-order propagation constant given by

$$\beta_{\mathrm{m}} = \left.\frac{d^{\mathrm{m}}\beta}{d\omega^{\mathrm{m}}}\right|_{\omega=\omega_0}. \tag{3-11}$$

Since β_{m} is related to the frequency, it is linked with the frequency dependence of the refractive index. The first order propagation constant is inversely related to the group velocity v_{g} which describes the speed of the envelope for a group of co-propagating waves

$$\beta_1 = \frac{d\beta}{d\omega} = \frac{1}{v_{\mathrm{g}}} = \frac{n_{\mathrm{g}}}{c} = \frac{1}{c}\left(n + \omega\frac{dn}{d\omega}\right), \tag{3-12}$$

where n_{g} is the group index. The second order propagation constant represents the dispersion of the goup velocity v_{g} and can be written as

$$\beta_2 = \frac{1}{c}\left(2\frac{dn}{d\omega} + \omega\frac{d^2n}{d\omega^2}\right), \tag{3-13}$$

which is known as the group velocity dispersion (GVD). In the telecommunication community, the dispersion parameter D_λ is widely used due to the ease of measurement

$$D_\lambda = \frac{d\beta_1}{d\lambda} = -\frac{2\pi c}{\lambda^2}\beta_2 = -\frac{\lambda}{c}\frac{d^2n}{d\lambda^2}. \tag{3-14}$$

It can be seen from Fig. 3.2 that in usual single-mode fibers the GVD reaches zero around 1300 nm. β_2 and D_λ approach zero in the vicinity of this wavelength region, which is thus called zero-dispersion wavelength λ_{ZDW}. It should be noted that dispersion does not completely vanish at λ_{ZDW} due to the non-zero higher order dispersion terms such as β_3. For special fibers such as HNLF, the value of λ_{ZDW} can be shifted by changing the fiber design.

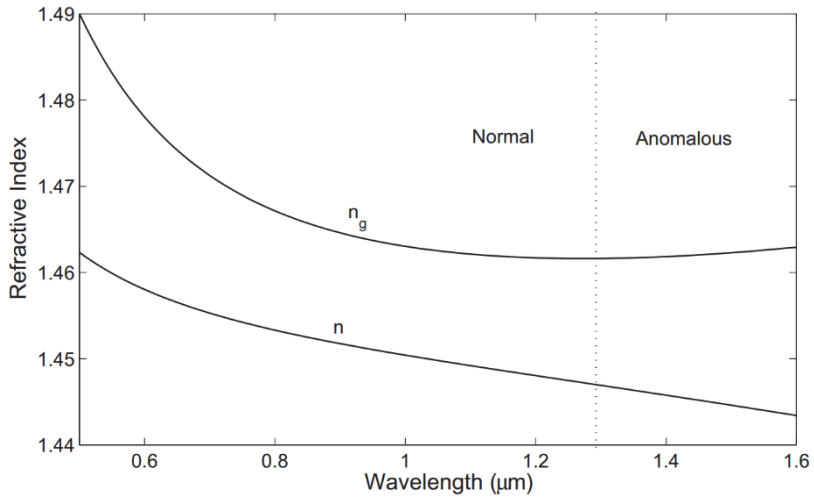

Fig. 3.2 Variation of refractive index n and group index n_g with respect to the wavelength in standard silica optical fiber.

According to the sign of dispersion parameter β_2 or D_λ, the nonlinear effects behave differently. When $\lambda < \lambda_{ZDW}$ where $\beta_2 > 0$, the fiber exhibits normal dispersion. The region where $\lambda > \lambda_{ZDW}$, i.e., $\beta_2 < 0$, is named anomalous dispersion regime. The latter is interesting for the community of telecommunications owing to the potential to balance the effects of dispersion and nonlinearity.

3.3 Wave propagation in fiber: nonlinear effects

As discussed above, owing to the inversion symmetric structure of silica, $\chi^{(2)}$ nonlinearity vanishes in optical fibers, giving rise to the domination of $\chi^{(3)}$ nonlinearities and thus of third-order parametric processes such as FWM and THG. In this section, the properties and the corresponding characteristics of $\chi^{(3)}$ nonlinearities and the related nonlinear phenomena will be introduced.

3.3.1 Self- and cross-phase modulation

In the context of nonlinear parametric processes, the intensity-dependent refractive index alters the speed of light in the medium and brings about additional phase changes for the propagating waves. This intensity induced phase shift ϕ_{SPM} is so-called self-phase modulation (SPM):

$$\phi_{\mathrm{SPM}} = \gamma P_0 L_{\mathrm{eff}}\,, \tag{3-15}$$

where P_0 is the average input optical power and also can be the peak power in the pulse regime. γ is related to the nonlinear Kerr coefficient n_2 as

$$\gamma(\omega_0) = \frac{\omega_0 n_2(\omega_0)}{cA_{\mathrm{eff}}}, \tag{3-16}$$

where A_{eff} holds for the effective mode area in the fiber, which is determind by the fabrication parameters such as core diameter and the difference core-cladding refractive indices. Since γ incorporates the contributions of nonlinear Kerr effect and the effective interaction mode area, it is hence regarded as the nonlinear parameter or the nonlinear coefficient.

If the power dependent phase modulation is introduced to or from other waves, the effect is known as cross-phase modulation (XPM) which also depends on the state-of-polarization (SOP) of the involving waves:

$$\phi_{\mathrm{XPM}} = 2\rho \cdot \gamma P_0 L_{\mathrm{eff}}\,, \tag{3-17}$$

where ρ is a polarization dependent term. Both SPM and XPM are valuable phenomena that have been widely discussed and exploited in various contexts.

3.3.2 Four-wave mixing

Due to the absence of $\chi^{(2)}$ nonlinearity, FWM, also called four-photon mixing, has become the primary and dominant nonlinear phenomenon in $\chi^{(3)}$ media, especially silica optical fiber. As illustrated in Fig. 3.1, for a $\chi^{(3)}$ medium, the nonlinear parametric interaction generally involves four waves or four photons. It should be recalled that the nature of nonlinear parametric processes is completely elastic and does not alter the quantum state of the medium. Thus in a fully quantum description, photons from one or more wave are annihilated and new photons are created simultaneously at one or more distinct frequencies in a manner that the energy and momentum are both conserved. In a completely classical term, FWM can be interpreted as the energy from one or more waves flowing to the other waves at different frequencies. The efficiency of the FWM process is determined by the phase matching condition amongst all the involved waves.

The overall efficiency of the nonlinear parametric process also depends on the changes of the SOP during the interaction. Following the discussion in the first section

of this chapter, we consider only the scalar case where all the waves are co-polarized and their SOPs do not change during interaction and propagation.

Consider two co-polarized waves with different frequencies ω_1 and ω_2 incident into a fiber in the same direction. The generation of the new frequency components can be described as follow: the strong beat note $\Delta\omega = \omega_1 - \omega_2$ modulates the refractive index of the fiber. This modulation will in turn modulate the two original incident waves, producing two side bands at both sides of each wave. At the same time, if another component with frequency ω_3 is added along with ω_1 and ω_2, it will inevitably be modulated by the beat note $\Delta\omega$. Similarily, the beat notes between ω_3 and ω_1 and ω_2 will again modulate all the involved waves. This way, FWM process and cascaded FWM processes take place.

Then, consider the circumstance in which a number of co-polarized incident waves of frequencies ω_i co-propagate through the nonlinear media. The total electric field then reads

$$E(x,y,z) = \frac{f(x,y)}{2} \sum_{i\in\{p,s,i\}} A_i(z) e^{j(\omega_i t - \beta_i z)} + c.c., \tag{3-18}$$

where $\beta_j = n_j\omega_j/c$ and n_j is the total refractive index. Eq. (3-1) must be taken with Eq. (3-18). The nonlinearity is expanded to third-order. The polarization is substituted with the forms of the electric fields and $f(x,y)$ represents the transverse mode shape. $A_i(z)$ is responsible for the slowly varying amplitude along the propagation direction. Obviously, owing to the third-order nonlinearity, new frequency components will be created. Meanwhile, waves with the same frequencies as the incident waves may also be generated and superpose with the incident waves in a coherent manner. All the possible frequency components should satisfy the energy conservation. This is usually express in the frequency domain as

$$\omega_m = \omega_j + \omega_k - \omega_l \tag{3-19}$$

where j, k, m, l represents any frequency components. These new frequency components are located symmetrically as

$$\Delta\omega = \omega_m - \omega_k = \omega_j - \omega_l \tag{3-20}$$

where ω_m, ω_j and ω_k, ω_l are the frequencies of the incident and created waves, respectively.

In quantum-mechanical terms, two photons of frequencies ω_m and ω_j annihilate

while two photons of frequencies ω_k and ω_l are created as the energy is conserved. In general, the incident waves with higher power are usually called pump while the generated waves are named signal or idler depending on the scenarios.

The above discussion has been conducted in the case where only two waves are incident. From a practical point of view, more than two waves can also be quite common. And in these cases, incident waves including the pumps and signal and idlers can be either degenerate or non-degenerate, namely, they can be of the same frequency or not.

Different FWM scenarios for different incident waves and distinct degeneracy cases are schematized in Fig. 3.3. When the frequencies of the incident pumps, signal, and idler are all different from each other, one refers to non-degenerate FWM as sketched in Fig. 3.3(a) and Fig. 3.3(b). If the signal and idler are absent, with only the pumps $P1$ and $P2$ at the input, due to the energy and momentum conservations the created signal and idler will be located on each side of the two pumps in a completely symmetric manner. This is quite similar to the case in Fig. 3.3(a) but with equal frequency spacings. In cases when one signal, or even both signal and idlers are incident along with the pumps, one generally ends up with the output as illustrated in Fig. 3.3(a) and Fig. 3.3(b), depending on the frequency relations at the input. And in some particular cases, these two cases can occur simultaneously, leading to the presence of four signals and idlers at the output.

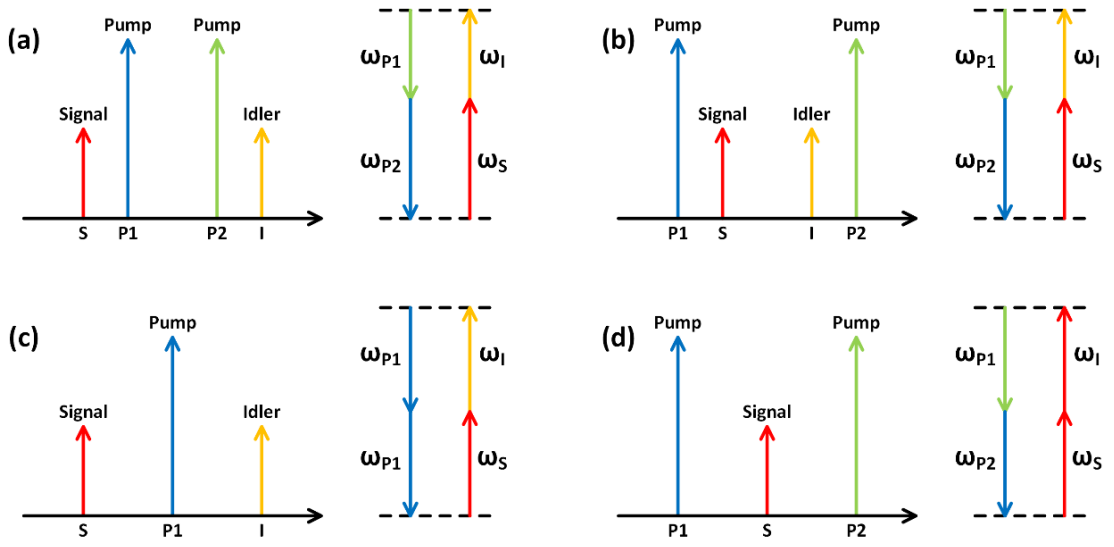

Fig. 3.3 Different FWM schemes with different input wave settings.

Different FWM schemes with different input wave settings. (a) Nondegenerate FWM; (b) Nondegenerate FWM; (c) Pump degenerate FWM; (d) Signal-idler degenerate FWM.

If the frequencies of the two incident pumps are identical, i.e., pumps are degenerate, the input signal will lead to the creation of an idler at the symmetric frequency as shown in Fig. 3.3(c). Quite analogously, the signal and idler can be also degenerate if pumps are not degenerate. This can be understood in a different point of view as the idler being generated and coherently superposed with the signal at the same frequency.

3.3.3 Phase matching

The underlying energy and momentum conservations fundamentally govern the FWM process, especially the annihilation and creation of the photons and their frequency relations.

Due to dispersion, as seen above, the effective refractive index is a function of frequency ω. This dispersion property is described by the propagation constant β as discussed in section 3.2.2 .

The phase velocities of the different frequency components are thus distinct. Therefore, the phase relation of the frequency components taking part in the nonlinear interactions will definitely be altered after a certain distance of propagation. As a result, the condition for momentum conservation would be no longer satisfied during the propagation, leading to a poor efficiency of the nonlinear interaction efficiency. It comes up that if the vectorial sum of the propagation constants of all the frequency components involved in the nonlinear interaction is zero, the phase relation amongst these waves can be preserved during the propagation. This phase relation is thus called phase matching. Since this phase matching only accounts for the linear effect, this is thus so-called the linear phase matching condition. Nonetheless, in order to incorporate the nonlinear effects, contributions coming from SPM and XPM should be accounted for and will be introduced later.

In particular, for FWM, the linear phase mismatch usually reads

$$\begin{aligned}\Delta\beta &= \beta_3 + \beta_4 - \beta_1 - \beta_2 \\ &= \left(n_3\omega_3 + n_4\omega_4 - n_1\omega_1 - n_2\omega_2\right)/c .\end{aligned} \tag{3-21}$$

In regard to the fiber dispersion, the perfect phase matching demands $\Delta\beta = 0$. This cannot be always satisfied, leading to the circumstance called phase mismatch

$$\Delta\beta \neq 0 . \tag{3-22}$$

In these cases, the efficiency of nonlinear interaction will be diminished. Therefore, the strength of the new components and efficiency of energy transfer will be reduced. The phase matching is one of the limiting factors for the efficiency of nonlinear processes.

3.4 Nonlinear Schrödinger equation

3.4.1 Generalized nonlinear Schrödinger equation

Derived from Maxwell's equation, the nonlinear Schrödinger equation (NLSE) governs the envelope dynamics of a quasi-monochromatic plane wave propagating in a nonlinear and dispersive medium when dissipative processes are negligible[102]. The generalized NLSE (GNLSE) should account for other practical effects involving loss effect, stimulated non-elastic processes such as SBS and SRS, and all the high-order dispersions. For the sake of simplicity, the SBS and SRS terms are ignored, leading to the NLSE reading

$$\frac{\alpha}{2}A+\frac{\partial A}{\partial z}+\frac{i\beta_2}{2}\frac{\partial^2 A}{\partial T^2}-\frac{\beta_3}{6}\frac{\partial^3 A}{\partial T^3}=i\gamma\left|A\right|^2 A, \tag{3-23}$$

where $A(z,t)$ is the slowly-varying envelope. The nonlinear coefficient γ is defined as in Eq. (3-16).

3.4.2 Coupled-wave equation

The coupled-mode wave equation can be directly derived from the wave equation or the GNLSE to obtain an analytical solution for the nonlinear interactions. In order to obtain a succinct solution, some hypothesis are imperative. We assume operation in quasi-continuous-wave (CW) condition so that the amplitude has a slowly-varying envelope, thus neglecting its time dependence. In order to further neglect the spatial distribution $F_j(x,y)$ of the fiber mode of j^{th} wave field propagating in the fiber, one can assume that all overlap integrals are nearly the same. This assumption is valid for SMF. With these appropriate simplifications, the coupled-mode equations that govern the slowly-varying amplitude $A_j(z)=\sqrt{P_j}e^{j\varphi_j}$, $j=1\sim4$, where P_j and φ_j are initial power and phase of j^{th} wave, respectively, in the optical fiber can be derived by taking Eq. (3-1) into NLSE Eq. (3-23) while substituting the polarization with the slowly-varying electric field

$$\begin{aligned}
\frac{dA_1}{dz} &= -\frac{\alpha}{2}A_1 + i\gamma\left[\left(|A_1|^2 + 2\sum_{k\neq 1}|A_k|^2\right)A_1 + 2A_2^* A_3 A_4 e^{i\Delta\beta z}\right], \\
\frac{dA_2}{dz} &= -\frac{\alpha}{2}A_2 + i\gamma\left[\left(|A_2|^2 + 2\sum_{k\neq 2}|A_k|^2\right)A_2 + 2A_1^* A_3 A_4 e^{i\Delta\beta z}\right], \\
\frac{dA_3}{dz} &= -\frac{\alpha}{2}A_3 + i\gamma\left[\left(|A_3|^2 + 2\sum_{k\neq 3}|A_k|^2\right)A_3 + 2A_1 A_2 A_4^* e^{-i\Delta\beta z}\right], \\
\frac{dA_4}{dz} &= -\frac{\alpha}{2}A_4 + i\gamma\left[\left(|A_4|^2 + 2\sum_{k\neq 4}|A_k|^2\right)A_4 + 2A_1 A_2 A_3^* e^{-i\Delta\beta z}\right],
\end{aligned} \tag{3-24}$$

where γ is the nonlinear coefficient given by Eq. (3-16) and $\Delta\beta$ is the wave-vector mismatch or linear phase mismatch given by Eq. (3-21). The set of coupled-wave equations of Eq. (3-24) describes the amplitude evolutions of four co-polarized waves co-propagating along the fiber.

It should be noted that even if only four waves are launched into the fiber, other extra frequency components may also be generated depending on the phase matching condition. However, here we focus on the main four waves.

The first term on the right-hand side in each of the equations in Eq. (3-24) containing amplitude and α holds for the loss effect during the propagation. The other terms in the middle-bracket represent different nonlinear phenomena: the first square modulus term represents the SPM effect; the second power summing term is responsible for the contribution due to XPM effect from other waves; the third term outside the inner parenthesis accounts for the third-order nonlinearity induced FWM effect, leading to phase matching governed phase shifts and energy transfer. Apparently, FWM efficiency is directly subject to the phase matching condition according to the $\Delta\beta$ term while those of SPM and XPM are affected only by the power of the interacting waves.

3.4.3 Approximate solution and total phase matching

Let us suppose that A_1 and A_2 represent the strong pumps while A_3 and A_4 are the signal and idler. In degenerate FWM cases, A_1 and A_2 or A_3 and A_4 can be degenerate. For insightfully investigating the physical properties of FWM, an approximate analytical solution is quite beneficial.

To this end, the additional hypothesis should be included: the dissipation in the medium is taken into account through either the effective length or by incorporating

propagation loss α; the pumps remain undepleted, assuming their intensities are much stronger than other waves. This way, an analytical solution of the set of differential equations Eq. (3-24) can be derived:

$$\begin{aligned}
\frac{dP_1}{dz} &= -\alpha P_1 - 4\gamma\sqrt{P_1P_2P_3P_4}\sin(\theta)\\
\frac{dP_2}{dz} &= -\alpha P_2 - 4\gamma\sqrt{P_1P_2P_3P_4}\sin(\theta)\\
\frac{dP_3}{dz} &= -\alpha P_3 + 4\gamma\sqrt{P_1P_2P_3P_4}\sin(\theta)\\
\frac{dP_4}{dz} &= -\alpha P_4 + 4\gamma\sqrt{P_1P_2P_3P_4}\sin(\theta),
\end{aligned} \tag{3-25}$$

$$\frac{d\theta}{dz} = \Delta\beta + \gamma\left(P_1 + P_2 - P_3 - P_4\right) + \left(\sqrt{\frac{P_1P_2P_3}{P_4}} + \sqrt{\frac{P_1P_2P_4}{P_3}} - 4\sqrt{P_3P_4}\right)\cos(\theta), \tag{3-26}$$

where θ represents the relative phase of the interacting waves that reads

$$\theta(z) = \left[\Delta\beta + \gamma\left(P_1 + P_2 - P_3 - P_4\right)\right]z + \left[\varphi_3(z) + \varphi_4(z) - \varphi_1(z) - \varphi_2(z)\right], \tag{3-27}$$

The power evolutions have a quite similar form as shown in Eq. (3-25). The first term on the right-hand side of Eq. (3-27) is responsible for the total phase-mismatch while the second term results from the initial relative phase. It should be noted that the phase-mismatch includes not only linear terms $\Delta\beta$ but also the contribution of intensities via nonlinear interactions. Therefore, the total phase mismatch can be written as

$$\begin{aligned}
\kappa &= \Delta\beta_L + \Delta\beta_{NL}\\
&= \left(\beta_1 + \beta_2 - \beta_3 - \beta_4\right) + \gamma\left(P_1 + P_2 - P_3 - P_4\right).
\end{aligned} \tag{3-28}$$

From a practical standpoint, one may exploit both the linear and nonlinear phase-mismatch to reach the perfect phase matching condition $\kappa = 0$.

The efficiency of the parametric process can be described by the so-called parametric gain g that can be derived from the analytical solution above, leading to:

$$\begin{aligned}
g &= \sqrt{\left[\gamma\left(P_1 + P_2\right)\frac{2\sqrt{P_1P_2}}{P_1 + P_2}\right]^2 - \left(\frac{\kappa}{2}\right)^2}\\
&= \sqrt{4P_1P_2\gamma^2 - \left(\frac{\kappa}{2}\right)^2}
\end{aligned}. \tag{3-29}$$

3.5 Fiber-optic parametric amplifier

3.5.1 Parametric amplification

One of the primary applications of nonlinear parametric processes in optical fiber exploits the underlying parametric gain to achieve parametric amplification. Such fiber-based amplifiers relying on FWM are thus known as FOPA[103].

For pump degenerate FWM, the process should involve signal and idler and one pump as shown in Fig. 3.3 (c). However, nondegenerate FWM can still occur even with only two pump waves. According to the energy conservation, new waves will be created at higher and lower frequencies with respect to the pumps. Their frequency separation equals the frequency difference between the two pumps. The new frequency components stem from the amplified quantum noise (AQE) which is also regarded as parametric ASE. The frequency locations of these new terms are subject to the pump-pump separation according to the energy conservation.

Parametric amplification is a process in which, when a signal is launched together with the pumps, the FWM process leads to energy transfer between the pumps and signals according to the phase matching condition. Undergoing the parametric process, the idler will be immediately created from AQE after a very short nonlinear interaction length and gradually evolve along the fiber together with other waves. With proper phase matching, both the signal and idler will gain energy from pumps, leading to the parametric amplification.

3.5.2 Phase-insensitive FOPA

As aforementioned, parametric processes must satisfy both energy and momentum conservations, resulting in a certain frequency relation. There is no exception for FOPA. On top of that, in absence of the idler at the input, the idler will be automatically created. Then the phase and frequency of this idler will strictly follow the relationship that leads to maximum parametric amplification. This way, the amplification gain for the signal does not depend on the initial relative phase but only on the phase matching. It is thereby a phase-insensitive amplification process.

In fact, most conventional amplifiers such as EDFA and Raman amplifier, are referred to as phase-insensitive amplifiers (PIA) as there is no phase-dependent gain. For the phase-insensitive FOPA (PI-FOPA), the signal gain is given by:

$$G_{\mathrm{PIA}} = \left\{1 + \left[\frac{\gamma\left(P_1 + P_2\right)}{g}\sinh\left(gL_{\mathrm{eff}}\right)\right]\right\}^2, \tag{3-30}$$

where undepleted pump assumption is preserved[32]. In the case where $\kappa = 0$ (perfect phase matching), when the FOPA is operating in the small signal regime, Eq. (3-30) can be reduced to a fully exponential form with respect to total pump power

$$G_{\mathrm{PIA}} = \frac{1}{4}\exp\left[2\gamma\left(P_1 + P_2\right)L_{\mathrm{eff}}\right]. \tag{3-31}$$

Meanwhile, in the case of worst phase matching, $\kappa = -2\gamma(P_1 + P_2)$, the signal gain is diminished to a quadratic relation with respect to the total pump power

$$G_{\mathrm{PIA}} = \left[2\gamma\left(P_1 + P_2\right)L_{\mathrm{eff}}\right]^2 \tag{3-32}$$

Note that in either case, pumps or signal and idlers cannot be degenerate according to the operation principle of the PIA.

The trace of development is quite similar to that of Raman amplifiers. Though the characteristics of FOPA have been widely studied in the 1980s[104], the practical researches have been hampered by the quality and performance of the devices. Ever since the demand for extra broadband amplification of WDM channel beyond the C-band has become essential to maintain the growth of transmission capacity, extensive researches on FOPA have been thrived again[105], [106]. Appreciable efforts have been carried out on the practical implementation of different FOPA configurations[107] such as degenerate or nondegenerate, one or dual-pumps as illustrated in Fig. 3.3. The gain spectrum of both single- and dual-pump configurations[32] have been insightfully investigated. The resulting exponential gain growth with respect to the pump power implies great potential amplification capability of the parametric process. On top of this, the gain spectrum of a typical FOPA is particularly restricted by the phase matching. Within the dispersive medium, the phase walk-off is determined by the deviation between the waves. As the dispersion of the commercial HNLF is optimized to be quite flat, the gain spectrum is capable of covering a vast spectral range including S-, C-, and L-band.

Apart from the broadband gain spectrum[105] and exponential gain property of FOPA, the underlying multi-wave interaction and ultra-fast nature of Kerr nonlinearity have led

to some particular operations including modulation instability and phase conjugation[108] that can be utilized for all-optical functionality in future telecommunication systems and networks. Regrettably, the noise performance of the FOPA is no better than that of those conventional amplifiers according to the 3 dB NF limit in the high gain regime.

3.5.3 Phase-sensitive FOPA

On the contrary, if both the pumps, the signal and the idler are incident and co-propagate together, the power evolution will depend on the relative phase among the waves. Note that the idler has to be accurately allocated at the frequency where it would have grown out of the AQE in PI-FOPA case, namely, the idler frequency has to be a direct copy of the signal frequency in a complete symmetric manner with respect to the pumps.

With the act of FOPA process, the signal and idler will evolve together along the fiber. Based on Eq. (3-25) to Eq. (3-27), the actual phase-sensitive gain can be derived[110]

$$G_{\mathrm{PSA}}(\theta_0) = 1 + \left\{1 + \frac{4\gamma^2 P_{\mathrm{P}}^2 \eta^2 + \kappa^2 + 4\gamma\kappa P_{\mathrm{P}} \eta \cos(\theta_0)}{4g^2}\right\} \sinh^2(gL) + \frac{\gamma P_{\mathrm{P}} \eta \sin(\theta_0)}{g} \sinh(2gL) \tag{3-33}$$

where $\eta^2 = P_i(0)/P_s(0)$ is the power ratio between the incident idler and signal and the initial relative phase is re-defined as $\theta_0 = \varphi_s + \varphi_i - \varphi_{P1} - \varphi_{P2}$, excluding the phase matching terms.

It can be observed from Eq. (3-33) that the power evolution, power flow, and signal gain strongly depend on the initial relative phase θ_0. With appropriate choices of θ_0, e.g., orthogonal values, the signal gain can be changed from the maximum to minimum corresponding to maximum amplification and de-amplification, respectively. It indicates a physical picture in which the energy can be transferred from pumps to signals while it could also flow back from signals to pumps, completely relying on the initial relative phase θ_0. Similarly, in the quantum mechanical description, the creation and the annihilation of the photons could occur at all the waves. FOPAs exploiting such phase-sensitive feature are known as PSA.

3.5.4 Phase sensitivity and squeezing

The unique phase-sensitivity has led to the particularly attractive nonlinear phenomenon, quadrature squeezing. The PSA gain response depends on the signal phase, provided the phases of the other interacting waves are fixed at the input. For example, in signal and idler degenerate FWM case, with fixed initial pump phases, only one quadrature of the signal will be amplified. More specifically, not only the signal but also the portion of the noise is amplified. As a matter of fact, all amplifiers treat signals and noises indiscriminately, no exception for PIA and PSA.

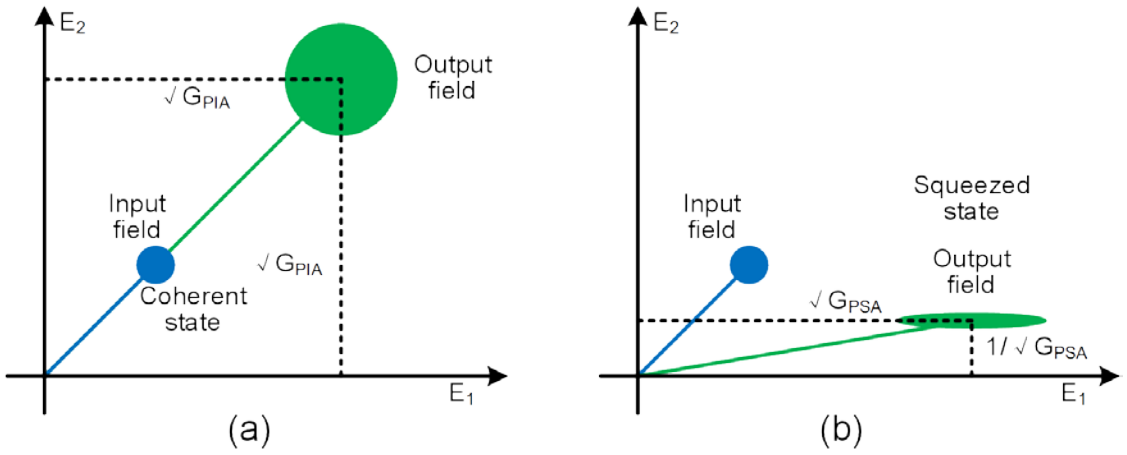

Fig. 3.4 Physical illustration of parametric amplification processes.

Physical illustration of parametric amplification processes: (a) Phase-insensitive amplification, G_{PIA} is the phase-insensitive parametric gain experienced; (b) Phase-sensitive amplification, G_{PSA} is the phase-sensitive parametric gain that experienced.

For any conventional PIA, all the associated noise will be amplified as indicated in Fig. 3.4 (a), and in addition, extra noises will be introduced by the amplifier itself[111]. Complying with the number-phase uncertainty, the amplitude, and the phase will be amplified simultaneously in the same manner with identical gain. The general procedure is sketched in Fig. 3.4 (a), and the circle size holds for the product of number-phase uncertainty. Both quadratures experience the same amplification process.

Nevertheless, this is not the case for PSA. Since the PSA treats the two quadratures differently, one quadrature is amplified with maximum gain $\sqrt{G_{PSA}}$ while the other quadrature undergoes a minimum gain $1/\sqrt{G_{PSA}}$. The fundamental noise performance is

limited by a more general uncertainty principle[112] where the uncertainty will be preserved during the amplification process. That is to say, during this phase-sensitive amplifying process, the total noise remains unchanged. Instead, the noise will be redistributed on the two quadratures in a manner that the noise on the in-phase portion can be reduced at the expense of the increased noise on the other orthogonal quadrature as shown in Fig. 3.4 (b). This is intuitively visualized as the so-called squeezing effect.

Since the amplifier treats signal and noise indistinguishable, the unique squeezing effect has led to the fact that the SNR on the amplified quadrature will not be degraded, giving rise to the ideal 0 dB NF. The in-phase component is “squeezed”. On the contrary, the amplified quadrature experiences noise amplification as an inversely squeezed state can be found on the quadrature component.

3.6 Multi-wave model

3.6.1 Single-pump and dual-pump PSA

According to the fundamental mechanism of FWM, it can be composed of different configurations as indicated in Fig. 3.3. Therefore, the FOPA and the PS-FOPA can be likewise constructed by different wave configurations, which can be roughly sorted out into two categories: single-pump configuration and dual-pump configuration.

In single-pump PSAs, the gain bandwidth strongly depends on the wavelength of the pump since it determines the phase matching conditions according to Eq. (3-28). The gain properties of single-pump configuration are therefore quite related to the wavelength of the pump. The maximum gain can be found when the signal is located away from the pump due to the contribution of the nonlinear phase matching to the total phase mismatch. This has led to the non-uniform gain spectrum. Meanwhile, the gain grows exponentially with the fiber length, the pump power, or the nonlinear coefficient at the perfect phase matching condition. Namely, the maximum gain scales exponentially with the product of fiber length, the pump power, and the nonlinear coefficient. Conversely, the gain bandwidth is inversely proportional to the fiber length. Therefore, trade-offs should be made between the peak gain and the gain bandwidth. Nevertheless, a flat gain spectrum can be hardly achieved. According to the phase matching, a deep dip can be observed in

the vicinity of the pump wavelength as shown in Fig. 3.5 (a). It is also worth mentioning that for the single-pump PSA, an extra idler is mandatorily required. This unwanted idler will occupy extra bandwidth, limiting the usable optical bandwidth for the actual signals.

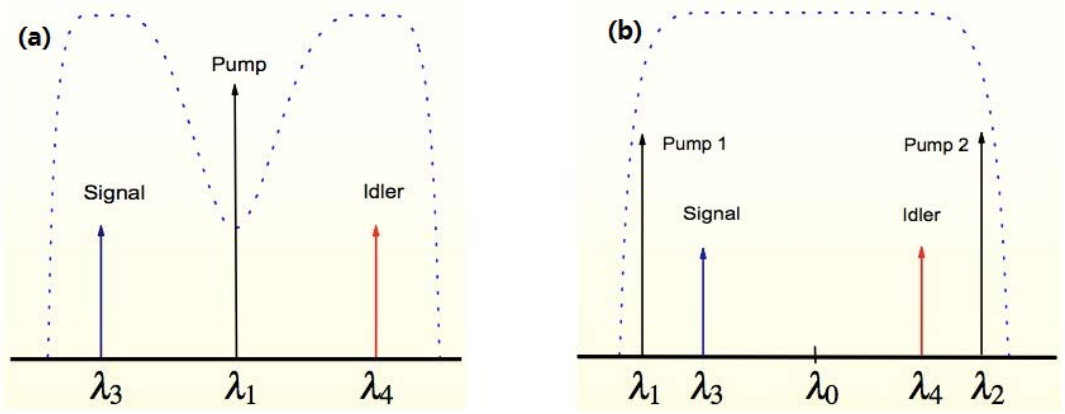

Fig. 3.5 Typical gain spectrum for PS-FOPA.

Typical gain spectrum for (a) single-pump PS-FOPA and (b) dual-pump PS-FOPA, respectively, illustrating the differences between the two cases.

In the context of fiber-optic communication systems and networks, a fairly uniform gain spectrum over the entire gain bandwidth is demanded. Although in single-pump PSA this can be realized by some particular techniques such as dispersion engineering of the fiber and connecting several fiber sections of suitable length and proper dispersive properties in tandem. Nevertheless, these techniques have difficulties in practical implementations.

On the contrary, dual-pump PSA is based on the nondegenerate FWM process that employs dual-pumps with distinct wavelengths. For this kind of PSA configurations, the phase matching condition can be satisfied over a much broader optical bandwidth. With appropriate pump wavelength allocations, it allows achieving a quite flat gain spectrum when the two pumps are located in a symmetrical manner with respect to the zero dispersion wavelength. The typical gain spectrum is shown in Fig. 3.5 (b). Moreover, with the presence of the two pump waves, the gain evolves quadratically with respect to the pump power. This allows achieving a certain gain with half of the power on each of the pumps, mitigating the SBS effect. This way, dual-pump PSA is of unique benefits from the practical point of view. One of the main drawbacks of the dual-pump PSA is that the gain property is sensitive to the random variation in refractive index resulting from the imperfections of the fiber parameters during the fabrication process. The effect

often manifests itself as the variation of the zero dispersion wavelength. Due to the influences of the phase matching conditions, such variations induce severe degradation in the gain spectrum, especially the flatness. In order to alleviate such effect, the two pumps are supposed to be located much closer to each other. However, the FWM process between the two pumps becomes non-negligible when they are not far away from each other, leading to the occurrence of cascaded FWM processes. The extra waves stem from the cascaded FWM processes may also constitute PS- or PS-FOPAs according to the phase matching conditions. Thus, these waves will in turn inevitably alter the phase sensitive process, i.e. the amplification process of the signal wave.

As a consequence, to precisely describe the behavior of the dual-pump PSA for the throughout comprehension and the overall analysis, a more accurate model taking into account the impact and influence of the high-order waves rather than the conventional 3-wave or 4-wave model is urgently demanded.

3.6.2 Cascaded FWM

The concept of the dual-pump degenerate PSA, as well as a preliminary experiment result as shown in Fig. 3.6 (a), illustrates what happens when co-polarized signal S_0 and pumps P_1 and P_2 are launched into a section of HNLF of length $L = 1011\text{m}$ (OFS standard HNLF) with a nonlinear coefficient $\gamma = 11.3\ \text{W}^{-1}\text{km}^{-1}$. The pump-pump separation is set to 40 GHz, with a central wavelength equal to $\lambda_{\text{ZDW}} = 1547.5\text{nm}$, corresponding to the zero-dispersion wavelength of the fiber. The total input power of the two pumps is equal to 23.5 dBm. At the output of the HNLF as can be seen from Fig. 3.6 (a), many high-order waves are generated by cascaded FWM of the two pumps and the pumps and signal. This leads to a significant deterioration of the signal gain compared to the value estimated from 3-wave model. The spectral broadening of the high-order waves is due to the phase modulation of the pumps used to suppress SBS. This SBS threshold can also be increased by using Spine HNLF or the cascade of different HNLF sections.

In the simplest 3-wave scalar optical parametric process, one considers two pumps denoted P_1 and P_2 and a degenerate signal and idler, denoted S_0 as illustrated in the left picture in Fig. 3.6 (a). Governed by the phase matching condition, extra high-order waves will be naturally generated according to the energy conservation. To take extra high-order four-wave mixing processes into account, we follow a more general 7-wave model

operating in continuous-wave regime involving four additional first order pumps and signals, as shown in the right panel of Fig. 3.6 (b).

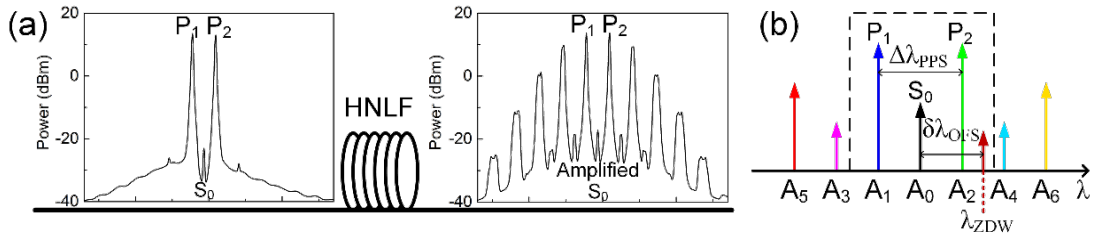

Fig. 3.6 Illustration of high-order wave generated by FWM process.
(a) Experimental result of dual-pump degenerate PSA: considerable high-order waves are generated by underlying high-order FWM processes. (b) Labeling of waves, separation, and offset for 7-wave model. The three waves in the dashed-line rectangle are those considered in the fundamental 3-wave model.

3.6.3 7-wave model based on coupled-wave equations

In order to investigate more accurately such a situation, we use a 7-wave model, as depicted in Fig. 3.6 (b). A similar 7-wave model has been independently developed by Maxime Baillot and Thierry Chartier, et al. in Lannion (see ref. [113] and [114]). Beyond the initially launched signal and pumps S_0, P_1, and P_2, we introduce the waves labeled 3 and 4 mainly generated by FWM of the signal with pumps 1 and 2, respectively, and the waves labeled 5 and 6 mainly generated by FWM of the pumps. The complex field of waves is written as

$$E_j(z,t) = \frac{1}{2}\left\{A_j(z)\exp\left[i\left(\beta_j z - \omega_j t\right) + i\varphi_j\right] + c.c.\right\} \quad (j = 0\ldots6) \tag{3-34}$$

where A_j, ω_j, and φ_j hold for the field slowly varying complex amplitudes, frequencies, and initial phase, respectively, and β_j is the wave-vector. The relative phase of the three input waves is denoted as $\varphi_{\mathrm{rel}} = 2\varphi_0 - \varphi_1 - \varphi_2$. Given that the initial pump phases are assumed to be zero, φ_{rel} only depends on the initial signal phase. Particularly, the initial signal phase that will lead to the maximum output signal gain is defined as $\varphi_{0,max}$. Even though this phase value varies for different pump wavelength configurations, we can always find an optimized $\varphi_{0,max}$ by numerical calculation in the different configurations. $\Delta\lambda_{\mathrm{PPS}} = |\lambda_{\mathrm{P1}} - \lambda_{\mathrm{P2}}|$ is the pump-pump wavelength separation while the wavelength

offset relative to zero dispersion wavelength $\delta\lambda_{\mathrm{OFS}} = \lambda_0 - \lambda_{\mathrm{ZDW}}$ corresponds to the deviation of the signal wave λ_0 with respect to the zero dispersion wavelength λ_{ZDW} of the fiber. In the following, A_3, A_4 and A_5, A_6 are also called high-order signals and pumps, respectively.

The field evolution of the seven co-polarized waves co-propagating in the z direction along the entire nonlinear medium with length L, attenuation coefficient α, nonlinear coefficient γ, and dispersion slope D_λ is governed by a set of seven complex coupled equations. The effect of random walk-off and differential group delay is neglected[115]. For the sake of clarity, we reproduce here only one of these equations, e.g. for input signal field A_0:

$$\begin{aligned}\frac{dA_0}{dz} = -\frac{\alpha}{2}A_0 + i\gamma\Bigg\{&\left[\left|A_0\right|^2 + 2\sum_{i=0,i\neq 0}^{6}\left|A_i\right|^2\right]A_0 + A_1^2A_3^*e^{-i\Delta\beta_{0311}z} + A_2^2A_4^*e^{-i\Delta\beta_{0422}z}\\ &+2A_1A_2A_0^*e^{-i\Delta\beta_{0012}z} + 2A_1A_6A_4^*e^{-i\Delta\beta_{0416}z} + 2A_1A_3A_5^*e^{-i\Delta\beta_{0513}z} + 2A_1A_4A_2^*e^{-i\Delta\beta_{0214}z}\\ &+2A_2A_5A_3^*e^{-i\Delta\beta_{0325}z} + 2A_2A_3A_1^*e^{i\Delta\beta_{2301}z} + 2A_2A_4A_6^*e^{i\Delta\beta_{2406}z} + 2A_4A_5A_1^*e^{i\Delta\beta_{4501}z}\\ &+2A_5A_6A_0^*e^{i\Delta\beta_{5600}z} + 2A_3A_4A_0^*e^{i\Delta\beta_{3400}z} + 2A_3A_6A_2^*e^{i\Delta\beta_{3602}z}\Bigg\}\end{aligned} \tag{3-35}$$

where the superscript * holds for complex conjugate. The term containing α accounts for the fiber linear attenuation, the two square modulus terms inside the square bracket are responsible for nonlinear phase shifts contributions due to SPM and XPM, respectively, and the other terms correspond to the energy transfers between the interacting waves due to FWM processes. All the relevant waves are equally spaced in frequency on the opposite sides of the signal wave ω_0 in a symmetrical fashion due to the energy conservation $\omega_m + \omega_n = \omega_k + \omega_l$ and $2\omega_m = \omega_k + \omega_l$ ($\omega_m + \omega_n = 2\omega_k$) representing the non-degenerate FWM (NDFWM) and degenerate (DFWM) processes respectively. If we consider one of the NDFWM processes, for which A_k and A_l play the roles of the pumps and A_m and A_n those of the signal and idler, the corresponding linear phase mismatch can be written as

$$\Delta\beta_{\mathrm{mnkl}} = \beta_{\mathrm{m}} + \beta_{\mathrm{n}} - \beta_{\mathrm{k}} - \beta_{\mathrm{l}} \tag{3-36}$$

where β_j is calculated at its frequency ω_j. This is done by expanding β to 4th order in Taylor power series around the signal frequency ω_0. The high-order derivatives of the propagation constant are deduced from the fiber dispersion coefficients. Eq. (3-36) is also valid for DFWM cases with either $\beta_m = \beta_n$ or $\beta_k = \beta_l$.

This set of complex coupled equations is quite general in the sense that it includes

effects such as depletion, high-order dispersion, and nonlinear phase shifts. For the 7-wave model, altogether 13 NDFWM and 9 DFWM processes are taken into account. The extension to extra interacting waves could improve the accuracy to some extent, especially for small values of $\Delta\lambda_{PPS}$, though at the expense of a much more complicated set of coupled equations due to the contribution of many more involved FWM processes. This would make any physical interpretation of the results almost impossible. The 7-wave model, which exhibits the similar tendency as models involving more waves and offers sufficient estimation accuracy with sustainable complexity, is thus adopted. By solving the set of complex coupled differential equations simultaneously in a numerical manner, one can obtain the field evolution of each wave along the fiber.

3.6.4 Multi-wave model

It is no doubt that by involving more interacting waves, namely, more high-order waves in the model will definitely lead to a more precise and accurate prediction, especially in the small pump-pump separation regime. However, this will bring about large computation consumptions. In this case, it might be better to directly turn to the solution for NLSE.

3.7 Conclusion

In this chapter, the FOPA has been introduced based upon the fundamental linear and nonlinear phenomena when wave propagates in optical fibers. The general description of the FOPA using the coupled-wave equations has been derived from the nonlinear Schrödinger equation. On this basis, the phase-sensitive property is introduced.

With the different configuration of the PS-FOPA, the general characteristics have been briefly discussed, leading to the necessities and demand of the multi-wave model rather than the conventional 3-wave model. To this end, the 7-wave model is derived and introduced.

Chapter IV

Gain properties of degenerate dual-pump phase-sensitive amplifier

In this chapter, the operation of a degenerate dual-pump PSA is thoroughly numerically investigated using a multi-wave model, taking into account high-order waves associated with undesired FWM processes. More accurate phase-sensitive signal gain characteristics are obtained compared to the conventional 3-wave model, leading to precise optimization of the pump configuration in a degenerate dual-pump PSA. The signal gain for different pump configurations, as well as the phase sensitivity, are obtained and interpreted by investigating the dominant FWM processes in terms of the corresponding phase matching. Moreover, the relation between the dispersion slope and the width of the signal gain curve versus the pump-pump wavelength separation is revealed, permitting the application-oriented arbitrary tailoring of the signal gains by manipulating the dispersion profile and pump wavelength allocation.

Although PSAs can be implemented in either single-pump configuration or dual-pump configuration, the gain properties of dual-pump configuration are more attractive because of the gain growth and the flat gain spectrum across a wider spectral range.

4.1 Gain spectrum of PS-FOPA

FOPA based PSAs[115], exploiting nonlinear parametric processes in HNLF, significantly benefit from intrinsically broadband[32] and noiseless amplification[31] and compatibility with current fiber-based systems[117]. They thus exhibit attractive prospects in a variety of research fields spanning from optical communication[117], metrology[115], to all-optical

signal processing[118]. In particular, owing to the essence of ultra-low distortion throughout the entire gain regime, it is of special potential for the state-of-the-art microwave photonics (MWP) applications[119], where ultra-low noise amplification with high linearity[120] and large gain is urgently demanded[121]. Compared to single-pump PSA, the dual-pump configuration, capable of providing a broadband flat gain spectrum with less power for each pump, and avoiding the generation of the unwanted idler, is of critical interest from the application point of view.

In such dual-pump PSAs, in order to generate a large and flat parametric gain over a broad spectrum, one can use a large wavelength separation between the two pumps that prevent the generation of spurious high-order waves due to multiple FWM in HNLF. However, phase locking two highly separated pump lasers requires advanced optical injection-locking and optical phase-locking techniques and is still difficult in practice. Moreover, though the use of strong dispersion-slope fiber can suppress the high-order waves, it is unfortunately not favorable for broad bandwidth gain. Additionally, it can be convenient and practical to fit all the waves within the gain bandwidth of a usual EDFA. Finally, Raman-induced power transfer, which is detrimental to the FWM efficiency[40], is easier to avoid with relatively small pump separations. For all these reasons, it is highly desirable to design a dual-pump PSA with a small pump separation while minimizing the generation of parasitic tones by FWM of the two pumps. Indeed, the existence of these undesired FWM processes associated with high-order waves can influence the phase-sensitive signal gain. To date, the PSA has been both theoretically and experimentally analyzed in depth based on a model describing a single FWM process consisting of 3-wave degenerate FWM (DFWM)[105], [106], [122] or 4-wave non-degenerate FWM (NDFWM)[123], [124]. The nondegenerate dual-pump PSA, introducing two additional idlers has been investigated based on the so-called 6-wave model[125], [126], [113]. More recently, high-order FWM has been addressed using a 7-wave model for the first time, accounting for sideband-assisted phase-sensitive gain extinction ratio enhancement in phase regeneration[127] and subsequently adopted for evaluation of intensity modulation transfer[128]. However, within the scope of a practical PSA, the thorough investigation and characterization of high-order FWM have been largely overlooked.

This chapter focus on the theoretical investigation of a degenerate dual-pump PSA by conducting a multi-wave, more precisely, 7-wave model similar to the one introduced in [127]. Following such a 7-wave model rather than the conventional 3-wave model, the

impact of the accompanying high-order FWM processes, as well as the relation between signal gain and dispersion, is investigated in terms of signal gain and power evolution when input phases are optimized for the maximum gain by extensive numerical simulations. Beyond this, we provide physical interpretations of the signal gain and phase sensitivity, based on the phase mismatch condition with regard to the relevant FWM processes and waves. Thanks to this physical interpretation, we can predict which processes limit the efficiency of the PSA. In particular, the phase sensitive signal gains can be precisely tailored and manipulated, thus enabling application-oriented optimization of various PSAs. This is particularly interesting for MWP links, where small pump separations can be sufficient owing to the limited bandwidth of the amplified signals.

4.2 Gain properties

4.2.1 Comparison between 3- and 7-wave models

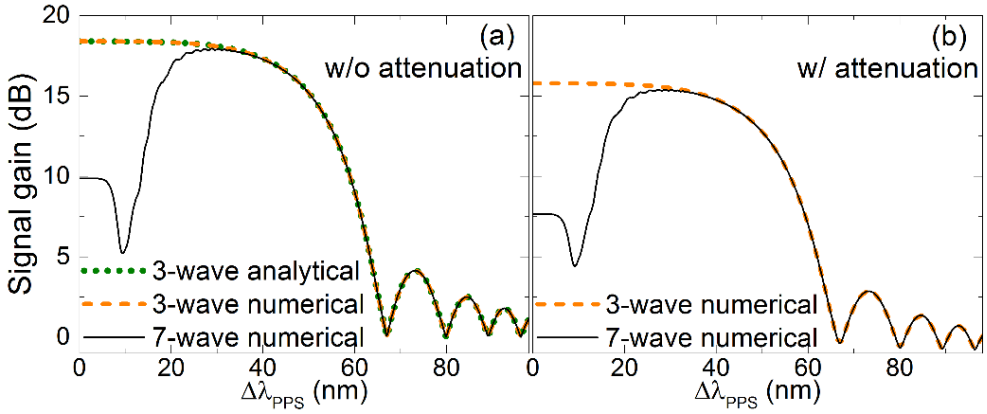

Fig. 4.1 Maximum signal gain when $\delta\lambda_{\mathrm{OFS}} = 0$ by both 3- and 7-wave models versus pump-pump wavelength separation $\Delta\lambda_{\mathrm{PPS}}$.

Maximum signal gain versus $\Delta\lambda_{\mathrm{PPS}}$ calculated with input signal phase $\varphi_{0,\max}$ maximizing the gain when $\delta\lambda_{\mathrm{OFS}} = 0$ using 3- and 7-wave models (a) Analytically and numerically without attenuation; (b) Numerically with attenuation, respectively. The fiber parameters are given in the text.

The signal gains are numerically obtained using the same OFS standard HNLF corresponding to experiment presented in Fig. 3.6., which we will keep throughout this

chapter. For $\delta\lambda_{\mathrm{OFS}} = 0$, Fig. 4.1 compares these results with those from the 3-wave model. The incident wave powers are 100 mW for each pump and 1 μW for the signal: we are thus in the small signal regime. All calculations in the following are performed by assuming zero pump phases and setting the initial signal phase at the value $\varphi_{0,\max}$ leading to maximum signal gain.

The dual-pump signal-idler degenerate FWM can be described by simplifying Eq. (3-24) to the 3-wave case when A_3 and A_4 are degenerate. The resulting conventional 3-wave analytical model [see the dotted line in Fig. 4.1 (a)] is valid only if the pumps remain undepleted and without fiber loss. This way, the power and phase evolutions as well as the PIA or PSA gain can be steadily obtained from Eq. (3-25), Eq. (3-26), Eq. (3-30) and Eq. (3-33), respectively. Taking the parameters of the previously adopted standard HNLF and neglecting the fiber attenuation, the gain can be calculated either analytically using above equations or numerically based on Eq. (3-24) using the conventional 3-wave model. Both calculations give the same prediction as indicated in the dotted and dashed lines in Fig. 4.1 (a). Meanwhile, the 7-wave model, in which pump depletion is involved by solving the 7-wave coupled-wave equations numerically as the solid line shown in Fig. 4.1 (a), indicates serious gain distortions in the small $\Delta\lambda_{\mathrm{PPS}}$ region. In particular, as the input signal power is quite small compared to the pump power, corresponding to the small signal regime, depletion is mainly caused by the high-order waves and not by signal amplification. This is a strong indication in favor of the usefulness of the 7-wave model. Not surprisingly, if attenuation is taken into account in both 3- and 7-wave numerical solutions, the maximum gain values become smaller compared to the previous cases as shown in Fig. 4.1 (b). From Fig. 4.1, it is clear that the 7-wave model exhibits improved accuracy for estimating and investigating the practical signal gain, especially in the small $\Delta\lambda_{\mathrm{PPS}}$ region where the 3-wave model is clearly invalid.

4.2.2 Gain spectrum of 3- and 7-wave models

By varying $\delta\lambda_{\mathrm{OFS}}$ and $\Delta\lambda_{\mathrm{PPS}}$ simultaneously while keeping $\varphi_{0,\max}$ and zero for the initial signal and pump phases, respectively, with fixed input powers, we generate the heatmaps for the maximum signal gain vs. $\delta\lambda_{\mathrm{OFS}}$ and $\Delta\lambda_{\mathrm{PPS}}$ using the 3- and 7-wave models, respectively, as presented in Fig. 4.2 (a) and Fig. 4.2 (b).

When the signal wave is in the vicinity of λ_{ZDW}, though significant gain deterioration is observed when the pumps are closely located, the gain profile tends to that of the 3-wave model when $\Delta\lambda_{PPS}$ is larger than 30.0 nm. However, compared to the 3-wave model, the peak gain in the 7-wave model is achieved when the signal wavelength is larger than λ_{ZDW} by about 6 nm. The predicted maximum gain is then even higher (17.5 dB) than the one (16.5 dB) predicted by 3-wave model. When the signal is located in the anomalous dispersion regime ($\delta\lambda_{OFS} > 0$), the decrease of the gain with $\Delta\lambda_{PPS}$ follows a similar tendency in the two models. Conversely, when the signal lies in the normal dispersion regime ($\delta\lambda_{OFS} < 0$), 7-wave model predicts serious gain distortions at small $\Delta\lambda_{PPS}$, including peaks and dips, which are absent from the 3-wave model predictions. Likewise, in the range of 20 nm $\leq \Delta\lambda_{PPS} \leq$ 100 nm, the two models exhibit similar behaviors.

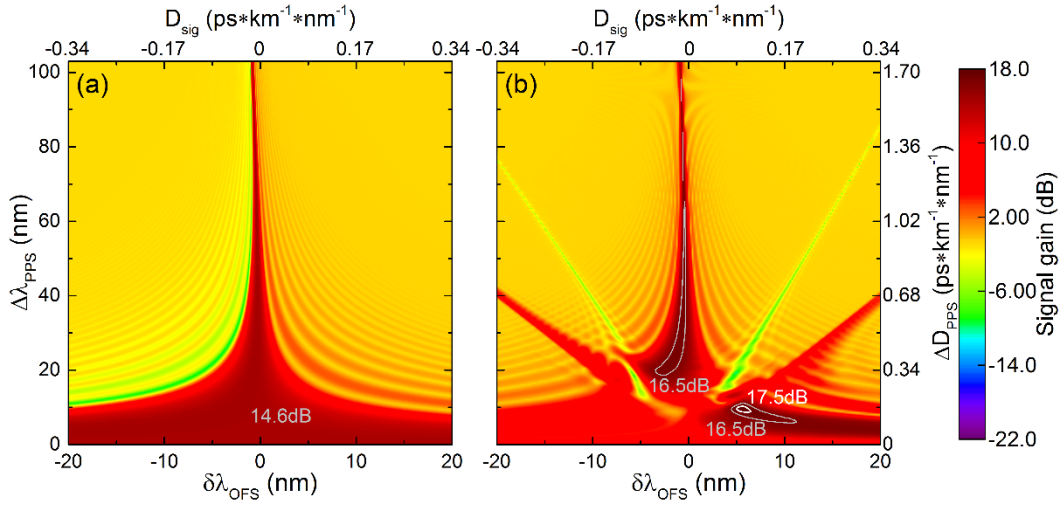

Fig. 4.2 Maximum signal gain vs. $\delta\lambda_{OFS}$ and $\Delta\lambda_{PPS}$.

Maximum signal gain vs. signal wavelength offset $\delta\lambda_{OFS}$ with respect to the zero dispersion wavelength λ_{ZDW} and vs. pump-pump separation $\Delta\lambda_{PPS}$ with input signal phase $\varphi_{0,max}$ to maximize the gain for (a) 3- and (b) 7-wave models. The right axis corresponds to the dispersion difference ΔD_{PPS} between the two pumps while the upper axis corresponds to the dispersion D_{sig} for the signal[129].

One striking feature of the 7-wave model with respect to the 3-wave one is that the gain peak vanishes and the gain decrease rapidly when the signal is moving further towards the normal dispersion regime, leaving only smaller gain peaks and dips around small $\Delta\lambda_{PPS}$ region, especially between – 10 nm and 0 deviation from λ_{ZDW}. The extra

gain peaks and dips that spread diagonally forming a star-shape pattern can be attributed to some phase matching situations at certain pump wavelength configurations, and will be investigated in the coming section.

4.3 Physical interpretation of gain properties

According to the phase matching essence of nonlinear FWM process [9, 21], the efficiency is governed by the effective phase mismatch κ_{mnkl} of the considered FWM process occurring between waves m, n, k, and l

$$\Delta\kappa_{\mathrm{mnkl}} = \Delta\beta_{\mathrm{mnkl}} + \gamma P_{\mathrm{mnkl}}, \tag{4-1}$$

where β_{mnkl} is the linear phase mismatch term as indicated in Eq. (3-36). γP_{mnkl} is the nonlinear phase mismatch term which depends on the powers of the involved waves through the relation:

$$\gamma P_{\mathrm{mnkl}} = \gamma\left(P_k + P_l - P_m - P_n\right), \tag{4-2}$$

where P_j is the power of wave j. Compared to the fundamental 3-wave model where only $\kappa_{0012} = \Delta\beta_{0012} + \gamma P_{0012} = (2\beta_0 - \beta_1 - \beta_2) + \gamma(P_1 + P_2 - 2P_0)$, associated with DFWM of the initial three waves, is relevant, the 7-wave model involves all the 22 FWM processes occurring simultaneously along the fiber, leading to much more complicated situations.

For the sake of clarity, the physical interpretation of the 7-wave model will be given by observing when these processes are phase matched, and thus expected to play a significant role. We do this by plotting the relevant κ_{mnkl} associated with the FWM process we want to consider and that we suspect to lead to a significant energy transfer between A_k, A_l and A_m, A_n. The nonlinear part of these κ_{mnkl} is calculated with the values of the powers P_{mnkl} obtained at the end of the fiber. In these plots, we multiply κ_{mnkl} by the fiber length: this leads to a phase mismatch expressed in units of an angle, and we expect the considered FWM process to be efficient only when the absolute value of this angle is small compared to π.

4.3.1 Zero dispersion region

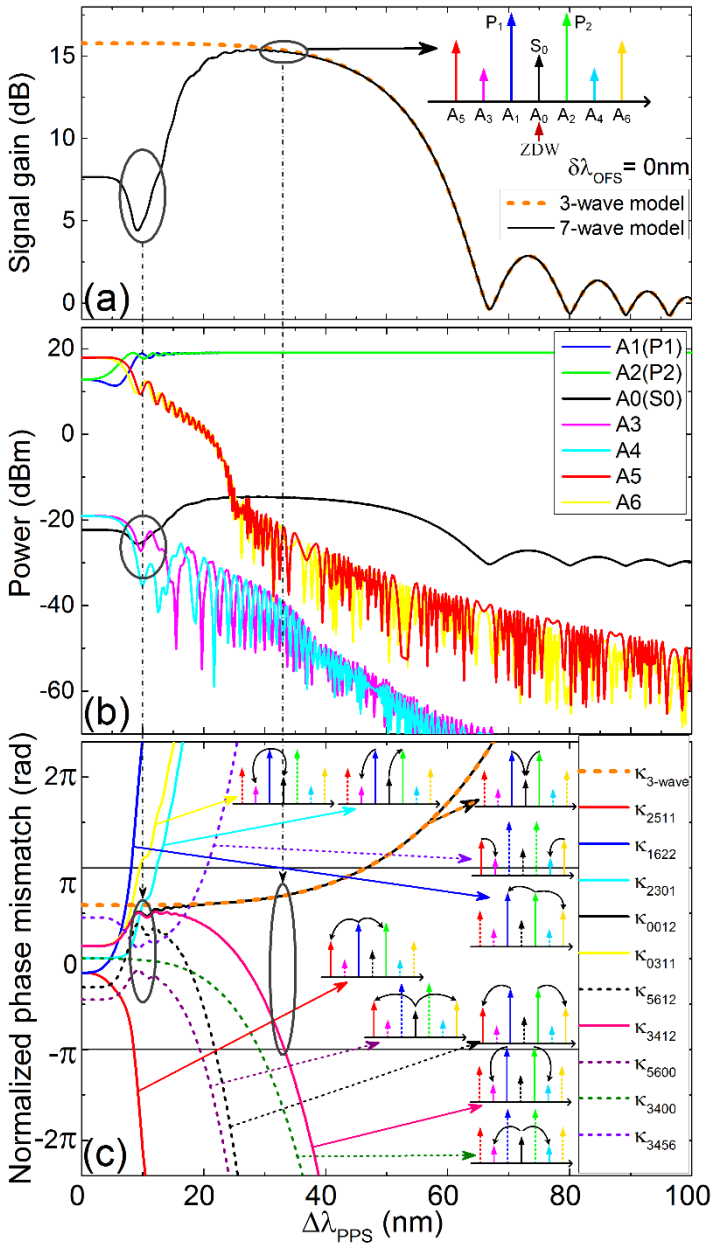

Fig. 4.3 Evolution of powers, gain, and phase mismatch when $\delta\lambda_{\mathrm{OFS}} = 0$ nm. Case where $\delta\lambda_{\mathrm{OFS}} = 0$ nm. The input signal phase is $\varphi_{0,\max}$ to maximize the gain for each configuration. (a) Maximum signal gain for 3- and 7-wave models versus pump-pump wavelength separation $\Delta\lambda_{\mathrm{PPS}}$; the inset shows the wavelengths configuration relatively to the λ_{ZDW}. (b) Corresponding evolution of the output powers of the seven waves. (c) Normalized phase mismatch angles of the relevant FWM processes. The input phases of the signal and pumps are chosen to correspond to the maximum gain of

the PSA in the ordinary 3-wave regime. The regions featured by ellipses are discussed in the text, and the corresponding dominant processes are given in the insets.

Let us start by considering the situation where $\delta\lambda_{\mathrm{OFS}} = 0$, for which λ_{ZDW} is at the center of all the waves, as illustrated in the inset of Fig. 4.3 (a). Then, the different FWM processes involving waves located in a symmetrical manner with respect to λ_{ZDW} can achieve perfect phase matching at some values of $\Delta\lambda_{\mathrm{PPS}}$. Fig. 4.3 (a) represents the maximum signal gain versus $\Delta\lambda_{PPS}$. The signal is launched with the phase $\varphi_{0,\mathrm{max}}$ that maximizes its gain and the pump phases are taken equal to zero [the same conditions as in Fig. 4.1 (b)], while Fig. 4.3 (b) reproduces the corresponding output powers of the 7 waves versus $\Delta\lambda_{\mathrm{PPS}}$. Fig. 4.3 (b) shows that the high-order signals and pumps (waves labeled 3, 4, 5, and 6), although they emerge only from the combination of high-order FWM processes, can exhibit significant output powers, even stronger than the incident signal and pumps, respectively. This happens for the small values of $\Delta\lambda_{\mathrm{PPS}}$, i.e., for $\Delta\lambda_{\mathrm{PPS}} < 20$ nm. This is explained by the values of the phase mismatch coefficients of the FWM processes that generate these high-order waves, as shown in Fig. 4.3 (c). Indeed, in this region, the phase mismatch coefficients κ_{0012}, κ_{5612}, κ_{3412}, κ_{3400}, κ_{5600}, κ_{3456}, remain within the $\pm\pi$ range for which the corresponding processes are efficient. As suggested by these κ's, besides the fundamental 3-wave phase mismatch κ_{0012}, which governs the energy transfer between pumps and signal, the energy is directed towards the high-order signals and pumps power from the input pumps and even from the input signal. This leads to the observed drastic pump depletion and the severe signal gain distortion. This is particularly striking at $\Delta\lambda_{\mathrm{PPS}} = 10nm$, where both κ_{3400} and κ_{5600} are close to 0, leading to almost perfect phase matching for the corresponding processes. However, according to the strength of the nonlinear coupling, the process corresponding to κ_{3400} is about 10 orders of magnitude weaker than the other pump-mediated processes. Thereby the dominant process associated with κ_{5600} is responsible for the remarkable signal gain dip at such value of $\Delta\lambda_{\mathrm{PPS}}$.

It is worth mentioning that, for κ_{2511} and κ_{1622}, even though the phase mismatch goes outside the $\pm\pi$ range even for small $\Delta\lambda_{\mathrm{PPS}}$, the intense interactions between the involved powerful waves contribute to the obvious pump depletion in small $\Delta\lambda_{\mathrm{PPS}}$ region as observed in Fig. 4.3 (b) and Fig. 4.3 (c). Beyond 20 nm separation, all the spurious processes have κ values outside the $\pm\pi$ range and vanish, leaving only the fundamental

process, namely κ_{0012}, within the $\pm\pi$ range: the gain predicted by the 3-wave model is then retrieved. It is worth noticing that, κ_{3400} and κ_{5600} become phase mismatched twice and three times quicker than κ_{0012}, respectively, due to the fact that these processes involve high-order signals and pumps with twice or three times larger frequency separations than the incident waves. This makes their linear phase mismatches much more sensitive to the increase of $\Delta\lambda_{\mathrm{PPS}}$. Similar behavior can also be found for κ_{3456} and κ_{5612}. Consequently, the signal gain completely retrieves the values predicted by the 3-wave model for $\Delta\lambda_{\mathrm{PPS}} \geq 30$ nm, where only κ_{0012} dominates over all the other processes, which are now completely phase mismatched.

4.3.2 Normal dispersion region

Let us now turn to the case where $\delta\lambda_{\mathrm{OFS}} = -10$ nm. Here also we maximize the signal gain by adjusting $\varphi_{0,\mathrm{max}}$ for the input signal and keeping zero input pump phases. The resulting maximum gain is shown in Fig. 4.4 (a-c). Despite some gain peaks, the gain predicted by the 7-wave model is completely different from the one derived from 3-wave model. For small values of $\Delta\lambda_{\mathrm{PPS}}$, owing to the intricate interplay of many processes whose values of κ are within the $\pm\pi$ range, one can hardly distinguish the dominant ones. The main FWM process associated with the phase mismatch κ_{0012} fades rapidly when $\Delta\lambda_{\mathrm{PPS}}$ increases because its phase mismatch exits the $\pm\pi$ range as soon as $\Delta\lambda_{\mathrm{PPS}} \geq 12$ nm. The signal gain becomes then extremely small. When $\Delta\lambda_{\mathrm{PPS}}$ reaches about 15 nm, the process governed by κ_{0624} becomes dominant, as indicated in Fig. 4.4 (c). This can be easily understood as A_0 and A_2 on the one hand and A_4 and A_6 on the other hand are then almost symmetrical with respect to λ_{ZDW}, as shown in the inset of Fig. 4.4 (a), thus approaching perfect phase matching. Through this process, A_0 and A_6 gain energy from A_2 and A_4, leading to the fact that A_6 becomes stronger than A_5 in the neighboring $\Delta\lambda_{\mathrm{PPS}}$ region. In the same region, the gain and power of A_0 start to increase a bit. Interestingly, A_4 exhibits some power losses for certain values of $\Delta\lambda_{\mathrm{PPS}}$, and for some others maintains a non-negligible level thanks to the FWM associated with κ_{4426}. When we further increase $\Delta\lambda_{\mathrm{PPS}}$, κ_{1604}, κ_{0422}, and κ_{1622} play an important role around $\Delta\lambda_{\mathrm{PPS}} = 20$ nm, leading to a significant power transfer from A_0, A_2, and A_4 to the other involved waves. This happens because A_2 is nearly located at λ_{ZDW} and all the FWM processes that are symmetric with respect to it are experiencing perfect phase matching. Thus it turns out

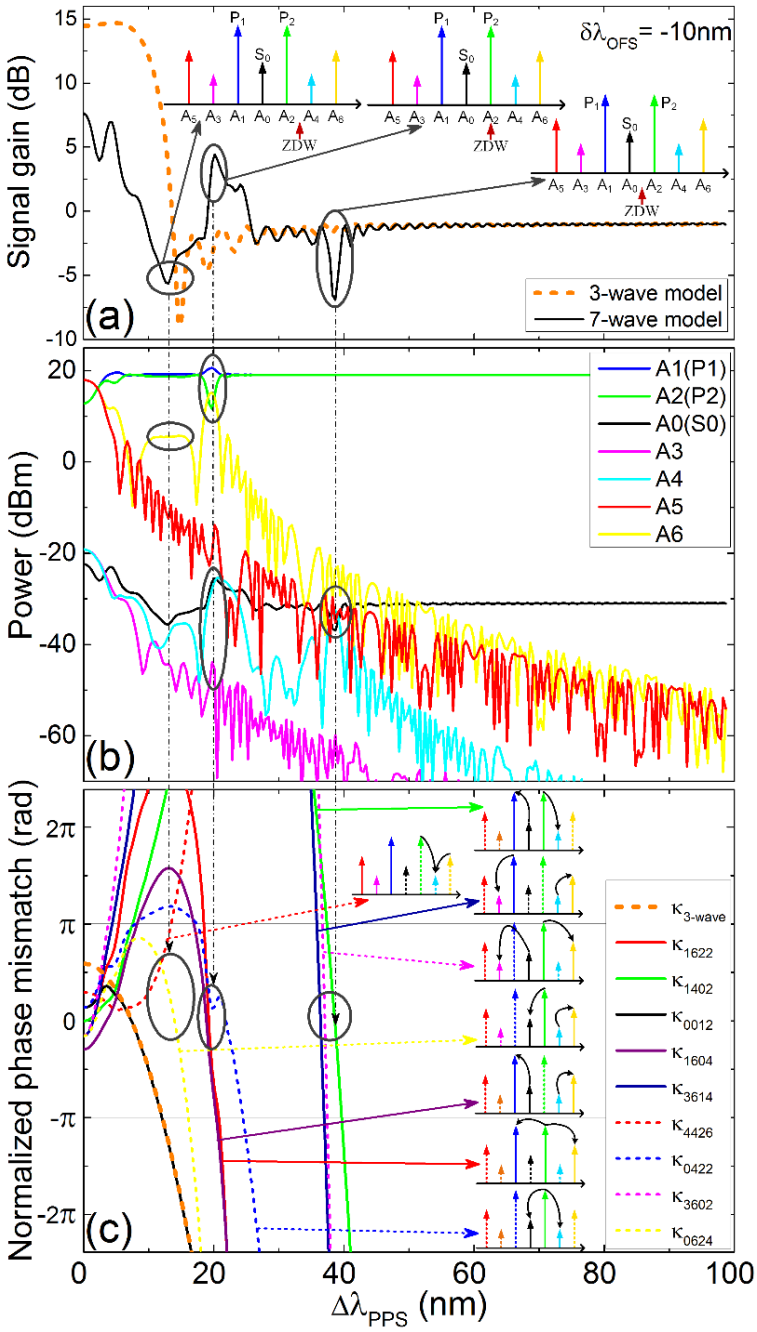

Fig. 4.4 Evolution of powers, gain, and phase mismatch when $\delta\lambda_{\mathrm{OFS}} = -10$ nm. (a-c) Same as Fig. 4 for $\delta\lambda_{\mathrm{OFS}} = -10$ nm (signal in normal dispersion region). All the cases are calculated with $\varphi_{0,\max}$ adjusted to maximize the signal gain and with zero input pump phases.

that the powers of A_6, A_4, and A_1 are more significant than those of A_5, A_3, and A_2, respectively, in the vicinity of such values of $\Delta\lambda_{\mathrm{PPS}}$. Specifically, even the pump A_1 gets

amplified owing to these processes. Beyond 30 nm separation, the signal gain almost vanishes and no significant depletion is observed, leaving only some tiny ripples in large $\Delta\lambda_{\mathrm{PPS}}$ regions. However, around $\Delta\lambda_{\mathrm{PPS}} = 40\,\mathrm{nm}$, one can observe a significant and narrow gain dip attributed to the phase matching of κ_{1402}, κ_{3614}, and κ_{3602}, as indicated in Fig. 4.4 (c). One must also notice the fact that the wavelength conversion process associated with κ_{1402} involves the two strong pumps while the other two processes involve only one initially launched pump combined with one high-order pump. As a consequence, κ_{1402} dominates over the other two processes: its nonlinear coupling is about 4 orders of magnitude stronger than the other two. Such a process pumps power out of A_0. In summary, throughout this normal dispersion region, one can hardly achieve an optimum pump configuration for signal amplification. This may make this regime unsuitable for practical applications.

4.3.3 Anomalous dispersion region

We finally turn to the opposite detuning $\delta\lambda_{\mathrm{OFS}} = +10$ nm with the same input conditions as in Fig. 4.3 and Fig. 4.4. Here also we focus on the maximum signal gain.

The signal is now located in the anomalous dispersion regime and a dramatic gain hump is observed for $\Delta\lambda_{\mathrm{PPS}} \approx 5$ nm as shown in [see Fig. 4.5 (a)], with much higher gain than predicted by the 3-wave model. This is mainly attributed to the fact that A_0 undergoes amplification not only thanks to the fundamental FWM process governed by κ_{0012}, which indeed remains between $-\pi$ and $+\pi$, but also thanks to two other phase matched FWM processes corresponding to κ_{0513} and κ_{0311} [see Fig. 4.5 (c)]. However, the process associated with κ_{0513} involves only one initially launched pump and is thus more than one order of magnitude weaker compared to the processes corresponding to κ_{0311} and κ_{0012} that involve the two strong pumps. It is thus negligible. Such a sideband-assisted gain enhancement has remained largely unexplored previously and will be further investigated below. As $\Delta\lambda_{\mathrm{PPS}}$ increases to larger separation regions, this gain peak decreases rapidly. A second but smaller gain peak is found at $\Delta\lambda_{\mathrm{PPS}} = 15$ nm. Although the process governed by κ_{0513} is no longer phase matched, this peak is explained by the process associated with κ_{0311}, which remains pretty well phase matched. In the vicinity of $\Delta\lambda_{\mathrm{PPS}} = 15\,\mathrm{nm}$, A_5, A_3, A_1, and A_0 are almost symmetric with respect of λ_{ZDW}, explaining the nearly perfect phase matching of κ_{0513}, κ_{3315} and κ_{0311}. Therefore, it turns

out that the power of A_5 and A_3 is larger than that of A_6 and A_4, respectively, owing to

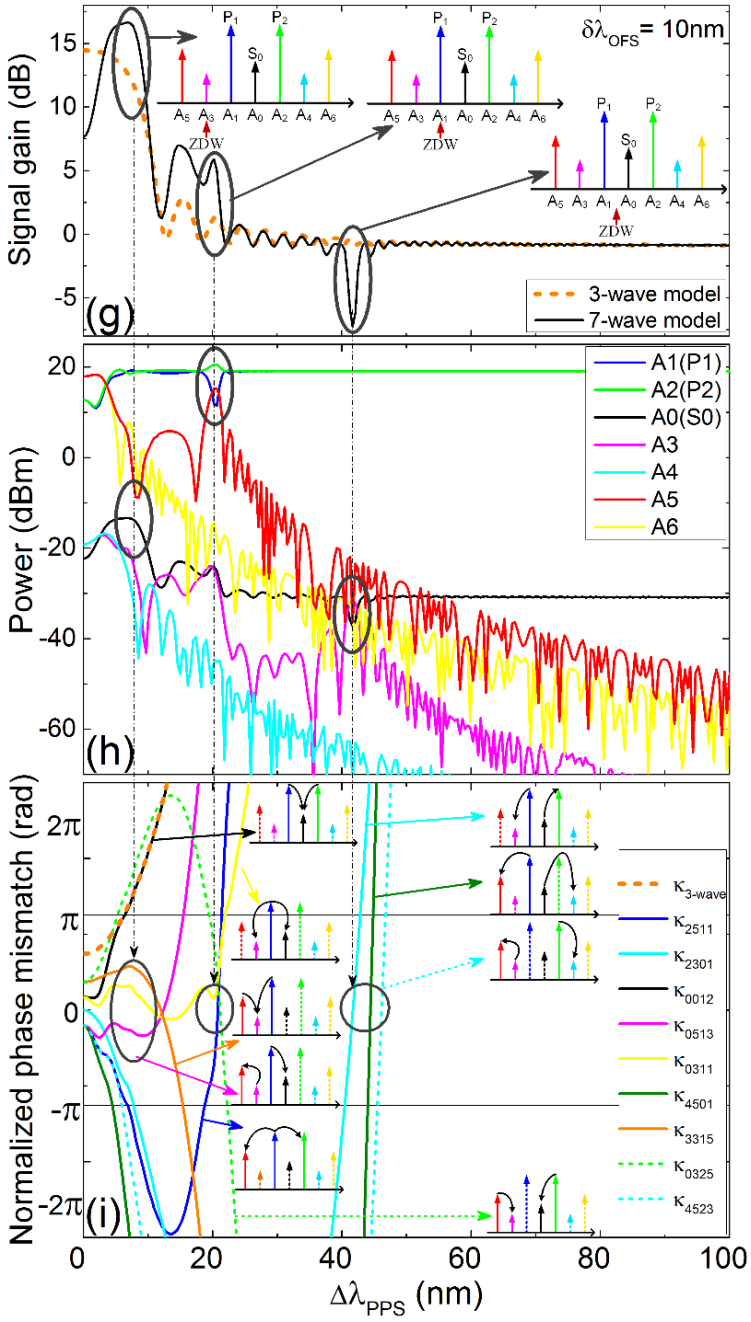

Fig. 4.5 Evolution of powers, gain, and phase mismatch when $\delta\lambda_{\mathrm{OFS}} = +10$ nm. (a-c) Same as Fig. 4.4 for $\delta\lambda_{\mathrm{OFS}} = +10$ nm (signal in anomalous dispersion region). All the cases are calculated with $\varphi_{0,\max}$ adjusted to maximize the signal gain and with zero input pump phases.

the energy transfers induced by the corresponding FWM processes. At larger separations,

about $\Delta\lambda_{\mathrm{PPS}} = 20$ nm, a situation similar to the one we met for $\delta\lambda_{\mathrm{OFS}} = -10$ nm occurs. Indeed, since A_0 is located nearby λ_{ZDW}, the waves positioned at symmetric positions with respect to A_0 can experience phase matched FWM. The FWM processes governed by κ_{0325} and κ_{2511}, become predominant in addition to the main one governed by κ_{0012}. This gives rise to the third gain peak in Fig. 4.5 (a). Since κ_{0012} is already far away from the $\pm\pi$ range, the two secondary gain peaks are smaller than the main one occurring at $\Delta\lambda_{\mathrm{PPS}} = 5$ nm. In the adjacent region for which $12\ \mathrm{nm} \leq \Delta\lambda_{\mathrm{PPS}} \leq 20\ \mathrm{nm}$, the power evolutions of A_5, A_3, and A_2, and of A_6, A_4, A_1, exhibit opposite evolutions with respect to the preceding case for which $\delta\lambda_{\mathrm{OFS}} = -10$ nm [compare Fig. 4.4 (b) and Fig. 4.5 (b)]. This is consistent with the fact that the phase mismatches for these processes have opposite values in the two cases $\delta\lambda_{\mathrm{OFS}} = +10$ nm and $\delta\lambda_{\mathrm{OFS}} = -10$ nm. Moreover, similarly to the normal dispersion regime case, a narrow gain dip is observed around $\Delta\lambda_{\mathrm{PPS}} = 40$ nm, owing to the fast evolution of κ_{2301}, κ_{4523}, and κ_{4501} around zero. Besides, the processes governed by κ_{4523} and κ_{4501} are about 4 orders of magnitude weaker than the process associated with κ_{2301} as they involve only one powerful pump. Therefore, the dominant process is the one governed by κ_{2301}, leading to the power increase of A_3 and the gain dip around as well.

Finally, compared to the case where the signal is located in the normal dispersion regime, in certain regions within the anomalous dispersion regime, the γP_{mnkl} term can cancel the $\Delta\beta_{\mathrm{mnkl}}$ in κ_{mnkl}, leading to better phase matching for the signal wave and subsequently to significant signal gain peaks for specific values of the pump-pump wavelength separation.

4.4 Impact of dispersion

In all three cases considered above, the signal gain becomes negligibly small beyond 40 nm pump-pump separation, a region in which the PSA becomes unusable for applications due to the large phase mismatch of the principal FWM process. The power evolution and signal gain, which we have just seen to be governed by the phase matching conditions, can be directly extended to other pump allocations. Remarkably, although the κ's are simply evaluated at the fiber output, rather than integrated along the fiber, the simple criterion consisting in looking whether the phase mismatch angle is within the $\pm\pi$ range

or not has been shown to be relevant to evaluate whether a given FWM process is dominant or negligible. This shows that, contrary to what could have been expected, one can build some intuition of what happens in such complicated multi-wave nonlinear problems. It is worth noting that the directions of the energy flows indicated in the insets of Fig. 4.4 and Fig. 4.5 are directly deduced from the power evolutions of the corresponding waves. They could be also obtained by looking at the relative phase of each process along the fiber. However, this is quite complicated and beyond the scope of the present research.

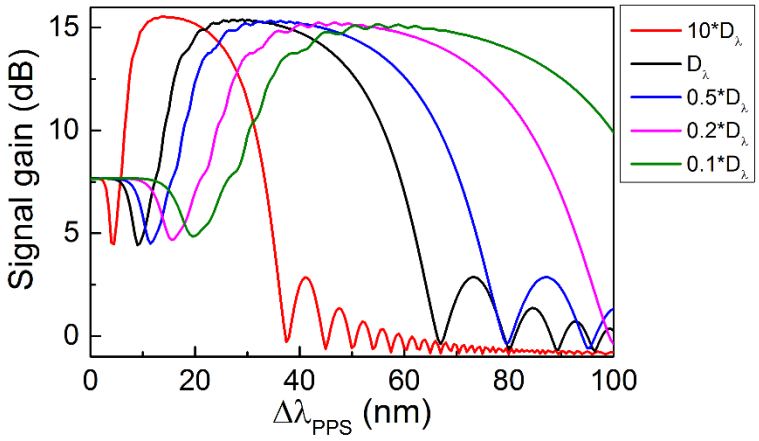

Fig. 4.6 Maximum signal gain vs. $\Delta\lambda_{\mathrm{PPS}}$ at different dispersion parameters.

Maximum signal gain vs. $\Delta\lambda_{\mathrm{PPS}}$ at different dispersion parameters. The input pump phases are equal to zero and the initial signal phase is taken at $\varphi_{0,\max}$ to optimize the gain. The plots are calculated for different factors multiplying the dispersion slope D_λ when $\delta\lambda_{\mathrm{OFS}} = 0$. The initial wave powers remain the same for all the values D_λ.

As mentioned above, the phase matching conditions, which determine the signal gain, depending on the wave powers, pump positions and thus dispersion properties of the fiber according to Eq. (4-1). To investigate the dispersion dependence of the gain characteristics, we change the dispersion slope D_λ of the HNLF with fixed initial wave powers. The width of the resultant maximum gain curves scales inversely proportional to D_λ, as illustrated in Fig. 4.6. Thus $\Delta\lambda_{\mathrm{PPS}}$ and $\delta\lambda_{\mathrm{OFS}}$ can be directly transposed in terms of dispersion profile, as illustrated by the top and right axes of Fig. 4.2 (a) and Fig. 4.2 (b). For these axes, D_{sig} is the dispersion at the signal wavelength and ΔD_{PPS} is the dispersion difference between two pumps. The gain versus $\Delta\lambda_{\mathrm{PPS}}$ can be subsequently normalized by the dispersion profile of the HNLF. When combined with the 7-wave model, the

precise tailoring of the signal gain by manipulating the dispersion profile permits a full optimization of the dual-pump PSA gain from the application point of view, such as the low distortion and low noise amplification on a single carrier in MWP links.

4.5 Phase-sensitivity

For the sake of thoroughly characterizing and investigating the phase sensitivity of the signal gain peak obtained in anomalous dispersion regime, we plot the gain versus input signal phase of the waves at various values of $\Delta\lambda_{\mathrm{PPS}}$ with $\delta\lambda_{\mathrm{OFS}} = +10$ nm, as represented below in Fig. 4.7.

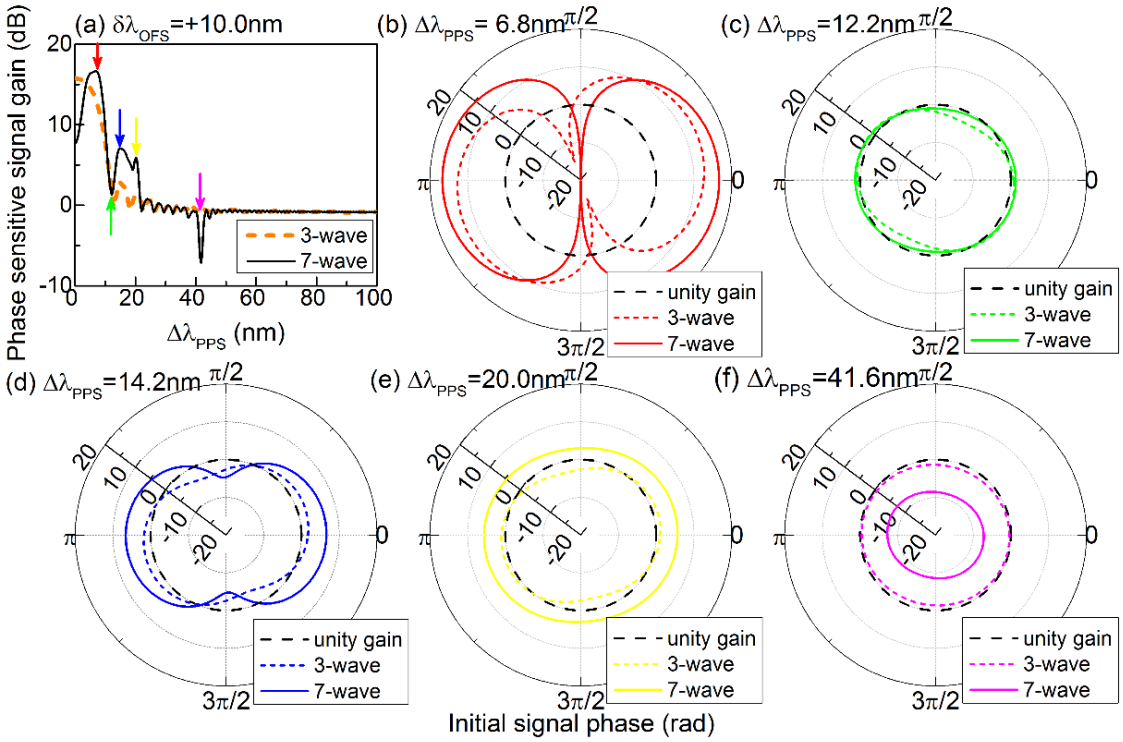

Fig. 4.7 Phase-sensitivity for different $\Delta\lambda_{\mathrm{PPS}}$ at $\delta\lambda_{\mathrm{OFS}} = +10$ nm.
(a) Same maximum signal gain versus pump-pump separation as in Fig. 4.5 (a), obtained for $\delta\lambda_{\mathrm{OFS}} = +10$ nm. The vertical arrows point at the values of $\Delta\lambda_{\mathrm{PPS}}$ corresponding to (b-f). (b-f) Gain (in dB) polar plot versus input signal phase with zero initial pump phases for the 3-wave (dashed line) and 7-wave (full line models) for (b) $\Delta\lambda_{\mathrm{PPS}} =$ 6.8 nm (first gain peak in (a)), (c) $\Delta\lambda_{\mathrm{PPS}} = 12.2$ nm (first gain dip in (a)), (d) $\Delta\lambda_{\mathrm{PPS}} =$ 14.2 nm (second gain peak in (a)), and (e) $\Delta\lambda_{\mathrm{PPS}} = 20$ nm (third gain peak in (a)), (f) $\Delta\lambda_{\mathrm{PPS}} = 41.6$ nm (second gain dip in (a)).

This figure shows how the gain depends on the input signal phase with zero initial pump phases for different values of the pump-pump separation $\Delta\lambda_{\mathrm{PPS}}$, indicated by the arrows in the signal gain curve of Fig. 4.7 (a). A very interesting feature can be noticed in Fig. 4.7 (b), which corresponds to the situation where the 7-wave model predicts more gain than the 3-wave model. Quite remarkably, this large gain is facilitated by the combination of phase-sensitive and phase-insensitive gain due to the processes corresponding to κ_{0012} and κ_{0311}, respectively.

Moreover, it is shown to be phase sensitive with an extinction ratio larger than 36 dB, larger than the one predicted with the 3-wave model. In addition, the value of the minimum gain (about -19.8 dB) is more than 3 dB smaller than the opposite of the maximum gain (about 16.7 dB) resulting from the dominant phase-insensitive process associated with κ_{0311} as discussed in the previous sections. It is worth noticing also that the maximum and minimum gains are slightly phase shifted compared to the 3-wave model. A similar behavior is observed at the second gain peak position, as shown in Fig. 4.7 (d). Conversely, the third gain peak is subject to less phase-sensitivity as a result of the corresponding large value of κ_{0012}, which shows that the fundamental gain process is no longer active. Additionally, since the dominant processes around the third gain peak are governed by κ_{0325} and κ_{0311}, and thus involve not only the initial three waves but also waves emerging from high-order FWM processes, we notice a strong degradation in the degree of phase-sensitivity of this gain and of its extinction ratio.

As shown in Fig. 4.7 (c), the phase sensitive gain around the first gain dip retrieves a similar tendency as in the 3-wave model, which agrees well with the gain curve in Fig. 4.7 (a) in the vicinity of this dip. As the gain varies around 0 dB, it exhibits weak phase-sensitivity. Similarly, though the phase-sensitivity is also observed at the narrow second gain dip with de-amplification as indicated in Fig. 4.7 (f), as discussed at the end of section 4.3, the dominant FWM process associated with κ_{2301} in this region is phase-insensitive wavelength conversion which decreases the signal power and amplifies the involved high-order waves A_3, besides the fundamental ones, thus impairing the phase-sensitivity at this dip.

4.6 Conclusion

In conclusion, high-order waves originating from the high-order FWM processes have

been shown to be properly described in the framework of a 7-wave model. Numerical integration of this model has led to the accurate signal gain calculation for the degenerate dual-pump PSA. It turns out that a PSA with an appropriate choice of wavelengths can achieve even higher signal gain than the one expected from the conventional 3-wave model, thanks to the extra gain provided by high-order FWM processes associated with high-order waves. The gains from the 7-wave model also revealed the regions where efficient gain can be obtained in different wave configurations, as well as some non-efficient configurations that should be avoided from the application point of view.

The physical interpretation of the complicated signal gain spectra and gain curve have been elaborated by further investigation of the dominant FWM processes in terms of the corresponding phase matching conditions. In addition, the phase sensitivity of the signal gain has been analyzed. The gain has been shown to be more or less phase sensitive in several PSA configurations, depending on whether the dominant FWM processes involve not only the fundamental 3-wave DFWM but also other higher-order FWM processes or not. Moreover, the width of the gain curve is shown to be scalable along with the dispersion of the fiber, permitting an arbitrary tailoring of these gains by manipulating the fiber dispersion profile. With the proposed 7-wave model, application-oriented arbitrary gains can be achieved together with a PSA configuration, which is optimized from a practical point of view. Especially for MWP links applications, where a large peak gain with low distortion and low noise is preferred rather than a broadband flat gain spectrum, the multi-wave model can easily select the most efficient configuration in view of maximizing the gain peak.

Chapter V

Regenerative functionality of phase-sensitive amplifier

In the last chapter, through the investigation of the phase-sensitivity and the phase-sensitive gain properties with respect to $\Delta\lambda_{\mathrm{PPS}}$ and $\delta\lambda_{\mathrm{OFS}}$, explicit physical pictures have been established on the basis of phase matching conditions of the FWM processes involved in the dual-pump PS-FOPA. With the help of the proposed 7-wave model, a more accurate numerical description of the PS-FOPA is enabled. This does not only allow simply accessing the gain properties within a broad spectral range, but also permits to obtain an insightful observation of the power and phase evolutions of the interacting waves. With such abundant information, we were allowed to attain a comprehensive and meaningful analysis for the design and the practical implementations of PS-FOPAs.

As introduced in the first chapter, in the context of fiber-optic communication systems and networks, PSAs can be utilized to mitigate the nonlinear impairments, especially for the now extensively deployed advanced high-order modulation formats. Thanks to the unique phase-sensitive property and the potential noiseless amplificative capability, PSAs are able to provide simultaneous phase and amplitude regeneration with ultra-low extra noises. To this end, various schemes have been proposed and demonstrated for the regeneration[130] and the quantization[131] of the signals with high-order phase and amplitude modulations such as binary phase-shift keying (BPSK), quadrature phase-shift keying (QPSK), differential QPSK (DQPSK), and quadrature amplitude modulation (QAM). Most of these approaches adopt sophisticated configurations in terms of such as cascaded FMW stages in order to achieve better regenerative performance or some particular functionalities. Nonetheless, the potential

regenerative capability of a fundamental PSA configuration has gone largely unexplored.

In this chapter, a thorough investigation aiming at the optimization of a fundamental PS-FOPA capable of simultaneous phase and amplitude regeneration is performed. The regeneration potential, quantified in terms of phase-sensitive extinction ratio, has been carefully assessed by a scalar model involving high-order waves associated with high-order four-wave mixing processes, going beyond the usual three-wave approach. Additionally, this model permits to unveil the physics involved in the high-order waves assisted regeneration. This permits a multi-dimensional and comprehensive optimization that allows to fully exploit the underlying regenerative capability and expedite the design of a transparent regenerator, showing the potential to act as a basic building block in future all-optical processing. We also compare different strategies when such regenerators are configured in concatenation. The approach can be readily applied to virtually any similar application for different all-optical processing functionalities.

5.1 Regenerative capability of PSA

In order to meet explosive traffic requirements, advanced modulation formats with complex constellations have been extensively employed[132] to scale up the transmission capacity. In such communication systems, all-optical processing, which outperforms electronic approaches in terms of traffic cost, bandwidth, power consumption, and flexibility, is highly desired in addition to the ceaseless pursuit of low noise repeating. To this end, PSA with the intrinsic ultra-fast response and quantum-limited amplification[117], has become a versatile and promising candidate towards all-optical functionalities[133], [134]. Particularly, the unique (phase and amplitude) squeezing property has led to the realization of all-optical regeneration and quantization of complex phase-encoded signals and the mitigation of nonlinear phase impairments[135], [136].

For a well-designed binary regenerator, a transparent step-like nonlinear phase transfer function[137] is required. This is indeed expected in an ideal PSA thanks to the inverse gains experienced by orthogonal quadratures: the in-phase field components are amplified with maximum gain while the quadrature components undergo maximum de-amplification. However, such phase-sensitive gain leads to an increase of amplitude fluctuations, which can nevertheless be alleviated by operating the amplifier in the saturated regime[138]. It has been inferred that maximizing the ratio of the maximum and

minimum phase-sensitive gains, the so-called phase-sensitive extinction ratio (PSER), is a fundamental approach to improve the processing efficiency[139], [140]:

$$PSER = \frac{G_{\max}}{G_{\min}} = G_{\max,\mathrm{dB}} - G_{\min,\mathrm{dB}} \tag{5-1}$$

Introducing large nonlinearities can directly lead to a high PSER. However, practical implementation of such solution requires large nonlinearities and/or large pump powers that are not always available. An alternative strategy consists in exploiting the extra waves stemming from high-order four-wave mixing (FWM) processes. Indeed, large PSER can be attained as a consequence of large phase-sensitive gain asymmetry (PSGA), defined as the product of the maximum and minimum gains:

$$PSGA = G_{\max} \cdot G_{\min} = G_{\max,\mathrm{dB}} + G_{\min,\mathrm{dB}} \tag{5-2}$$

This is especially true since the resulting large de-amplification owing to the high-order processes can lead to a large PSER. This has led to efficient phase regeneration and decomposition[139], [140] at relatively low nonlinear phase shifts (NPS). Regeneration and quantization can also be achieved by coherent superposition of weighted signals[141] and idlers in sequentially concatenated stages[142], [143], [144]. More recently, polarization-assisted vector PSA[145], taking advantage of polarization effects in FWM, has been proposed for regeneration and phase quantization[146]. This method mitigates the NPS requirement at the expense of diminished net gain and additional complexity[137]. To study the squeezing property and in turn optimize the regenerator, phase-sensitive transfer functions under some particular phase matching conditions have been discussed both in HNLF[138], [147] and semiconductor optical amplifiers (SOA)[148], based on the conventional 3-wave model[117] and time-dependent rate equations, respectively. The influence of NPS to PSER has been initially introduced and explored using a 7-wave model[127]. As a promising candidate for future all-optical processing, the limit of such a fundamental PSA setup in the context of regeneration is of particular importance. To date, a thorough analysis and optimization for the basic quadrature operations is still imperative and remains to be done.

In order to fully exploit the regenerative potential of a single PSA based signal processor, we exploit the scalar 7-wave model[129] developed in Chapter 3 and already exploited in Chapter 5. Using this precise model, we study quadrature squeezing in terms of nonlinear phase-sensitive transfer characteristics and trajectories in a wide spectrum

range with varied phase matching conditions in both small signal and saturation regimes. This enables, for the first time, multi-dimensional optimization of quadrature operations from the regeneration point of view. In addition, different schemes to concatenate two amplifier sections are also discussed to optimize their operation. Based on our investigations, the quadrature squeezing potential acting as a basic building block of the regenerative and processing operations is thoroughly exploited. The proposed approach can be considered a general guiding tool for a variety of application scenarios.

5.2 Gain properties, PSER and PSGA

In order to investigate the potential regenerative capabilities, let us first study the relation, or more precisely the dependence, between PSER and PSGA. In the last chapter, the maximum phase-sensitive gain has been calculated and elaborated through the 7-wave model as shown in Fig. 4.2. It is straightforward to obtain the minimum phase-sensitive gain, i.e. de-amplification of the signal, from the 7-wave model as shown in Fig. 5.1 with the same HNLF parameters and pump power as illustrated in Fig. 4.2. Based on these preliminarily calculated maximum and minimum gain profiles for varying values of $\Delta\lambda_{\mathrm{PPS}}$ and $\delta\lambda_{\mathrm{OFS}}$, the PSER and PSGA estimated by the 7-wave model can be derived with simple mathematical calculations, as depicted in Fig. 5.2 (a) and Fig. 5.2 (b), respectively. These results were obtained with the same 23 dBm total pump power.

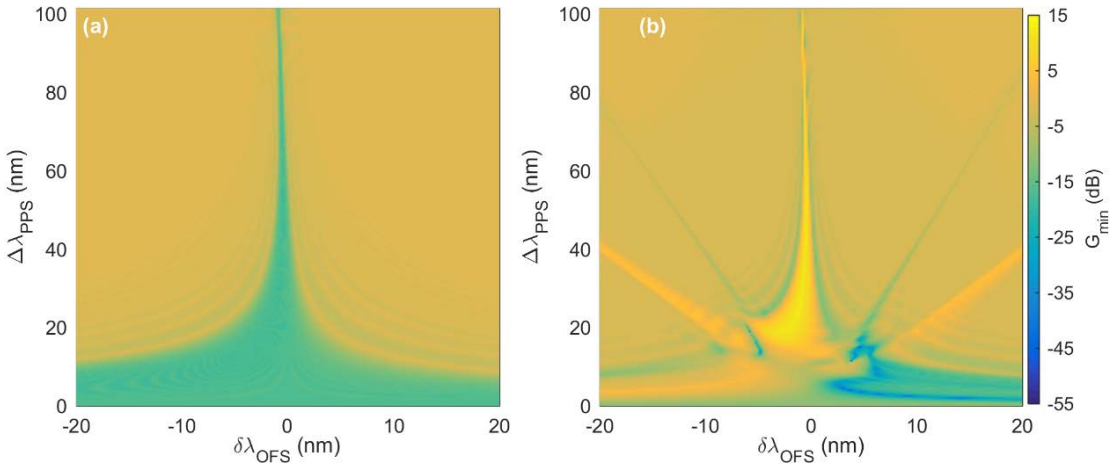

Fig. 5.1 Minimum signal gain vs. $\delta\lambda_{\mathrm{OFS}}$ and $\Delta\lambda_{\mathrm{PPS}}$.

Minimum signal gain vs. signal wavelength offset $\delta\lambda_{\mathrm{OFS}}$ with respect to the zero dispersion wavelength λ_{ZDW} and vs. pump-pump separation $\Delta\lambda_{\mathrm{PPS}}$ with input signal phase $\varphi_{0,\mathrm{max}}$ to maximize the gain for both (a) 3- and (b) 7-wave models.

According to the standard 3-wave model, the predicted PSER barely depends on the PSGA since the maximum and minimum gains are almost symmetric with respect to the unitary gain. The PSGA is then almost around 0 dB, and the PSER is about twice the maximum gain. By contrast, according to the 7-wave model, the maximum and minimum gain profiles are drastically modified owing to the high-order FWM processes. Thus the PSER and PSGA exhibit completely disparate behaviors. Though in most cases, the PSER evolution agrees with the PSGA one to some extent, the gain profiles are no longer symmetric, leading to distorted and abruptly varying PSER and PSGA maps as functions of $\delta\lambda_{\mathrm{OFS}}$ and $\Delta\lambda_{\mathrm{PPS}}$, as can be seen in Fig. 5.2.

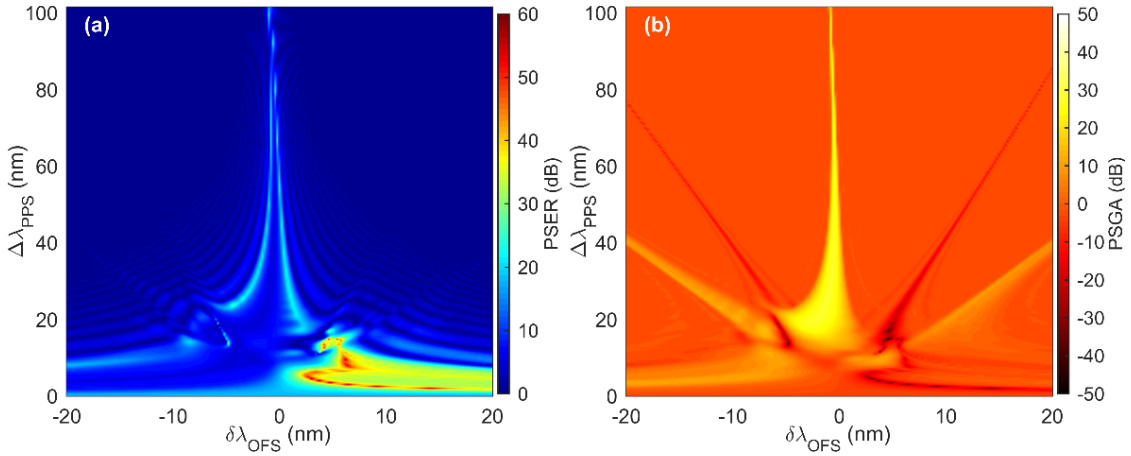

Fig. 5.2 PSER and PSGA vs. $\delta\lambda_{\mathrm{OFS}}$ and $\Delta\lambda_{\mathrm{PPS}}$ estimated from 7-wave model. (a) PSER and (b) PSGA vs. $\delta\lambda_{\mathrm{OFS}}$ and $\Delta\lambda_{\mathrm{PPS}}$ estimated by the 7-wave model for 23 dBm total pump power in the small signal regime. The nonlinear medium is the typical standard HNLF as used in the previous experiments and calculations with $\lambda_{\mathrm{ZDW}} = 1547.5$ nm. All other parameters are the same as the figures regarding the maximum and the minimum gains and are given in text.

In the configuration where $\delta\lambda_{\mathrm{OFS}} = 0$, where all the waves are centered at λ_{ZDW}, it is worth noticing that for $10\ \mathrm{nm} \leq \Delta\lambda_{\mathrm{PPS}} \leq 20\ \mathrm{nm}$, the PSER exhibits an anomalously low value around 10 dB while the PSGA shows a positive value larger than 20 dB. This implies that the minimum gain is positive (in dB) in this region. This can be understood by the fact that owing to the multiple interactions of all high-order processes, phase-insensitive processes dominate over phase-sensitive ones, resulting in a non-negative gain of the output signals in this region. Similar behaviors are also found for small $\Delta\lambda_{\mathrm{PPS}}$ in the normal dispersion ($\delta\lambda_{\mathrm{OFS}} \leq 0$) regime, corresponding to the positive PSGA area

[see the yellow part in the left part of Fig. 5.2 (b)]. This parameter range thus exhibits no promising operation point. In the rest part of the normal dispersion regime, where the PSGA profile is almost flat, implying more symmetric gain profiles, and it is therefore not surprising to find only a moderate PSER value of about 20 dB.

The situation appears to be quite different in the anomalous dispersion regime ($\delta\lambda_{\mathrm{OFS}} > 0$). As indicated in Fig. 5.2, when $\Delta\lambda_{\mathrm{PPS}}$ is relatively small, various nontrivial zigzag-shaped negative PSGA dips are located in this regime, exhibiting a strong overlap with regions of large PSER. The minimum PSGA reaches almost -50 dB, revealing the large deamplification that leads to a high PSER reaching up to about 60 dB. Nonetheless, it is not surprising that the most significant PSER is found in the anomalous dispersion regime. The numerical result has already claimed the prediction of the extraordinary gain peak illustrated in Fig. 4.7. Particularly, in Fig. 4.7 (b), the phase-sensitivity at this pump wavelength configuration is manifested as the huge difference between the maximum and minimum gains. Likewise, in the vicinity of this gain peak, attributed to the phase matching conditions, the phase-sensitivity stays above a high value, leading to the high PSER in this area. Therefore, this configuration is particularly promising and will be carefully investigated in the following sections.

Besides, in both normal and anomalous dispersion regimes, one can observe two diagonal stripes of PSGA dips and peaks, respectively, expanding towards relatively large absolute values of $\delta\lambda_{\mathrm{OFS}}$ and $\Delta\lambda_{\mathrm{PPS}}$. This overall tendency is similar to the gain profile presented in Fig. 4.2. However, these dips and peaks do not coincide with large values of the PSER except for some inconspicuous periodical ripples. If incorporating the results of the minimum gain, it suddenly becomes superficial. In these diagonal stripes, the relatively prominent PSGA is the result of the negative maximum gain, for which cannot be cancelled out in the calculation of PSGA. While they actually hardly contribute much to the PSER. So that the PSER in these regions are quite limited. This is mainly due to the fact that in large $\delta\lambda_{\mathrm{OFS}}$ and $\Delta\lambda_{\mathrm{PPS}}$ regime, as a result of the strong dispersion, the large phase mismatch hinders the emergence of high-order FWM processes, eliminating the influence of high-order waves and thus diminishing the phase-sensitivity. For instance, when $\delta\lambda_{\mathrm{OFS}} \approx 0$, all spurious processes vanish when $\Delta\lambda_{\mathrm{PPS}}$ gets large, leaving only the fundamental 3-wave FWM leading process. In this case, PSGA sums up to nearly zero because of the almost symmetric gain profiles, giving rise

to a moderate PSER.

To summarize, the PSER and PSGA are not always positively related, and a large PSGA is a necessary but not sufficient condition to obtain a large PSER.

The substantial PSER predicted by 7-wave model allows improving the steepness of the phase transfer function, thus permitting excellent squeezing efficiency. On top of that, the amplitude fluctuation associated with the phase-to-amplitude conversion becomes prominent and will be studied in the following section.

5.3 Nonlinear phase shift

Starting from the wavelength allocation giving rise to a large PSER as predicted in Fig. 5.2, we calculate the evolution of the amplifier performance as a function of the NPS, defined as the product of γ, the total input pump power $P = P_1 + P_2$ (with $P_1 = P_2$), and L. The results are reproduced in Fig. 5.3(a) for the 3-wave (dashed lines) and the 7-wave (full lines) models with $\delta\lambda_{\mathrm{OFS}} = 3.0$ nm and $\Delta\lambda_{\mathrm{PPS}} = 4.5$ nm.

When the NPS increases, the maximum gain (G_{max}) and minimum (negative) gain (G_{min}) calculated by the 3-wave model evolve almost symmetrically with respect to the unitary gain (0 dB). As a consequence, the PSGA remains close to 0 dB, and the PSER grows almost independently from the PSGA. This is consistent with the results regarding the wavelength allocation $\delta\lambda_{\mathrm{OFS}}$ and $\Delta\lambda_{\mathrm{PPS}}$ discussed in the last section for the 3-wave model. Now, in the 7-wave model, G_{max} is slightly smaller than in the 3-wave model. This phenomenon was expected since the high-order waves consume a significant part of the pump power that becomes unavailable for amplification of the signal. On the contrary, the most surprising difference between the two models comes from the minimum gain G_{min}, which exhibits two abrupt dips for particular NPS values. These dips are also visible on the PSGA at the same NPS values. This is reflected on the PSER as well. By conducting an analysis similar to Ref. [129] and chapter IV, one can identify the FWM mechanisms whose total phase mismatch is close to zero, and thus play a significant role in the energy transfer between the 7 waves. In the vicinity of the gain dips, this analysis shows that the processes that extract power from A_0 are much more efficient than those that amplify A_0. Taking advantage of the first PSER peak, excellent performances can be expected with moderate total pump power ($P = 18.9$ dBm), for which one still remains in the small NPS region.

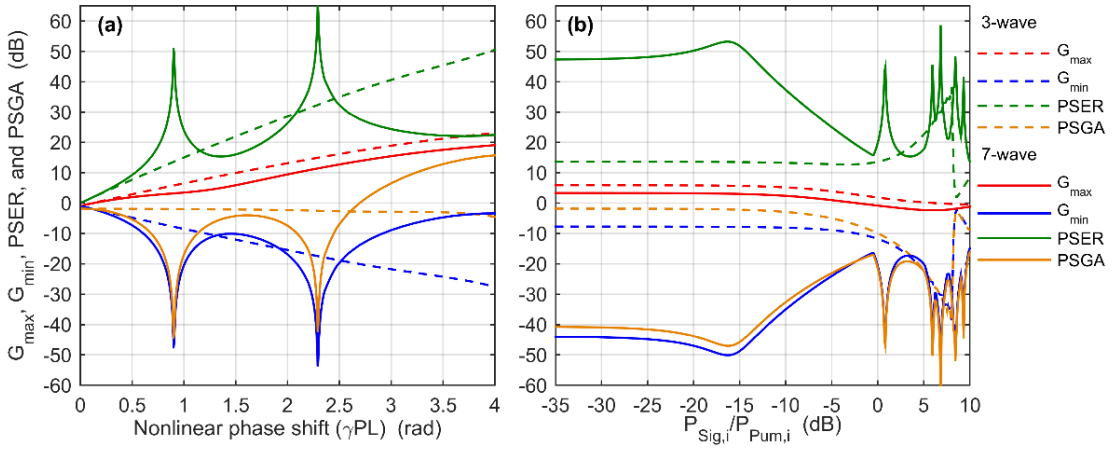

Fig. 5.3 Gain profiles with respect to nonlinear phase shift and degree-of-saturation. Gain profiles including maximum gain (G_{max}), minimum gain (G_{min}), PSER, and PSGA with respect to (a) total nonlinearity: nonlinear phase shift (NPS), and (b) degree-of-saturation (DoS), respectively, from both the 3- and 7-wave models[149] when $\delta\lambda_{\mathrm{OFS}} = 3.0$ nm and $\Delta\lambda_{\mathrm{PPS}} = 4.5$ nm with total pump power $P = 18.9$ dBm, namely, the optimum wavelength allocation and pump power that we found above.

As mentioned above, the associated phase-to-amplitude conversion of the amplifier can induce severe amplitude noise, which is detrimental to the quality of regeneration. This problem should be carefully addressed to achieve regeneration without sacrificing amplitude noise. Analogous to the phase-to-phase transfer characteristics, a step-like phase-to-amplitude response is therefore highly desirable. To this end, the instantaneous saturation property, which exploits the power-dependent gain saturation, due to which the output signal amplitude is distorted, is conventionally investigated to cope with the accompanying intensity variations. However, care should also be taken as the operation in saturation regime will, in turn, change the PSER performance. For this reason, the influence of the degree-of-saturation (DoS), i.e., the ratio of the incident signal power to the total input pump power, should be investigated. This is performed in Fig. 5.3 (b) for the optimized wavelength allocation ($\delta\lambda_{\mathrm{OFS}} = 3.0$ nm and $\Delta\lambda_{\mathrm{PPS}} = 4.5$ nm) and total pump power that we found above.

Starting from the small signal region where $\mathrm{DoS} \leq -30$ dB, Fig. 5.3 (b) shows that both G_{max} and G_{min} reduce with saturation. However, G_{min} decreases faster than G_{max}, leading to a drop of the PSGA and a small increase in the PSER. With a further increase of the DoS towards the full saturation regime, the absolute values of G_{max} and G_{min} both

diminish as well as the PSER as a result. The fluctuations on different gain properties after DoS ≥ 0 dB are quite similar to the behavior observed in conventional optical parametric amplifiers attributed to the intense interaction between comparably strong waves. Nonetheless, the particular demand on signal power makes this fully saturated region impractical. It appears that operation in the gain-limited saturation brings about a limited improvement in terms of PSER. However, it could be particularly beneficial for the mitigation of the associated amplitude variations as will be discussed in the following sections regarding the overall optimization.

5.4 Phase-sensitive transfer characteristics

We have just seen that the DoS directly modifies the phase-to-amplitude response and in turn the PSER as well. Consequently, in order to provide a visual picture of the trade-off between phase squeezing and amplitude/power fluctuation management, we plot three different phase transfer characteristics of the amplifier in Fig. 5.4 for both 3- and 7-wave models. We represent in false colors the phase-to-gain, phase-to-power, and phase-to-phase transfer functions for the DoS varying from -40 to 5 dB and a total pump power equals to $P = 18.9$ dBm. Other parameters are chosen based on the results from the preceding optimizations.

First, the phase-to-gain transfer characteristics from 3- and 7-wave models are represented in Fig. 5.4 (a) and Fig. 5.4 (b), respectively. Compared to the quite uniform evolution in the small signal region in the 3-wave model, the 7-wave transfer function reveals a much deeper minimum gain, which confirms our preceding discussions. Considering the effect of saturation, the gain distortion is obviously more intense in the 7-wave model than in the 3-wave one. When the DoS lies between -3 dB and -20 dB, both maximum and minimum gain plateaus become much flatter than in 3-wave model. Assisted by the high-order waves, one can observe strong signal depletion when the signal power just becomes comparable with the pump power in the full saturation region, permitting potential all-optical processing opportunities.

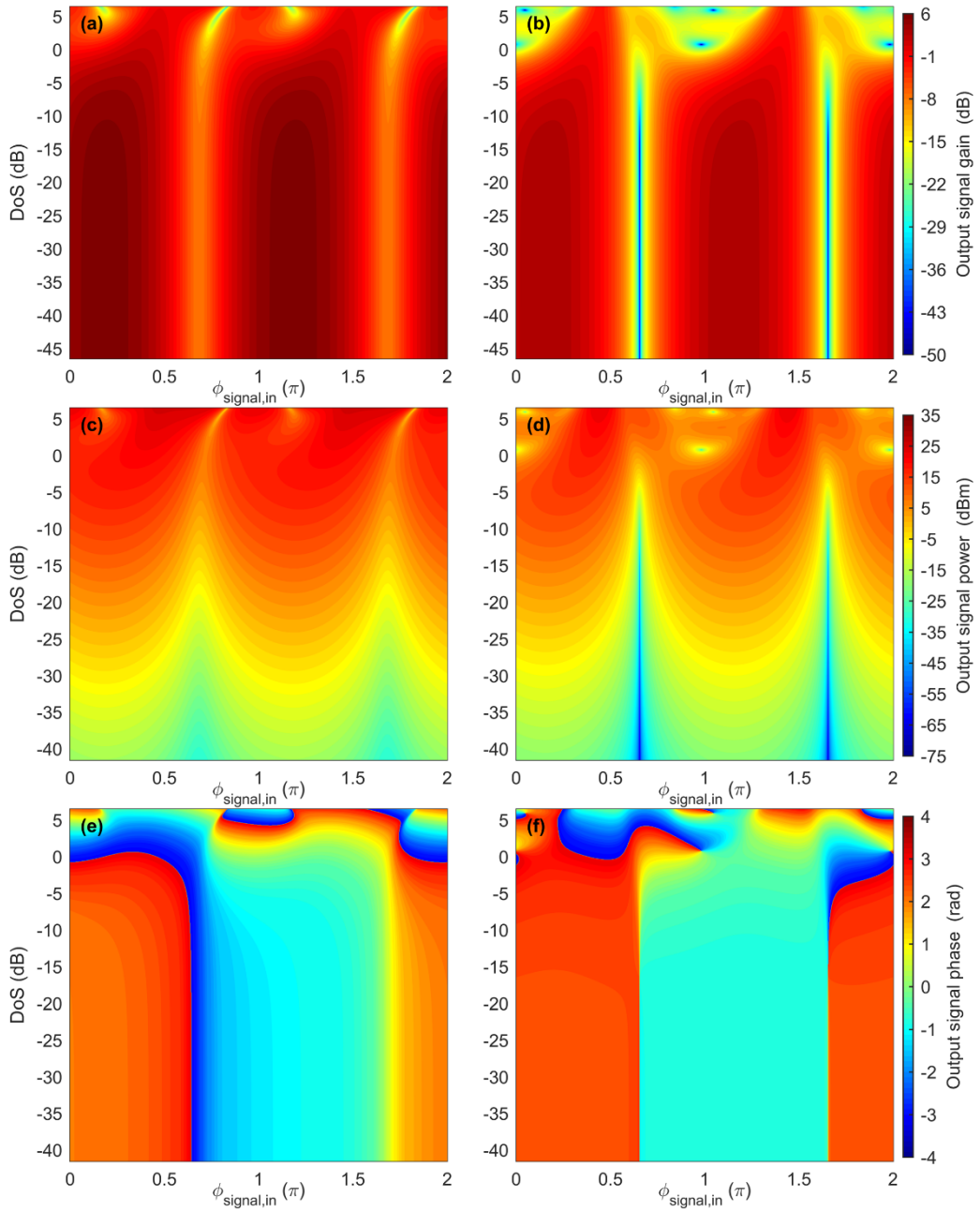

Fig. 5.4 Phase transfer characteristics vs. signal phase and degree-of-saturation. (a, b) Phase-to-gain, (c, d) Phase-to-power, and (e, f) Phase-to-phase transfer characteristics with respect to input signal phase and DoS, numerically estimated by the 3-wave (left, (a, c, and e)) and the 7-wave (right, (b, d, and f)) model, respectively, using the optimum wavelength allocation ($\delta\lambda_{\mathrm{OFS}} = 3.0$ nm and $\Delta\lambda_{\mathrm{PPS}} = 4.5$ nm) and total pump power ($P = 18.9$ dBm) that obtained above.

The estimation of signal gain is also illustrated by the phase-to-power transfer

properties shown in Fig. 5.4 (c) and Fig. 5.4 (d). One can also observe the fluctuations along the maximum and minimum plateaus, which will influence the amplitude behavior of the squeezing effect. Both transfer characteristics indicate the possibility to mitigate the associated amplitude noise. However, as discussed from Fig. 5.3 (b) above, gain limitation using saturation, in turn, degrades the PSER and thus affects the regeneration capability. Considering now the phase-to-phase response plotted in Fig. 5.4 (e) and Fig. 5.4 (f), in the small signal regime, the 7-wave model offers a high detail precision for the transition between two squeezed quadratures. As the squeezing effect is directly connected with PSER, the substantially higher PSER estimated by the 7-wave model indeed leads to better squeezing of both quadratures. This much higher PSER offers some extra margin before the phase squeezing is affected by gain saturation, eventually allowing better suppression capability for amplitude variations. In 3-wave model, the phase squeezing is compromised for saturation regimes corresponding to $-10\ \mathrm{dB} \leq \mathrm{DoS} \leq -3\ \mathrm{dB}$. The steepness of the transitions between quadratures is impaired and, more seriously, the phase plateau is no longer flat but fluctuates around 0 rad input signal phase. This is not the case according to the 7-wave model, as the impact due to the saturation does not degrade the sharp transition that much. Only negligible ripples in phase plateaus are then observed.

5.5 Complex plane trajectory

The output signal trajectories in complex plane from linear to saturation regime provide intuitive observations for the simultaneous squeezing effects on both phase and amplitude, as illustrated in Fig. 5.5 (a) and Fig. 5.5 (b). The input signal phase is varying along the unit circle and the output trajectories are normalized with respect to the input signal. They clearly exhibit the gain degradation due to the high-order waves in the 7-wave model. Except for the distortion on the trajectories, it should be noted that in both 3- and 7-wave models the maximum gain axis rotates with saturation towards the same direction. This shift of the principal gain axis is more significant with stronger DoS.

In small signal linear regime, instead of amplified circles for the conventional phase-insensitive amplifier, squeezed elliptical output trajectories are explicitly observed. Phase squeezing along the gain axes occurs simultaneously with a large associated amplitude variation in both models. Notably, in this small signal regime, the elliptical

trajectory predicted by the 7-wave model is more closed than that in 3-wave model, indicating a more efficient squeezing effect in 7-wave model. This is attributed to the higher PSER with the assistance of the high-order waves.

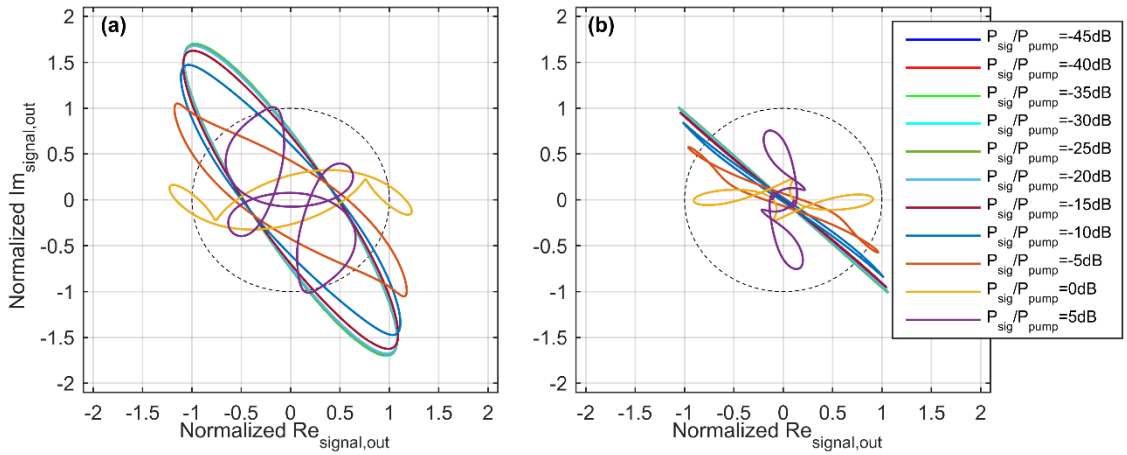

Fig. 5.5 Output trajectory of the signal in both 3- and 7-wave prediction.
Output signal trajectory in the complex plane estimated by (a) the 3- and (b) the 7-wave model for various DoS, respectively. The input signal is represented as the unit circle. The output trajectories are normalized in amplitude with respect to the input signal. The wavelength allocation ($\delta\lambda_{\mathrm{OFS}} = 3.0$ nm and $\Delta\lambda_{\mathrm{PPS}} = 4.5$ nm) and the total pump power ($P = 18.9$ dBm) are the optimum values that we obtained above.

With the increase of the saturation, the principal gain axis further rotates towards the horizontal axis. This is more clearly observed started from DoS = -10 dB, possibly due to the relatively large signal power that gives rise to the intense interaction between waves. When DoS = -5 dB, we can observe some moderate amplitude squeezing occurring together with the phase squeezing. This is especially striking in the 7-wave model where some small spirals are buckling around the two terminal vertexes of the trajectory. It is well confirmed that, with adequate saturation, it could be possible to achieve the desired phase squeezing while alleviating the amplitude noise.

5.6 Regenerative capability

5.6.1 BPSK regeneration

Using the proposed optimization approach, the regenerative capability is firstly

numerically evaluated in the case of BPSK modulation. The BPSK signal is contaminated by additive white Gaussian noise with 20 dB SNR. The root-mean-square error vector magnitude (EVM) is used as the performance metric.

The EVM represents the Euclidian distance between the ideal symbol coordinate and the actual symbol from the real measurements. In general, EVM is averaged over an ensemble of symbol trajectories and can be defined as:

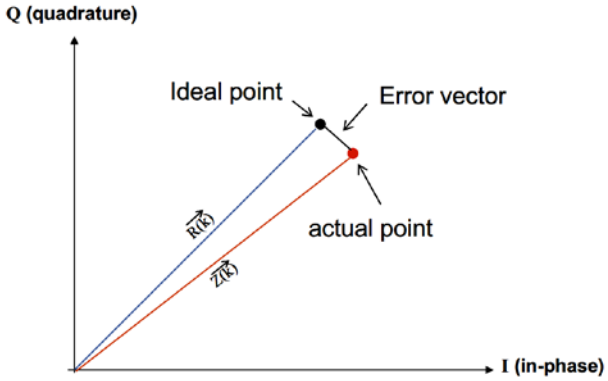

Fig. 5.6 Definition of Error vector magnitude (EVM) in the I/Q space.
Definition of Error vector magnitude (EVM) with the I/Q signal space indicating reference vector, $\vec{R}(k)$, and the measurement vector, $\vec{Z}(k)$.

Therefore, for the collection of EVM for each of the measurement, the root-mean-square EVM, EVM_{rms} is given by the ratio of the amplitude of the error vector to the root mean square amplitude of the reference vector:

$$EVM_{\text{rms}} = \sqrt{\frac{\sum_{k=1}^{M}\left|Z(k)-R(k)\right|^2}{\sum_{k=1}^{M}\left|R(k)\right|^2}} \tag{5-3}$$

In the absence of noise and nonlinearities, namely an ideal system, where no signal distortion is introduced, the measured vector and reference vector should be identically overlapped on the I/Q space. This way, the EVM equals to zero. Consider the case when the noise and distortion are no longer negligible, the displacement between the measured vector from the reference vector due to the noise and distortion effects will become significant. This suggests that the SNR and EVM should share an inverse relationship.

In our case, EVM_{rms} is assessed with respect to the varied DoS as presented in Fig.

5.7 in order to verify the impact of DoS. It can be easily inferred that the 7-wave model predicts better EVM improvement. The most efficient regeneration configuration in terms of EVM_{rms} is achieved at about DoS = -7.5 dB, which agrees well with the predictions of sections before (5.4 and 5.5). It is worth noticing that this DoS does not correspond to the optimized PSER [see Fig. 5.3 (b)]. However, taking into consideration the phase-to-amplitude noise transfer, the total quadrature noises, including phase and amplitude portions, become well balanced, thus leading to this promising value of the EVM_{rms} around such DoS.

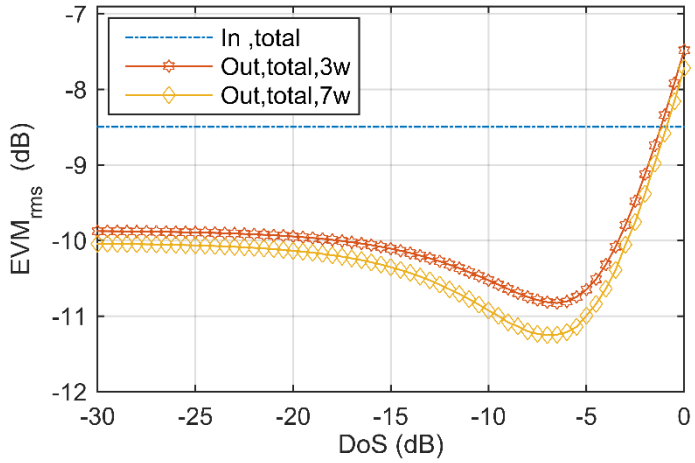

Fig. 5.7 Error vector magnitude (EVM) of the input and output BPSK signal vs. DoS. EVM_{rms} of the input and the output BPSK signal vs. DoS numerically estimated by the 3- and the 7-wave models, respectively, using the optimum wavelength allocation ($\delta\lambda_{OFS} = 3.0$ nm and $\Delta\lambda_{PPS} = 4.5$ nm) and total pump power ($P = 18.9$ dBm) that we obtained above.

The BPSK constellations at input and output with -20 dB, -7.5 dB, and 0 dB DoS are reproduced in Fig. 5.8, respectively. Unlike at DoS = -20 dB where the amplitude squeezing is almost negligible, both phase and amplitude squeezing are observed at -7.5 dB as shown in Fig. 5.8 (c).

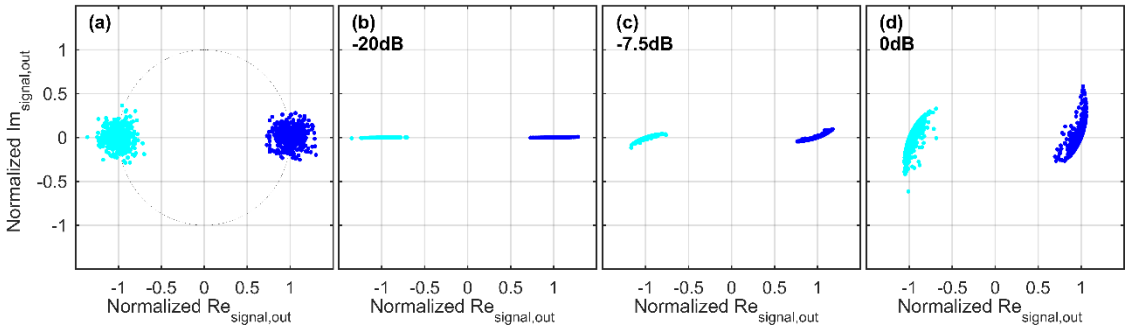

Fig. 5.8 Normalized constellations of the input and output BPSK signals.

Normalized constellations of the (a) input and output BPSK signals with (b) DoS = -20 dB, (c) DoS = -7.5 dB, and (d) DoS = 0 dB, respectively, numerically estimated from the 7-wave model using the optimum wavelength allocation ($\delta\lambda_{\mathrm{OFS}} = 3.0$ nm and $\Delta\lambda_{\mathrm{PPS}} = 4.5$ nm) and total pump power ($P = 18.9$ dBm) that we obtained above.

The constellation is then distorted in a similar manner as inferred in Fig. 5.5. In contrast, further increase of the DoS only brings intense energy interchange amongst waves, leading to highly distorted squeezing in both quadratures that is of no application interest.

5.6.2 Field decomposition of QPSK

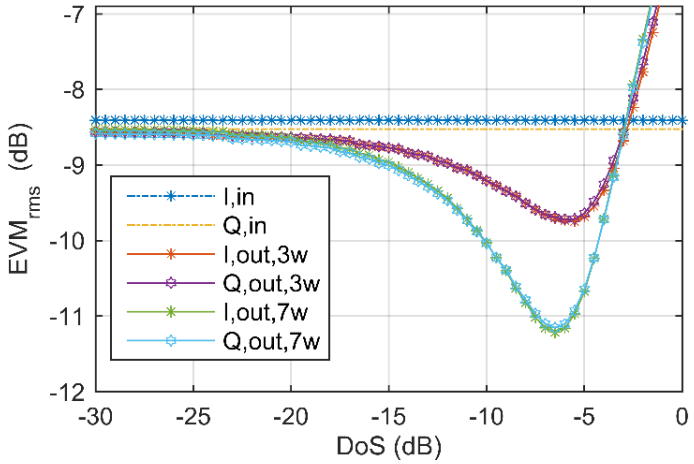

Fig. 5.9 $\mathrm{EVM_{rms}}$ of the input and output QPSK signals vs. DoS.

$\mathrm{EVM_{rms}}$ of the input and the output QPSK signals including in-phase (I) and quadrature (Q) components vs. DoS numerically estimated by the 3- and the 7-wave models, respectively, using the optimum wavelength allocation ($\delta\lambda_{\mathrm{OFS}} = 3.0$ nm and $\Delta\lambda_{\mathrm{PPS}} = 4.5$ nm) and total pump power ($P = 18.9$ dBm) that we obtained above.

All-optical decomposition and regeneration of both in-phase and quadrature components are indispensable functionalities for future all-optical networks that require transparent modulation format conversion as well as some other signal processing capabilities. To this end, by precisely managing the gain axis, i.e., the relative phase between the signal and pumps, for example, it is feasible to extract the orthogonal quadratures individually. In this scenario, we take the decomposition of a QPSK signal as an example test bench.

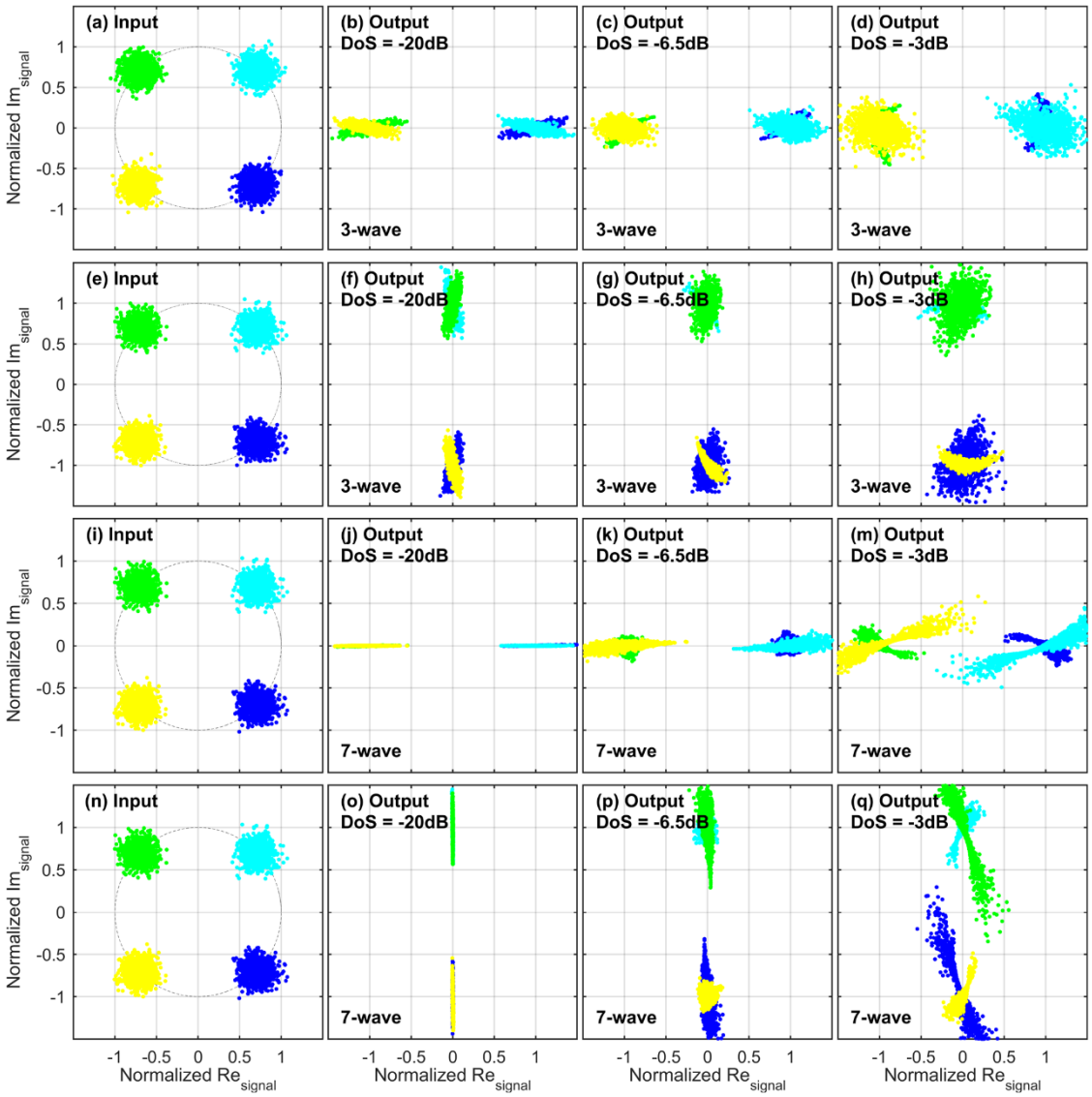

Fig. 5.10 Normalized constellations of the decomposed QPSK I and Q components. Constellations of the I and Q components of the QPSK signals at (a, e) [respectively, (i, n)] the input and the output with (b, f) [respectively, (j, o)] DoS = -20.0 dB, (c, g) [respectively, (k, p)] DoS = -6.5 dB, and (d, h) [respectively, (m, q)] DoS = -3.0 dB,

respectively, numerically calculated from the 3-wave (respectively, 7-wave) model using the optimum wavelength allocation ($\delta\lambda_{\mathrm{OFS}} = 3.0$ nm and $\Delta\lambda_{\mathrm{PPS}} = 4.5$ nm) and total pump power ($P = 18.9$ dBm) obtained above. All the constellations are normalized.

By controlling the phases of the incident pumps, the gain axis of the regenerative PSA can be aligned to either in-phase (I) or quadrature (Q) for decomposition. In Fig. 5.9, the $\mathrm{EVM_{rms}}$ of both I and Q components are numerically estimated by the 3- and 7-wave models in the cases of the decomposition of each component, respectively. The overall tendency of the $\mathrm{EVM_{rms}}$ is quite similar to that in BPSK case. Though the $\mathrm{EVM_{rms}}$ evolution with respect to the DoS in both 3-wave and 7-wave models exhibits a similar trend, the values from the two models are different. In the small signal regime, although the squeezing is more efficient in 7-wave model thanks to the high-order waves, the EVM performances in the two models are quite close to each other. However, while entering the saturation regime, the divergence increases more and more.

The optimum $\mathrm{EVM_{rms}}$ for I and Q quadratures occurs at about -6.5 dB DoS, suggesting that some degree of saturation is helpful. Meanwhile, the 7-wave model predicts about 1.5 dB further improvement of $\mathrm{EVM_{rms}}$. Similar to the BPSK case, distortion of the constellations as represented in Fig. 5.10 is observed in the fully gain-saturated regime, which in turn deteriorates the EVM performance.

It is worth noting that in the saturation regime, the occurrence of the distinct distortions on the squeezed constellations is mainly attributed to the fact that the transfer characteristics have been severely modified in the saturation regime as implied by Fig. 5.4 and Fig. 5.5. This eventually leads to the non-orthogonal relation between the maximum and minimum gain axes, resulting in the differences in the constellations.

5.7 Concatenation

According to the discussions above, the simultaneous regeneration in both amplitude and phase in a saturated PSA has been investigated and systematically optimized. Nonetheless, by far, one question still remains: whether the simple concatenation of two or more than two such regenerative PSA stages can possibly outperform the separated regeneration in two successive stages.

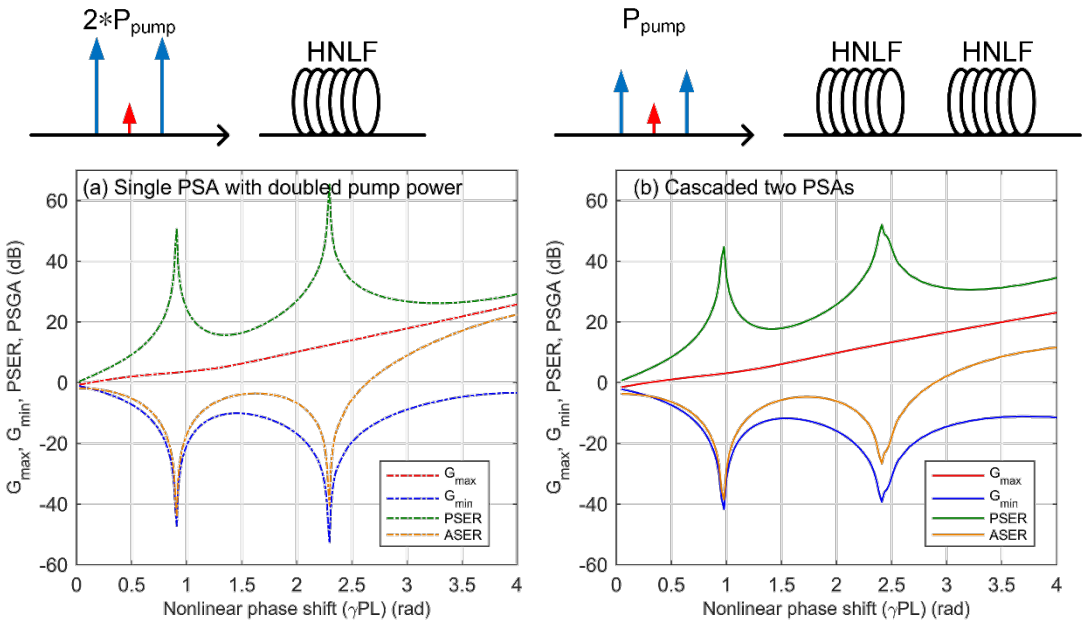

Fig. 5.11 Gain properties with respect to NPS for single and cascaded PSA stages. Gain properties including G_{max}, G_{min}, PSER, and PSGA as respect to NPS for (a) single stage of HNLF (dot-dashed lines) with twice the total pump power and (b) cascaded two stages of HNLF (solid lines), respectively, using the optimum wavelength allocation as in Fig. 5.3 in the small signal regime.

It is intuitive to first consider cascading the same PSA, extending to twice the length of the nonlinear medium, hence doubling the value of the NPS. To perform the comparison with the same NPS values, this should be directly compared with the results obtained when the total input pump power is doubled. The resulting gain properties are reproduced as shown in Fig. 5.11 (a) and Fig. 5.11 (b), respectively.

It appears that, compared to the same amount of NPS, both strategies exhibit quite similar tendencies of the evolution of the gain properties. However, more precisely, for the cascaded two stages of HNLF, G_{max} is slightly lower than the first case, as well as the G_{min}. While similar PSGA and PSER are achieved, but with a slightly higher NPS requirement in the second case. This is simply due to the fact that in the cascaded two stages case, the higher NPS comes at the price of the stronger losses attributed to the longer HNLF. Nevertheless, in the single PSA case, only the total pump power is elevated, without introducing any extra losses (here the SBS effect is neglected).

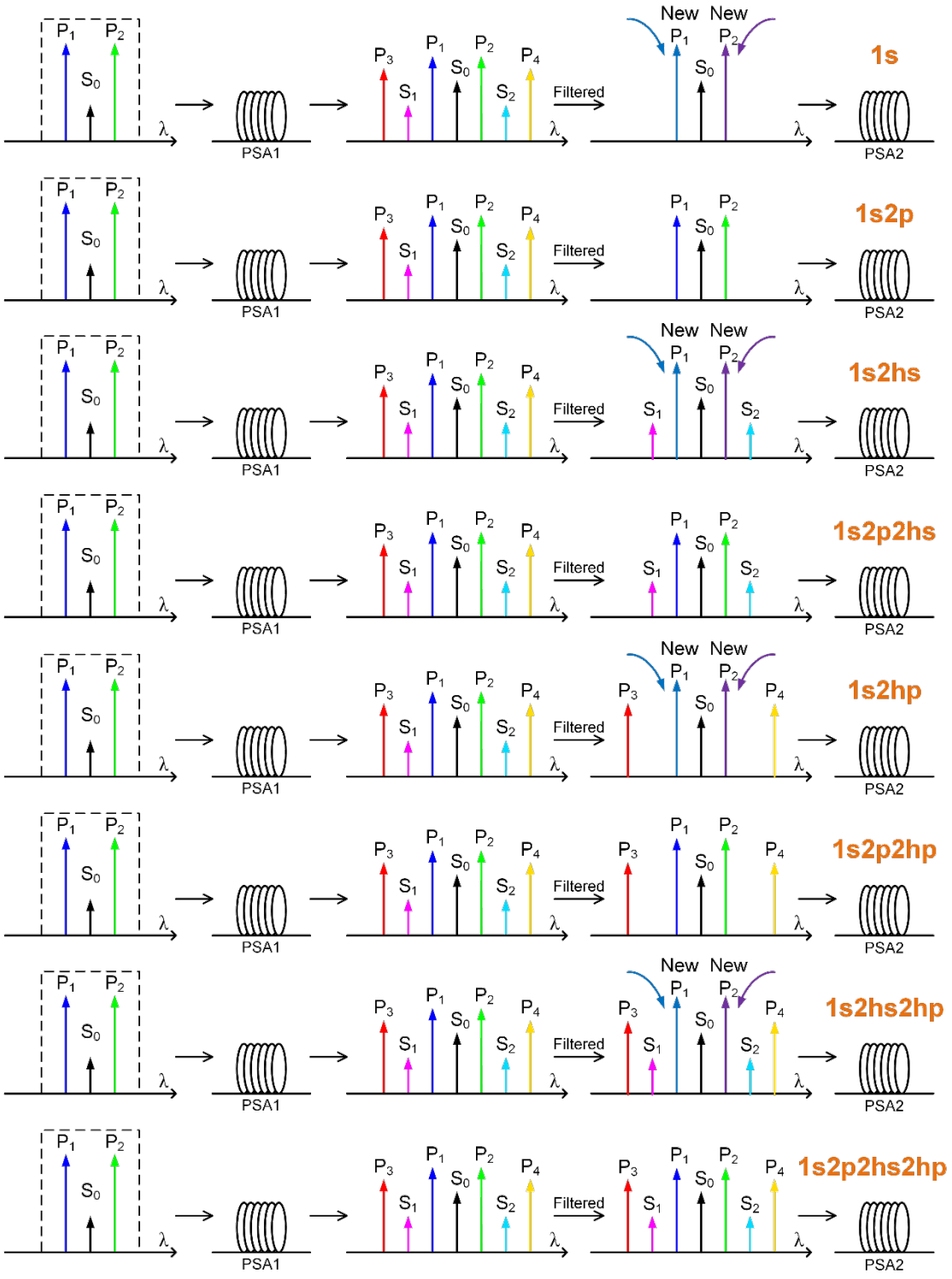

Fig. 5.12 Definitions of different concatenation scenarios.

Distinct strategies for different combinations of waves excited into the 2nd PSA stage:

1s, 1s2p, 1s2hs, 1s2p2hs, 1s2hp, 1s2p2hp, 1s2hs2hp, and 1s2p2hs2hp stand for exciting signal with regenerated dual pumps, signal with pumps from the first stage, signal and high-order signals from the first stage with regenerated dual pumps, signal with pump and high-order signals all from the first stage, signal and high-order pumps with regenerated dual pumps, signal and pumps with high-order pumps all from the first stage, signal with high-order signals and pump and regenerated dual pumps, and all the seven waves from the first stage, respectively.

Since the generation of the high-order waves aids at improving the regeneration capability as they enhance the phase-sensitivity, we evaluate different strategies with different combinations of waves at the input of the second PSA stage, as illustrated in Fig. 5.12. In these different scenarios, different combinations of waves will be excited to the second PSA stage. These different cases are named as 1s, 1s2p, 1s2hs, 1s2p2hs, 1s2hp, 1s2p2hp, 1s2hs2hp, and 1s2p2hs2hp which stand for exciting signal with regenerated dual pumps, signal with pumps from the first stage, signal and high-order signals from the first stage with regenerated dual pumps, signal with pump and high-order signals all from the first stage, signal and high-order pumps with regenerated dual pumps, signal and pumps with high-order pumps all from the first stage, signal with high-order signals and pump and regenerated dual pumps, and all the seven waves from the first stage, respectively.

The final outputs are assessed with respect to either the initial input or the output of the first stage. This is because, for some application scenarios, the signals will be used in the mid-stages.

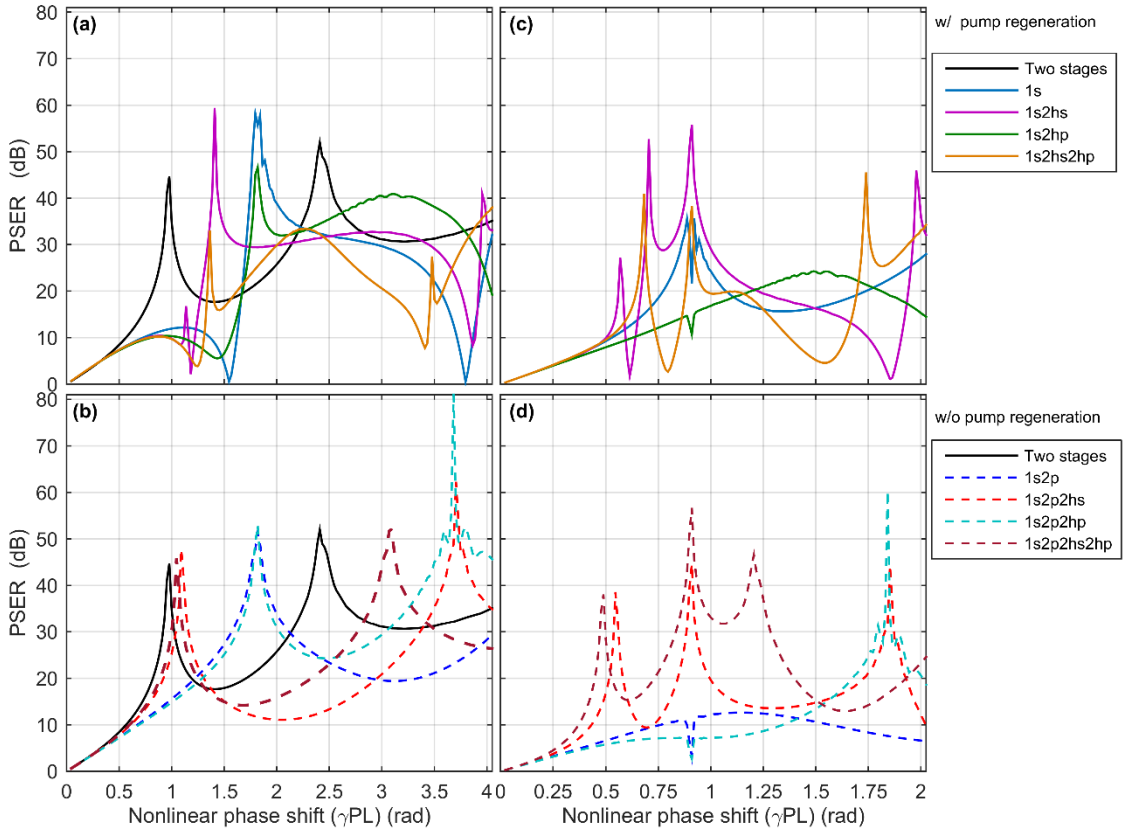

Fig. 5.13 PSER evolutions in different concatenation cases.

PSER numerically evaluated with distinct strategies for different combinations of waves excited into the 2nd stage where the cascaded two stages case correspond to the scenarios shown in Fig. 5.12. The final outputs are assessed with respect to (a) and (c) the initial input at the first stage, (b) and (d) the output of the first stage, respectively.

In the former case, no other strategy exhibits a superior performance compared with the straightforward concatenation [the first case “Two stages” with a black solid line in Fig. 5.13 (a)] or just directly exciting all the seven waves into the second stage [the last case “1s2p2hs2hp” with a dark brown dashed line in Fig. 5.13 (b)]. In another general application scenario, considering regeneration at relay points or intermediate sections or relay stages, the output is assessed against the input of the second stage as presented in Fig. 5.13 (c) and Fig. 5.13 (d). The most promising strategy is still the overall excitation of all the waves for the second stage. In both scenarios, the more waves from the first stage are used, the better obtainable efficiency in terms of PSER. It is important to note that, even if compared with the tactics in which the dual pumps are regenerated before sending to the second stage thus achieving higher NPS, the direct excitation of as many

as possible waves from the first stage still offers the most competitive prospect. Such phenomena could be probably interpreted as according to the phase matching conditions determined by the nonlinear medium and the wavelength allocation, the high-order processes will inevitably take place, therefore leading to the emergence of high-order waves stemming from those processes with certain phase relation in between. This way, no matter what extra waves would be excited, all the waves will unavoidably grow and propagate along the medium with an expectable phase relation and share the limited total power. It should be also noted that the regeneration of some designated waves, usually the pumps, could increase the NPS in the second stage, however, at the expense of modifying the phase relations amongst the waves. As these kinds of regeneration do not change or impair the overall tendency of the evolution of all the waves, the growth of the waves has to be steered and reconstituted according to the phase matching condition and eventually again comply with their specified trends. Such that, to arrive at the same PSER peak, the cases with regenerated pumps demands a bit larger PSER. And the peak value is slightly higher due to the stronger NPS induced. Thereby, in a word, the most promising and potential concatenation strategy lies in the straightforward excitation of all the waves with their well-established phase relation.

5.8 Conclusion

In this chapter, a systematic optimization approach has been proposed for a regenerative PSA based on the more precise 7-wave model. On top of this, the performance of regenerative dual-pump degenerate PSA has been thoroughly investigated and analyzed for simultaneous phase and amplitude regeneration, an important building block of future all-optical processing. To bring the untapped regenerative potentialities into full play, we perform numerical estimations to exploit fundamental regenerative PSA through precise optimization comprising the wavelength allocation, nonlinear phase shift, and degree-of-saturation. Compared with the conventional 3-wave model, the predicted high PSER provides a relaxed margin for the underlying gain-saturation operation. Therefore, it permits to alleviate the accompanying amplitude fluctuation in phase squeezing with moderate power requirement. Such an optimized configuration facilitates the realization of simultaneous regeneration without compromising the performance. It also exhibits great potential to relieve the rigorous power restriction allowed for the input of an HNLF

due to the stimulated Brillouin scattering from the application point of view. With the proposed approach, the phase and amplitude noise reduction for regeneration of either BPSK or QPSK has been numerically studied.

Moreover, the interpretations and discussions regarding different concatenation strategies unveil the fact that, governed essentially by the phase matching conditions, one could hardly find a more promising solution than the straightforward excitation of all the relevant waves involved for cascaded identical PSA stages. Such comprehensive and versatile optimization approach could fully exploit the potential regenerative capability of PSA, providing a powerful tool for the application-oriented optimization in future all-optical processing networks.

Chapter VI

Conclusions and perspective

6.1 Conclusions and contribution

It is clear that the unique properties of the PSA are of particular benefit for the modern optical and photonic systems and subsystems. This thesis has been devoted to the theoretical investigation, characterization, evaluation, and optimization of the FOPA based PSA adopting comprehensive numerical analysis on the basis of the multi-wave model. Aiming at the thorough investigation and analysis of the PSA for the comprehensive optimization, in this work, we have established a more general 7-wave model that takes into account the high-order pumps, signals, and idlers stemming from the cascaded FWM processes in a dual-pump PS-FOPA configuration. With this model, it is allowed to precisely study and assess the phase-sensitive processes, leading to the accurate investigation of the behavior of the dual-pump PSA. Numerical analysis is carried out with the scope of comprehensive interpretation in order to sketch the physical picture of the underlying nonlinear interactions.

The gain properties, which are regarded as the most important characteristics of an amplifier, have been primarily studied using the proposed 7-wave model. The underlying relations between the phase matching conditions and interaction strength and the FWM efficiency have been unveiled. The signal gain at various pump configurations, as well as the phase-sensitivity, is obtained and interpreted by investigating the dominant FWM processes in terms of phase matching conditions. Moreover, the relation between the dispersion slope and the profile of the signal gain versus the pump-pump wavelength separation is revealed, permitting the application-oriented arbitrary tailoring of the signal gains by manipulating the dispersion profile and pump wavelength allocation.

From a more practical point of view, the analysis of regenerative capability of the PSA has been performed. This thus permits the overall optimization of the fundamental PSA configuration, offering the opportunities to fully exploit the untapped regenerative potential.

This model, as well as the proposed optimization approach, has enabled application-oriented optimization of the PSA and can be readily applied to virtually any similar applications for different all-optical processing functionalities.

6.2 Prospective

The remarkable progress of the PSAs, in particular, the PS-FOPA, has allowed the emergence of novel opportunities in not only fiber-optic communications and telecom communities but also many other fields in the entire ICT ecosystem.

Nowadays, advanced modulation formats usually explore the SOP of the lightwave to enlarge the transmission capacities. For example, polarization multiplexing quadrature phase shift keying (PM-QPSK) is the modulation technique of choice for 100 G and has become the standard for the commercial fiber-optical transmission systems. In this regard, the polarization characteristics of optical amplifiers have become critical. As a matter of fact, due to the polarization sensitive nature of FWM parametric processes, the PS-FOPA are highly dependent on the SOP of the pumps and the signals[17], [150]. A comprehensive description incorporating the polarization effects requires a fully vectorial form of the coupled-wave equations[151]. The polarization dependence on the gain properties would have particular importance for the relevant community[152]. On one hand, an ideal optical amplifier is supposed to be completely polarization independent, providing the same amplificative effect on the both SOP[153]. On the other hand, the polarization dependent peculiarity can be utilized for the regenerative purpose for polarization modulated signals[154]. Therefore, the investigation on the dependence of gain properties on the SOP of the interacting lightwaves is of special interest. This can be carried out by taking into account effects of the SOP of the waves. To this end, we will further extend our 7-wave model to a vectorial form. This is expected to have a lot of valuable findings.

Another important performance metric is the noise property, namely, the noise figure of the amplifiers. Since the gain properties are strongly dependent on the PSA configurations, it could be expected that the NF should behave quite similarly. However,

in the current literature, most of the analysis in NF are performed with conventional 3-wave model[155]. Though it could be difficult to end up with a uniform analytical result[156] for the NF in the cases when high-order waves are accounted for, it is still very important to understand the impact of these high-order waves on the NF of the signal of interest. For this purpose, the analysis of the noise performance based on the 7-wave model would be quite attractive. We can start this study following our findings in the noise transfer of BPSK and QPSK.

For the practical implementation of the PSAs, the volume, power consumption, and compatibility are also very critical issues that must be addressed. However, the state-of-the-art PS-FOPAs are still bulk and the systems are also sophisticated, which hampers the practical deployment. In this context, nano-scale on-chip photonic integration is one of the most promising directions[157]. Advanced materials and structures exhibit unprecedented nonlinearities than conventional silica optical fibers. For instance, materials with photonic crystal structure can manipulate and control the propagating lightwave by exploiting a photonic bandgap region in which light cannot travel[158], giving rise to a strong confinement of the light, and thus highly efficient nonlinearity. Due to the compatibility to the well-established industrial manufacturing technologies, silicon photonic integration has become the pioneer. Other materials, such as III-V semiconductors, exhibit considerable nonlinearities compared with silicon platforms. In addition, with a proper choice of the alloys, it allows exhibiting a large photonic bandgap at telecom wavelength, drastically reducing the nonlinear absorptions that are regarded as one main limiting factor when optical energy density becomes very large[159]. The investigation and exploitation of these novel materials will be of practically positive meanings. Towards these practical requirements, we focus on the GaP photonic crystal waveguide. This particular material combined a lot of attractive properties such as large bandgap at telecom wavelength ($\sim 2.26\,\mathrm{eV}$), silicon comparable high thermal conductivity ($110\ \mathrm{W/m \cdot K}$), large refractive index ($n = 3.06$) at 1550 nm, and transparency over a wide spectral range[160]. Collaborating with the researchers from the III-V laboratory at Thales Research Technologies, we have made a preliminary experimental characterization of the slow-light enhanced suspended GaP photonic crystal waveguide. Further investigation regarding the linear and nonlinear properties of such waveguide will be carried out.

Besides the PS-FOPA itself, other application fields that require low noise amplification are all the underlying beneficiary of the PSA technologies. In microwave photonics, one critical issue lies in the fact that the large conversion losses between the electrical domain and optical domain, which can be somewhat compensated by the amplifiers. Moreover, the noise of the optical amplifiers will be converted to the electrical domain by a factor of two due to the optical-power-to-electrical-current conversion at photodetectors[161]. This makes the low noise feature of PSA particularly valuable. In microwave photonics links, conventional EDFAs are not able to perform bi-directional amplification[162] while PSA features bi-directional optical amplification. Though in bi-directional transmission, the SBS effect and Rayleigh backscattering may lead to implementation challenges, the superb traits of PSA will still benefit a lot the performance of microwave photonics links. Low noise and high efficient microwave photonics link is one of the primary aims for our researches on the PS-FOPA and will be sought for in the future.

References

[1] F. Bretenaker and N. Treps, Laser 50 years of discoveries, Singapore: World Scientific, 2015.

[2] Laser and Optics, Verlag Berlin Heidelberg: Springer, 2012.

[3] P. A. Humblet and M. Azizoglu, "On the bit error rate of lightwave systems with optical amplifiers," *Journal of Lightwave Technology*, vol. 9, no. 11, pp. 1576–1582, Nov. 1991.

[4] K. C. Kao and G. A. Hockham. "Dielectric-fibre surface waveguides for optical frequencies," *Proc. IEE.*, vol. 113, no. 7, pp. 1151–1158, Jul. 1966.

[5] K. C. Kao and T. W. Davies, "Spectrophotometric Studies of Ultra Low Loss Optical Glasses - I: Single Beam Method," *Journal of Scientific Instruments (J. Physics E)*, Series 2, Vol. 1, pp. 1063-1068, 1968.

[6] F. Idachaba, D. U. Ike, and O. Hope, "Future Trends in Fiber Optics Communication," *Proc. World Congress on Engineering (WCE 2014)*, London UK., Jul. 2014.

[7] I. Hayashi, M. B. Panish, P. W. Foy, and S. Sumski, "Junction lasers which operate continuously at room temperature," *Appl. Phys. Lett.*, vol. 17, pp. 109–111, 1970.

[8] Z. I. Alferov, V. M. Andreev, D. Z. Garbuzov, Y. V. Zhilyaev, E. P. Morozov, E. L. Portnoi, and V. G. Triofim, "Investigation of the influence of the AlAs–GaAs heterostructure parameters on the laser threshold current and the realization of continuous emission at room temperature," *Fiz. Tekh. Poluprovodn.*, vol. 4, pp. 1826, 1970.

[9] T. Ikegami and Y. Suematsu, "Resonance-like characteristics of the direct modulation of a junction laser," *Proc. IEEE*, vol. 55, pp. 122–123, 1967.

[10] R. P. Rietz, "High speed semiconductor photodiodes," *Rev. Sci. Inst.*, vol. 33, pp. 994–999, 1962.

[11] J. E. Bowers, C. A. Burrus, and R. J. McCoy, "InGaAs PIN photodetectors with modulation response to millimeter wavelengths," *Electron. Lett.*, vol. 21, pp. 812–814, 1985.

[12] N. Thorsen, Fiber Optics and the Telecommunication Explosion, New York: Prentice Hall, 1998.

[13] R. H. Blumenthal, "Design of a microwave frequency light modulator," *Proc. IRE*, vol. 50, pp. 452–456, 1962.

[14] K. M. Johnson, "Microwave light modulation by the Pockel effect," *Microwave J.*, vol. 7, pp. 51–56, 1964.

[15] R. D. Standley and G. D. Mandeville, "Performance of an 11 GHz optical modulator using LiTaO," *Appl. Opt.*, vol. 10, pp. 1022–1023, 1971.

[16] K. Berchtold, O. Krumpholz, and J. Suri, "Avalanche photodiodes with a gain-bandwidth product of more than 200 GHz," *Appl. Phys. Lett.*, vol. 26, pp. 585–587, 1975.

[17] G. P. Agrawal, Lightwave Technology: Telecommunication Systems, New Jersey: John Wiley & Sons, 2005.

[18] D. N. Payne and W. A. Gambling, "Zero material dispersion in optical fibers," *Electron. Lett.*, vol. 11, pp. 176–178, 1975.

[19] T. Miya, Y. Terunuma, T. Hosaka, and T. Miyashita, "Ultimate low-loss single mode fiber at 1.55um," *Electron. Lett.*, vol. 15, pp. 106–108, 1979.

[20] G. E. Keiser, "A review of WDM technology and application," *Opt. Fiber Technol.*, vol. 5, pp. 3-39, Jan. 1999.

[21] E. Desurvire, Erbium-Doped Fiber Amplifiers, New York: Wiley, 1994.

[22] Y. Yamamoto and T. Mukai, "Fundamentals of optical amplifiers," *Fiber & Integrated Optics*, vol. 21, Special Issue on "Optical Amplifiers," pp. S1-S14, 1989.

[23] K. Fukuchi, T. Kasamatsu, M. Morie, R. Ohhira, T. Ito, K. Sekiya, D. Ogasahara, and T. Ono, "10.92-Tb/s (273 x 40-Gb/s) triple-band/ultra-dense WDM optical-repeated transmission experiment" *Proc. Optical Fiber Commun. Conf.*, 2001 Optical Society of America, Washington, DC, Paper PD24, 2001.

[24] T. Welsh, R. Smith, H. Azami, and R. Chrisner, "The FLAG cable system," *IEEE Commun. Mag.*, vol. 34, no. 2, pp. 30-35, Feb. 1996.

[25] W. C. Marra, and J. Schesser, "Africa ONE: the Africa Optical Network," IEEE Commun. Mag., vol. 34, no. 2, pp. 50-57, Feb. 1996.

[26] N. S. Bergano and H. Kidorf, "Global undersea cable networks," Opt. Photon. News, vol, 12, no. 3, pp. 32-35, 2001.

[27] A. K. Dutta, N. K. Dutta, and M. Fujiwara, *WDM Technologies: Passive Optical Components*, Burlington, MA: Academic Press, 2003.

[28] L. F. Mollenauer and K. Smith, "Demonstration of soliton transmission over more than 4000 km in fiber with loss periodically compensated by Raman gain", Opt. Lett., vol. 13, no. 8, pp. 675-677, Aug. 1988.

[29] S. Namiki and Y. Emori, "Ultrabroad-band Raman amplifiers pumped and gain-equalized by wavelength-division-multiplexed high-power laser diodes," IEEE J. Sel. Topics in Quantum Electron., vol. 7, no. 3, pp. 3-16, Feb. 2001.

[30] A. Hasegawa and F. Tappert, "Transmission of stationary nonlinear optical pulses in dispersive dielectric fibers. I. Anomalous dispersion", Appl. Phys. Lett., vol. 23, pp. 142, 1973.

[31] C. M. Caves, "Quantum limits on noise in linear amplifiers," Physical Review D, vol. 26, no. 8, pp. 1818-1839, Oct. 1982.

[32] J. Hansryd, P. A. Andrekson, M. Westlund, J. Li, and P.-O. Hedekvist, "Fiber-Based Optical Parametric Amplifiers and Their Applications," *IEEE J. Sel. Topics in Quantum Electron.*, vol. 8, no. 3, pp. 506-520, May/Jun. 2002.

[33] M. E. Marhic, N. Kagi, T.-K. Chiang, and L. G. Kazovsky, "Broadband fiber optical parametric amplifiers," *Opt. Lett.*, vol. 21, pp. 573–575, 1996.

[34] M.-C. Ho, K. Uesaka, M. E. Marhic, Y. Akasaka, and L. G. Kazovsky, "200-nm-bandwidth fiber optical amplifier combining parametric and Raman gain," *J. Lightwave Technol.*, vol. 19, pp. 977–981, Jul. 2001.

[35] S.-K. Choi, R.-D. Li, C. Kim, and P. Kumar, "Traveling-wave optical parametric amplifier: Investigation of its phase-sensitive and phase-insensitive gain response," *J. Opt. Soc. Amer. B*, vol. 14, pp. 1564–1575, 1997.

[36] K. O. Hill, D. C. Johnson, B. S. Kawasaki, and R. I. MacDonald, "CW three-wave mixing in single-mode optical fibers," *J. Applied Physics*, vol. 49, no. 10, pp. 5098-5106, 1978.

[37] M. Onishi, T. Okuno, T. Kashiwida, S. Ishikawa, N. Akasaka, and M. Nishimura, "Highly nonlinear dispersion-shifted fibers and their application to broadband wavelength converter," *Opt. Fiber Technol.*, vol. 4, pp. 204–214, 1998.

[38] D. L. Philen, D. W. Peckham, and I. Brener, "Measurement of the nonlinear index of refraction, N_2, for various fiber types," in *Proc. Optical Fiber Communication Conf.*, vol. 4, Baltimore, MD, 2000, pp. 184–186. Paper ThL5.

[39] J. Hansryd and P. A. Andrekson, "Broad-band continuous-wave-pumped fiber optical parametric amplifier with 49-dB gain and wavelength-conversion efficiency," *IEEE Photon. Technol. Lett.*, vol. 13, no. 3, Mar. 2001.

[40] G. P. Agrawal, Nonlinear Fiber Optics, 2nd ed. San Diego, CA: Academic, 1995.

[41] R. H. Stolen and J. E. Bjorkholm, "Parametric amplification and frequency conversion in optical fibers," *IEEE J. Quantum Electron.*, vol. QE-18, no. 7, pp. 1062–1072, 1982.

[42] G. Cappellini and S. Trillo, "Third-order three-wave mixing in single-mode fibers: Exact solutions and spatial instability effects," *J. Opt. Soc. Am. B*, vol. 8, no. 4, Apr. 1991.

[43] M. Karlsson, "Four-wave mixing in fibers with randomly varying zero dispersion wavelength," *J. Opt. Soc. Amer. B*, vol. 15, pp. 2269–2275, 1998.

[44] J. A. Levenson, I. Abram, Th. Rivera, and P. Grangier, "Reduction of quantum noise in optical parametric amplification," *J. Opt. Soc. Amer. B*, vol. 10, pp. 2233–2238, 1993.

[45] M. Karlsson, "Transmission Systems with Low Noise Phase-Sensitive Parametric Amplifiers," *J. Lightw. Technol.*, vol. 34, no. 5, pp. 1411-1423, Mar. 2016.

[46] L. Eldada, "Optical add/drop Multiplexing Architecture for Metro Area Networks," *SPIE Newsroom*, 1200801.0950, 2007.

[47] M. Westlund, J. Hansryd, P. A. Andrekson, and S. N. Knudsen, "Transparent wavelength conversion in fiber with 24 nm pump tuning range," *Electron. Lett.*, vol. 38, pp. 85–86, 2002.

[48] R. H. Stolen and J. E. Bjorkholm, "Parametric amplification and Frequency Conversion in Opitcal Fibers," *IEEE J. Quantum Electronics*, vol. QE-18, no. 7, pp. 1060-1072, Jul. 1982.

[49] K. Inoue, "Polarization independent wavelength conversion using fiber four-wave mixing with two orthogonal pump lights of different frequencies," *J. Lightwave Technol.*, vol. 12, pp. 1916–1920, Nov. 1994.

[50] Z. Tong, A. O. Wiberg, E. Myslivets, B. P. Kuo, N. Alic, and S. Radic, "Broadband parametric multicasting via four-mode phase-sensitive interaction," *Optics Express*, vol. 20, no. 17, pp. 19363–19373, 2012.

[51] A. D. Ellis, N. Mac Suibhne, D. Saad, and D. N. Payne, "Communication networks beyond the capacity crunch," *Phil. Trans. R. Soc. A*, vol. 374, no. 2062, 20150191, 2016.

[52] H. J. Thiele, A. D. Ellis, and I. D. Phillips, "Recirculating loop demonstration of 40 Gbit/s all-optical 3R data regeneration using a semiconductor nonlinear interferometer," *Electron. Lett.*, vol. 35, no. 3, pp, 230–231, 1999.

[53] M. A. Sorokina, "Design of multilevel amplitude regenerative system," *Optics Letters*, vol. 39, no. 8, pp. 2499–2502, 2014.

[54] T. Roethlingshoefer, G. Onishchukov, B. Schmauss, G. Leuchs, "All-optical simultaneous multilevel amplitude and phase regeneration," *IEEE Photon. Technol. Lett.*, vol. 26, no. 6, pp. 556–559, 2014.

[55] K. Sponsel, K. Cvecek, C. Stephan, G. Onishchukov, B. Schmauss, and G. Leuchs, "Optimization of a Nonlinear Amplifying Loop Mirror for Amplitude Regeneration in Phase-

Shift-Keyed Transmission," *IEEE Photon. Technol. Lett.*, vol. 19, no. 22, Nov. 2007.

[56] T. Roethlingshoefer, T. Richter, C. Schubert, G. Onishchukov, B. Schmauss, and G. Leuchs, "All-optical phase-preserving multilevel amplitude regeneration," *Optics Express*, vol. 22, no. 22, pp. 27077–27085, 2014.

[57] J. Leuthold, B. Mikkelsen, R. E. Behringer, G. Raybon, C. H. Joyner, and P.-A. Besse, "Novel 3R regenerator based on semiconductor optical amplifier delayed-interference configuration," *IEEE Photon. Technol. Lett.*, vol. 13, no. 8, pp. 860–862, 2001.

[58] S. Koenig, R. Bonk, H. Schmuck, W. Poehlmann, Th. Pfeiffer, C. Koos, W. Freude, and J. Leuthold, "Amplification of advanced modulation formats with a semiconductor optical amplifier cascade," *Optics Express*, vol. 22, no. 15, pp. 17854-17871, Jul. 2014.

[59] Z. Zhu, M. Funabashi, P. Zhong, L. Paraschis, D. L. Harris, and S. J. B. Yoo, "High-performance optical 3R regeneration for scalable fiber transmission system applications," *J. Lightwave Technol.*, vol. 25, no. 2, pp. 504–511, 2007.

[60] J. Kakande, R. Slavik, F. Parmigiani, A. Bogris, D. Syvridis, L. Gruner-Nielsen, R. Phelan, P. Petropoulos, and D. J. Richardson, "Multilevel quantization of optical phase in a novel coherent parametric mixer architecture," *Nat. Photonics*, vol. 5, no. 12, pp. 748–752, 2011.

[61] S. Sygletos, M. E. McCarthy, S. J. Fabbri, M. A. Sorokina, M. F. C. Stephens, I. D. Phillips, E. Giacoumidis, N. M. Suibhne, P. Harper, N. J. Doran, S. K. Turitsyn, and A. D. Ellis, "Multichannel regeneration of dual quadrature signals," in *Proc. ECOC 2014*, paper We.1.5.4.

[62] A. D. Ellis, J. Zhao, and D. Cotter, "Approaching the non-linear Shannon limit," *J. Lightwave Technology*, vol. 28, no. 4, pp. 423–433, Feb. 2010.

[63] K. S. Turitsyn and S. K. Turitsyn, "Nonlinear communication channels with capacity above the linear Shannon limit," *Opt. Lett.*, vol. 330, no. 17, pp. 3600–3602, Sep. 2012.

[64] D. J. Richardson, "Filling the light pipe," *Science*, vol. 37, pp. 327–328, Oct. 2010.

[65] Z. Zhu, M. Funabashi, P. Zhong, X. Bo, L. Paraschis, and S. J. B. Yoo, "Jitter and amplitude noise accumulations in cascaded all-optical regenerators," *IEEE J. Lightwave Technol.*, vol. 26, no. 12, pp. 1640–1652, 2008.

[66] J. Capmany and D. Novak, "Microwave photonics combines two worlds," *Nature Photonics*, vol. **1**, pp. 319-330, 2007.

[67] A. J. Seeds and K. J. Williams, "Microwave Photonics," *Journal of Lightwave Technology* **24**(12), 4628-4641 (2006).

[68] J. Yao, "Microwave Photonics," *J. Lightwave Technology*, vol. 27, no. 3, pp. 314-335, Feb. 2009.

[69] J. Capmany and P. Munoz, "Integrated Microwave Photonics for Radio Access Networks," *J. Lightwave Technology*, vol. 32, no. 16, pp. 2849-2861, Aug. 2014.

[70] L. Bui, M. Pelusi, T. D. Vo, N. Sarkhosh, H. Emami, B. J. Eggleton, and A. Mitchell, "Instantaneous frequency measurement system using optical mixing in highly nonlinear fiber," *Optics Express*, vol. 17, no. 25, pp. 22983–22991, 2009.

[71] H. Emami and M. Ashourian, "Improved dynamic range microwave photonic instantaneous frequency measurement based on four-wave mixing," *IEEE Trans. Microw. Theory Technol.*, vol. 62, no. 10, pp. 2462–2470, 2014.

[72] P. Berger, J. Bourderionnet, F. Bretenaker, D. Dolfi, S. Ó Dúill, G. Eisenstein, and M. Alouini, "Intermodulation distortion in microwave phase shifters based on slow and fast light propagation in semiconductor optical amplifiers," *Opt. Lett.*, vol. 35, no. 16, pp. 2762-2764, Aug. 2010.

[73] A. Bhatia, H.-F. Ting, and M. A. Foster, "Linearization of phase-modulated analog optical links using a four-wave mixing comb source," *Opt. Expr.*, vol. 22, no. 25, pp. 30899-30909, Dec. 2014.

[74] C.-S. Brès, A. O. J. Wiberg, B. P.-P. Kuo, B. Stossel, and S. Radic, "Characterization of Distortionless Analog Signal Multicasting by Parametric Mixer," *Technical Digest Optical Fiber Communication Conference (OFC 2010)*, paper OWT2.

[75] R. Loudon, The Quantum Theory of Light, Oxford University Press, 2000.

[76] J. D. Kraus, Radio Astronomy, McGraw-Hill, 1966.

[77] J. P. Gordon, H. J. Zeiger, and C. H. Townes, "The Maser – New type of microwave amplifier, frequency standard, and spectrometer," *Physical Review*, vol. 99, no. 4, pp. 1264-1274, Aug. 1955.

[78] A. L. Schawlow and C. H. Townes, "Infrared and Optical Masers," *Physical Review*, vol. 112, no. 6, pp. 1940-1949, Dec. 1958.

[79] T. H. Maiman, "Optical and Microwave-optical Experiments in Ruby," *Physical Review Letters*, vol. 4, no. 11, pp. 564-567, Jun. 1960.

[80] T. H. Maiman, “Stimulated optical radiation in ruby masers,” *Nature*, vol. 187, pp. 493–494, 1960.

[81] P. A. Franken, A. E. Hill, C. W. Peters, G. Weinreich, "Generation of Optical Harmonics," *Physical Review Letters*, vol. 7, no. 4, pp. 118–119, Aug. 1961.

[82] R. W. Boyd, Nonlinear Optics, 3rd ed, Academic Press, 2003.

[83] Y. R. Shen, Principles of Nonlinear Optics, Wiley, 1984.

[84] J. A. Armstrong, N. Bloembergen, J. Ducuing, and P. S. Pershan, "Interactions between light waves in a nonlinear dielectric," *Physical Review*, vol. 127, no. 6, pp. 1918-1939, Sep. 1962.

[85] N. M. Kroll, "Parametric amplification in spatially extended media and application to the design of tuneable oscillators at optical frequencies," *Proceedings of the IEEE*, vol. 51, no. 1, pp. 110-114, Jan. 1963.

[86] D. J. Lovering, J. A. Levenson, P. Vidakovic, J. Webjorn, and P. S. J. Russell, "Noiseless optical amplification in quasi-phase-matched bulk lithium niobate," *Optics Letters*, vol. 21, no. 18, pp. 1439-1441, Sep. 1996.

[87] R. H. Stolen, "Phase-matched-stimulated four-photon mixing in silica-fiber waveguides," *IEEE Journal of Quantum Electronics*, vol. QE-11, no. 3, pp. 100-103, Mar. 1975.

[88] D. Hewak, Properties, processing, and applications of glass and rare earth-doped glasses for optical fibres, Stevenage, GB, EMIS Group, 1998.

[89] S. F. Jacobs, M. Sargent III, J. F. Scott, and M. O. Scully, "Laser Applications to Optics and Spectroscopy," vol. 2, Addison-Wesley, 1975.

[90] T. Okuno, M. Onishi, T. Kashiwada, S. Ishikawa, and M. Nichimura, "Silica-based functional fibers with enhanced nonlinearity and their applications," *IEEE J. Sel. Topics Quantum Electron.*, vol. 5, no. 5, pp. 1385-1391, Sep./Oct. 1999.

[91] M. A. Newhouse, D. L. Weidman, and D. W. Hall, "Enhanced-nonlinearity single-mode lead silicate optical fiber," *Optics Letter*s, vol. 15, no. 21, pp. 1185-1187, 1990.

[92] I. Kang, T. D. Krauss, F. W. Wise, B. G. Aitken, and N. F. Borrelli, "Femtosecond measurement of enhanced optical nonlinearities of sulfide glasses and heavy metal doped oxide glasses," *J. Opt. Soc. Am. B*, vol. 12, no. 11, pp. 2053–2059, Nov. 1995.

[93] R. E. Slusher, G. Lenz, J. Hodelin, J. Sanghera, L. B. Shaw, and I. D. Aggarwal, "Large Raman gain and nonlinear phase shifts in high-purity As2Se3 chalcogenide fibers," *J. Opt. Soc. Am. B*, vol. 21, no. 6, pp. 1146=1155, 2004.

[94] L. B. Fu, M. Rochette, V. G. Ta'eed, D. J. Moss, and B. J. Eggleton, "Investigation of self-phase modulation based optical regeneration in single mode As2Se3 chalcogenide glass fiber," *Opt. Express*, vol. 13, no. 19, pp. 7637-7644, 2005.

[95] L. Brilland, F. Smektala, G. Renversez, T. Chartier, J. Troles, T. Nguyen, N. Traynor, and A. Monteville, "Fabrication of complex structures of Holey Fibers in Chalcogenide glass," *Opt. Express*, vol. 14, no. 3, pp. 1280-1285, 2006.

[96] R. H. Stolen, E. P. Ippen, and A. R. Tynes, "Raman Oscillation in Glass Optical Waveguide,"

Appl. Phys. Lett., vol. 20, no. 2, pp. 62-64, Jan. 1972.

[97] E. P. Ippen and R. H. Stolen, "Stimulated Brillouin scattering in optical fibers," *Appl. Phys. Lett.*, vol. 21, no. 11, pp. 539-541, Dec. 1972.

[98] R. G. Smith, "Optical Power Handling Capacity of Low Loss Optical Fibers as Determined by Stimulated Raman and Brillouin Scattering," *Appl. Opt.*, vol. 11, no. 11, pp. 2489, Nov. 1972.

[99] R. H. Stolen, "The Early Years of Fiber Nonlinear Optics," *J. Lightwave Technology*, vol. 26, no. 9, pp. 1021-1031, May 2008.

[100] T. Li, Ed., Optical Fiber Communications: Fiber Fabrication, vol. 1 (Academic Press), 1985.

[101] U. C. Paek, "High-speed high-strength fiber drawing," J. Lightwave Technol., vol. 4, no. 8, pp. 1048-1060, 1986.

[102] C. Sulem and P.-L. Sulem, The Nonlinear Schrödinger Equations: Self-Focusing and Wave Collapse, Springer, 1999.

[103] M. Ohashi, K. Kitayama, Y. Ishida, and N. Uchida, " Stress-induced frequency tuning for stimulated four-photon mixing in a birefringent single-mode fiber," *Appl. Phys. Lett.*, vol. 41, no. 4, pp. 1111-1113, 1982.

[104] I. Bar-Joseph, A. A. Friesem, R. G. Waarts, and H. H. Yaffe, "Parametric interaction of a modulated wave in a single-mode fiber," *Opt. Lett.*, vol. 11, no. 8, pp. 534, Aug. 1986.

[105] M. E. Marhic, N. Kagi, T. K. Chiang, and L. G. Kazovsky, "Broadband fiber optical parametric amplifiers," *Opt. Lett.*, vol. 21, no. 8, pp. 573-575, Apr. 1996.

[106] M. E. Marhic, Y. Park, F. S. Yang, and L. G. Kazovsky, "Broadband fiber-optical parametric amplifiers and wavelength converters with low-ripple Chebyshev gain spectra," *Opt. Lett.*, vol. 21, no. 17, pp. 1354-1356, Sep. 1996.

[107] F. S. Yang, "High-nonlinearity fiber optical parametric amplifier with periodic dispersion compensation," *J. Lightwave Technol.*, vol. 17, no. 2, pp. 210-215, 1999.

[108] S. Watanabe and M. Shirasaki, "Exact compensation for both chromatic dispersion and Kerr effect in a transmission fiber using optical phase conjugation," *J. Lightwave Technol.*, vol. 14, no. 3, pp. 243-248, Mar. 1996.

[109] F. Yaman, Q. Lin, S. Radic, and G. P. Agrawal, "Impact of dispersion fluctuations on dual-pump fiber-optic parametric amplifiers," *IEEE Photon. Technol. Lett.*, vol. 16, no. 5, pp. 1292-1294, May 2004.

[110] R. Tang, J. Lasri, P. S. Devgan, V. Grigoryan, P. Kumar, and M. Vasilyev, "Gain characteristics of a frequency nondegenerate phase-sensitive fiber-optic parametric amplifier with phase self-

stabilized input," *Opt. Expr.*, vol. 13, no. 26, pp. 10483-10493, Dec. 2005.

[111] H. Heffner, "The fundamental noise limit of linear amplifiers," *Proceedings of the IRE*, vol. 50, no. 7, pp. 1604–1608, Jul. 1962.

[112] C. J. McKinstrie and S. Radic, "Phase-sensitive amplification in a fiber," *Opt. Expr.*, vol. 12, no. 20, pp. 4973–4979, Sep. 2004.

[113] M. Baillot, T. Chartier, and M. Joindot, "Multiple four-wave mixing in optical fibers," in *European Conference on Optical Communication*, (ECOC, 2014), p. We.3.7.2.

[114] M. Baillot, M. Gay, C. Peucheret, M. Joindot, and T. Chartier, "Phase quadrature discrimination based on three-pump four-wave mixing in nonlinear optical fibers," *Opt. Expr.*, vol. 24, no. 23, pp. 26930–26941, Nov. 2016.

[115] M. E. Marhic, A. A. Rieznik, G. Kalogerakis, C. Braimiotis, H. L. Fragnito, and L. G. Kazovsky, "Accurate numerical simulation of short fiber optical parametric amplifiers," *Opt. Expr.*, vol. 16, no. 6, pp. 3610–3622, 2008.

[116] Z. Tong, C. Lundstrom, P. A. Andrekson, C. J. McKinstrie, M. Karlsson, D. J. Blessing, E. Tipsuwannakul, B. J. Puttnam, H. Toda, and L. Grüner-Nielsen, "Towards ultrasensitive optical links enabled by low-noise phase-sensitive amplifiers," *Nat. Photonics*, vol. 5, no. 7, pp. 430–436, 2011.

[117] Z. Tong and S. Radic, "Low-noise optical amplification and signal processing in parametric devices," *Adv. Opt. Photonics*, vol. 5, no. 3, pp. 318, 2013.

[118] C.-S. Brès, A. O. J. Wiberg, B. P.-P. Kuo, E. Myslivets, N. Alic, B. Stossel, and S. Radic, "RF photonic link employing optical phase sensitive amplification," *Optical Fiber Communication Conference*, OSA Technical Digest (Optical Society of America, 2012), paper OM3B.5.

[119] A. Agarwal, T. Banwell, and T.K. Woodward, "Low distortion multicasting of an analog signal by self-seeded parametric mixer," *IEEE Photonics Technol. Lett.*, vol. 22, no. 5, pp. 332–334, 2010.

[120] I. Fsaifes, T. Labidi, F. Goldfarb, and F. Bretenaker, "Intermodulation distortion analysis of an analog photonic link employing parametric phase-sensitive amplification," in *European Conference on Optical Communication*, (ECOC, 2014), paper P.1.10.

[121] A. Bhatia, H.-F. Ting, and M. A. Foster, "Linearization of phase-modulated analog optical links using a four-wave mixing comb source," *Opt. Expr.*, vol. 22, no. 25, pp. 30899–30909, 2014.

[122] A. Vedadi, A. Mussot, E. Lantz, H. Maillotte, and T. Sylvestre, "Theoretical study of gain distortions in dual pump fiber optical parametric amplifiers," *Opt. Commun.*, vol. 267, no. 1, pp.

244–252, 2006.

[123] G. Ferrini, I. Fsaifes, T. Labidi, F. Goldfarb, N. Treps, and F. Bretenaker, "Symplectic approach to the amplification process in a nonlinear fiber: role of signal-idler correlations and application to loss management," *J. Opt. Soc. Am. B*, vol. 31, no. 7, pp. 1627–1641, 2014.

[124] C. J. McKinstrie and S. Radic, "Parametric amplifiers driven by two pump waves with dissimilar frequencies," *Opt. Lett.*, vol. 27, no. 13, pp. 1138–1140, 2002.

[125] A. Vedadi, M. E. Marhic, E. Lantz, H. Maillotte, and T. Sylvestre, "Investigation of gain ripple in two-pump fiber optical parametric amplifiers," *Opt. Lett.*, vol. 33, no. 19, pp. 2203–2205, 2008.

[126] M. E. Marhic, A. A. Rieznik, and H. L. Fragnito, "Investigation of the gain spectrum near the pumps of two pump fiber-optic parametric amplifier," *J. Opt. Soc. Am. B*, vol. 25, no. 1, pp. 22–30, 2008.

[127] M. Gao, T. Inoue, T. Kurosu, and S. Namiki, "Evolution of the gain extinction ratio in dual-pump phase sensitive amplification," *Opt. Lett.*, vol, 37, no. 9, pp. 1439–1441, 2012.

[128] Y. Meng, J. Lian, S. Fu, M. Tang, P. Shun, and D. Liu, "All-optical DPSK regenerative one-to-nine wavelength multicasting using dual-pump degenerate phase sensitive amplifier," *J. Lightwave Technol.*, vol. 32, no. 15, pp. 2605–2612, 2014.

[129] W. Xie, I. Fsaifes, T. Labidi, and F. Bretenaker, "Investigation of degenerate dual-pump phase sensitive amplifier using multi-wave model," *Opt. Expr.*, vol. 23, no. 25, pp. 31896-31907, Dec. 2015.

[130] M. Karlsson, "Transmission Systems with Low Noise Phase-Sensitive Parametric Amplifiers," *J. Lightwave Technol.*, vol. 34, no. 5, pp. 1411–1423, Mar. 2016.

[131] A. Bogris, and E. Pikasis, "Enhanced Multi-Level Phase Quantizer for the Optical Processing of M-PSK Signals," *J. Lightwave Technol.*, vol. 34, no. 10, pp. 2571–2577, May 2016.

[132] R. J. Essiambre, G. Kramer, P. J. Winzer, G. J. Foschini, and B. Goebel, "Capacity limits of optical fiber networks," *J. Lightwave Technol.*, vol. 28, no. 4, pp. 662–701, 2010.

[133] R. Slavík, F. Parmigiani, J. Kakande, C. Lundström, M. Sjödin, P. A. Anderson, R. Weerasuriya, S. Sygletos, A. D. Ellis, L. Grüner-Nielsen, D. Jakobsen, S. Herstrom, R. Phelan, J. O'Gorman, A. Bogris, D. Syvridis, S. Dasgupta, P. Petropoulos, and D. J. Richardson, "All-optical phase and amplitude regenerator for next generation telecommunications systems," *Nat. Photonics*, vol. 4, no. 10, pp. 690–695, 2010.

[134] J. Parra-Cetina, A. Kumpera, M. Karlsson, and P. A. Andrekson, "Phase-sensitive fiber-based

parametric all-optical switch," *Opt. Express*, vol. 23, no. 26, pp. 33426–33436, 2015.

[135] M. Karlsson, "Transmission systems with low noise phase-sensitive parametric amplifiers," *J. Lightwave Technol.*, vol. 34, no. 5, pp. 1411–1423, 2016.

[136] S. L. Olsson, M. Karlsson, and P. A. Andrekson, "Nonlinear phase noise mitigation in phase-sensitive amplified transmission systems," *Opt. Express*, vol. 23, no. 9, pp. 11724–11740, 2015.

[137] F. Parmigiani, G. Hesketh, R. Slavík, P. Horak, P. Petropoulos, and D. J. Richardson, "Polarization-assisted phase-sensitive processor," *J. Lightwave Technol.*, vol. 33, no. 6, pp. 1166–1174, 2015.

[138] C. Lundström, B. Corcoran, M. Karlsson, and P. A. Andrekson, "Phase and amplitude characteristics of a phase sensitive amplifier operating in gain saturation," *Opt. Expr.*, vol. 20, no. 19, pp. 21400–21412, 2012.

[139] M. Gao, T. Kurosu, T. Inoue, and S. Namiki, "Efficient phase regeneration of DPSK signal by sideband-assisted dual-pump phase-sensitive amplifier," *Electron. Lett.*, vol. 49, no. 2, pp. 140–141, 2013.

[140] M. Gao, T. Kurosu, T. Inoue, and S. Namiki, "Low-penalty phase de-multiplexing of QPSK signal by dual-pump phase sensitive amplifiers." 39th *European Conference and Exhibition on Optical Communication*, OSA Technical Digest (CD) (Optical Society of America, 2013), p. We. 3. A. 5.

[141] J. Kakande, R. Slavík, F. Parmigiani, A. Bogris, D. Syvridis, L. Grüner-Nielsen, R. Phelan, P. Petropoulos, and D. J. Richardson, "Multilevel quantization of optical phase in a novel coherent parametric mixer architecture," *Nat. Photonics*, vol. 5, no. 12, pp. 748–752, 2011.

[142] T. Kurosu, M. Gao, K. Solis-Trapala, and S. Namiki, "Phase regeneration of phase encoded signals by hybrid optical phase squeezer," *Opt. Expr.*, vol. 22, no. 10, pp. 12177–12188, 2014.

[143] R. P. Webb, M. Power, and R. J. Manning, "Phase-sensitive frequency conversion of quadrature modulated signals," *Opt. Expr.*, vol. 21, no. 10, pp. 12713–12727, 2013.

[144] K. R. H. Bottrill, F. Parmigiani, L. Jones, G. Hesketh, D. J. Richardson, and P. Petropoulos, "Phase and amplitude regeneration through sequential PSA and FWM saturation in HNLF," in *Proceedings of the European Conference on Optical Communication* (IEEE, 2015), p. We.3.6.3.

[145] F. Parmigiani, K. R. H. Bottrill, R. Slavík, D. J. Richardson, and P. Petropoulos, "Multi-channel phase regenerator based on polarization-assisted phase-sensitive amplification," *IEEE Photonics Technol. Lett.*, vol. 28, no. 8, pp. 845–848, 2016.

[146] F. Parmigiani, G. D. Hesketh, R. Slavík, P. Horak, P. Petropoulos, and D. J. Richardson, "Optical

phase quantizer based on phase sensitive four wave mixing at low nonlinear phase shift," *IEEE Photonics Technol. Lett.*, vol. 26, no. 21, pp. 2146–2149, 2014.

[147] C. Lundström, Z. Tong, M. Karlsson, and P. A. Andrekson, "Phase-to-phase and phase-to-amplitude transfer characteristics of a nondegenerate-idler phase-sensitive amplifier," *Opt. Lett.*, vol. 36, no. 22, pp. 4356–4358, 2011.

[148] K. Saito and H. Uenohara, "Analytical investigation of operating conditions for simultaneous intensity and phase noise suppression using phase sensitive semiconductor optical amplifiers," *Optical Fiber Communication Conference*, OSA Technical Digest (CD) (Optical Society of America, 2013), p. JTh2A.31.

[149] W. Xie, I. Fsaifes, and F. Bretenaker, "Optimization of a degenerate dual-pump phase-sensitive optical parametric amplifier for all-optical regenerative functionality," *Opt. Expr.*, vol. 25, no. 11, pp. 12552-12565, May 2017.

[150] M. E. Marhic, Fiber Optical Parametric Amplifiers, Oscillators and Related Devices, Cambridge University Press, 2008.

[151] C. J. McKinstrie, S. Radic, and C. Xie, "Phase conjugation driven by orthogonal pump waves in birefringent fibers", *J. Opt. Soc. Am. B*, vol. 20, no. 7, pp. 1437-1446, Jul. 2003.

[152] C. J. McKinstrie and S. Radic, "Phase-sensitive amplification in a fiber", *Opt. Expr.*, vol. 12, no. 20, pp. 4973-4979, Sep. 2004.

[153] Qiang Lin and Govind P. Agrawal, "Vector theory of four-wave mixing: polarization effects in fiber-optic parametric amplifiers", *J. Opt. Soc. Am. B*, vol. 21, no. 6, pp. 1216-1224, Jun. 2004.

[154] W. Yang, Y. Yu, M. Ye, G. Chen, C. Zhang, and X. Zhang, "Phase regeneration for polarization-division multiplexed signals based on vector dual-pump nondegenerate phase sensitive amplification", *Opt. Expr.*, vol. 23, no. 3, pp. 2010-2020, Jan. 2015.

[155] Z. Tong, A. Bogris, C. Lundström, C. J. McKinstrie, M. Vasilyev, M. Karlsson, and P. A. Andrekson, "Modeling and measurement of the noise figure of a cascaded non-degenerate phase-sensitive parametric amplifier", *Opt. Expr.*, vol. 18, no. 14, pp. 14820-14835, Jun. 2010.

[156] K. Inoue, “Quantum noise in parametric amplification under phase-mismatched conditions”, *Optics Communications*, vol. 366, pp. 71-76, 2016.

[157] M. A. Foster, A. C. Turner, M. Lipson, and A. L. Gaeta, "Nonlinear optics in photonic nanowires", *Opt. Expr.*, vol. 16, no. 2, pp. 1300-1320, Jan. 2008.

[158] T. Baba, "Photonic crystals - Remember the light", *Nat. Photon.*, vol. 1, pp. 11-12, Jan. 2007.

[159] I. Cestier, S. Combrié, S. Xavier, G. Lehoucq, A. de Rossi, and G. Eisenstein, "Chip-scale

parametric amplifier with 11 dB gain at 1550 nm based on a slow-light GaInP photonic crystal waveguide", *Optics Letters*, vol. 37, no. 19, pp. 3996-3998, Oct. 2012.

[160] K. Rivoire, Z. Lin, F. Hatami, W. Ted Masselink, and J. Vuckovic, "Second harmonic generation in gallium phosphide photonic crystal nanocavities with ultralow continuous wave pump power", *Optics Express*, vol. 17, no. 25, pp. 22609-22615, Nov. 2009.

[161] V. J. Urick, M. E. Godinez, P. S. Devgan, J. D. McKinney, and F. Bucholtz, "Analysis of an Analog Fiber-Optic Link Employing a low-biased Mach–Zehnder modulator followed by an erbium-doped fiber amplifier", *J. Lightw. Technol.*, vol. 27, no. 12, pp. 2013-2019, Jun. 2009.

[162] A. Karim and J. Devenport, "Noise figure reduction in externally modulated analog fiber-optic links", *IEEE Photon. Technol. Lett.*, vol. 19, no. 5, pp. 312-314, Mar. 2007.

RÉSUMÉ (EN FRANÇAIS)

La capacité et les performances des systèmes et sous-systèmes photoniques à fibres optiques déployés sur de grandes distances dépendent fortement des performances des amplificateurs optiques comme leurs propriétés de bruit, leur bande passante de gain, et leurs non-linéarités. Les amplificateurs optiques conventionnels, même s'ils sont basés sur différents processus physiques, imposent tous sans exception un bruit supplémentaire pendant le processus d'amplification. Ceci entraîne une dégradation du rapport signal à bruit, conduisant à un facteur de bruit d'au moins 3 dB pour ces amplificateurs conventionnels. Ces derniers sont souvent appelés amplificateurs insensibles à la phase (PIA). Dans ce contexte, les amplificateurs paramétriques à fibre optique (PS-FOPA), reposant sur l'interaction non-linéaire à quatre ondes (FWM) dans les fibres optiques de silice, surpassent les PIA conventionnels grâce à leur propriété unique de compression de phase. La plupart de leurs caractéristiques, y compris le gain et le facteur de bruit, dépendent de la phase relative initiale des quatre ondes qui interagissent. Par conséquent, ils peuvent être exploités pour améliorer les caractéristiques fondamentales de l'amplification, c'est-à-dire l'amplification sans bruit ajouté et l’ obtention d’un spectre de gain ultra-large, ainsi que pour diverses applications avancées telles que la compensation de la distortion non linéaire et la régénération du signal. Avec d'autres fonctionnalités intéressantes comme la conversion de longueur d'onde et la conjugaison de phase, les PS-FOPA sont considérés comme des candidats prometteurs pour les prochaine générations d'amplificateurs optiques utilisables en communications tout optiques, traitement de signal et dans les réseaux.

Le PS-FOPA peut être décrit de manière classique par les équations d'ondes couplées fondamentales, qui peuvent être dérivées de l'équation de Schrödinger non linéaire. La forme générale des équations d'ondes couplées régissant les FOPA ne

contient généralement que trois ou quatre équations différentielles ordinaires, correspondant aux trois ou quatre ondes en interaction selon le mécanisme FWM. Cependant, dans des situations plus générales, les ondes d'ordre élevé qui sont inévitablement générées par les processus de FWM en cascade affecteront forcément les caractéristiques des PS-FOPA. Elles modifieront les propriétés de gain, la sensibilité en phase et la valeur du facteur de bruit. Par conséquent, il est très important de disposer d'un modèle théorique plus précis qui fournit une description détaillée du PS-FOPA en tenant compte de la contribution de toutes les harmoniques. Avec l'aide d'un tel modèle, nous pouvons espérer maîtriser plus précisément les caractéristiques du PS-FOPA, conduisant à l'exploitation efficace de la capacité d'amplification potentielle.

A cette fin, l'objectif de cette thèse est d'étudier de manière approfondie les propriétés linéaires et non linéaires du PS-FOPA dégénéré à double pompe, en termes de propriétés de gain et de sensibilité en phase pour différentes configurations. À partir de l'équation de Schrödinger non linéaire fondamentale, le modèle dit à 7 ondes, contenant un ensemble de sept équations différentielles ordinaires complexes a été établi. Outre les trois ondes fondamentales, le signal et deux pompes, ce modèle incorpore également les équations représentant les signaux d'ordre plus élevé et les pompes d'ordre plus élevé issues des processus FWM en cascade. Avec l'apparition de ces ondes supplémentaires, ce modèle permet de décrire l'interaction complexe non linéaire entre toutes les ondes, conduisant à une analyse numérique plus précise du PS-FOPA dégénéré à double pompe. Par conséquent, ce modèle permet de donner une interprétation physique plus précise des interactions multi-ondes basée sur les conditions d'accord de phase et l'efficacité de l'interaction, révélant les relations sous-jacentes entre la dispersion, la sensibilité de phase et les propriétés de gain. De plus, la capacité de régénération simultanée de phase et d'amplitude d'un PS-FOPA est évaluée dans le but d'une optimisation globale du processus de régénération. Ceci permet d'exploiter pleinement la capacité de régénération potentielle d'une configuration PS-FOPA de base agissant comme un bloc de construction fondamental des futures fonctionnalités tout-optiques. L'approche basée sur ce modèle permet une optimisation orientée vers l'application et est particulièrement utile pour la conception et l'optimisation de tels PS-FOPAs, et peut être appliquée de manière répétée dans divers scénarios d'application.

Appendix I

Works related to co-supervision

In the framework of a co-supervision agreement between Shanghai Jiao Tong University and Universite Paris-Sud, part of my Ph.D. works has been accomplished in the two countries. In the following, I summarize the work I have done in the group led by Prof. Yi Dong in Shanghai Jiao Tong University.

State-of-the-art laser-based optical frequency combs have become valuable tools for an ever-increasing number of applications and have to date revolutionized a wide range of fields from fundamental science to modern applications. Most of the application scenarios have extended beyond the original purpose of accurate frequency metrology, such as laser spectroscopy, molecular sensing, coherent measurement, LIDAR, coherent optical communication, coherent beam steering, and microwave photonics. Modern optical frequency combs usually act as a precise frequency grid operating in the optical domain capable of providing a large number of equally spaced comb modes across a broad optical spectral range with unprecedented accuracy and stability. The endless progress and the emerging applications have driven the comb generation for higher precision and accuracy, as well as a broader spectral range with better tunability and flexibility across the entire spectrum.

To this end, there are mainly three techniques that can be utilized for the generation of advanced optical frequency combs. As a first technique, mode-locked lasers (MLLs) can be applied to generate frequency combs extending up to an optical bandwidth broader than an octave. Especially the comb synthesizer with self-referenced MLL, exhibiting superb precision and stability are explored and contribute to progress in comb generation. A second approach lies in the electro-optic modulation on the conventional continuous-wave laser. In order to achieve the high precision and accuracy on the comb modes, the mode spacing should be maintained stable. In general, this is achieved by phase-locking

the mode spacing to a highly stable microwave reference. Aiming at diversified instrumental objectives, technical requirements in terms of mode-spacing, center frequency, spectral coverage and shape, phase noise i.e. coherence, and stability, a growing number of research groups have focused on the nonlinear optical technology. By exploring the latest advent of highly nonlinear dispersion-engineered on-chip nanophotonic waveguides, resonators, and other active devices, it allows generating frequency combs with a variety of unique properties such as direct synthesis in mid-infrared range and ultra-wide mode spacings.

Nevertheless, the relatively large mode spacing has limited the performance in many applications. Therefore, a frequency comb with tunable mode spacing is highly desirable. Furthermore, in application scenarios such as spectroscopy, coherent sensing, microwave photonics, and LIDAR, phase-continuous tunability of the mode spacing is of unique benefit. According to the operation principle of the mode-locked laser and the electro-optic modulation, it is not straightforward to achieve this phase-continuous tunability of the mode spacing while preserving the stability of the comb. Thus, such unique property of the frequency comb has gone largely overlooked so far.

To this end, on the basis of the operational principle, the frequency comb generation based on electro-optic modulation has been explored. In order to preserve the stable operation of the whole frequency comb while tuning the mode spacing, the difference between the electrical and the optical propagation delays is precisely measured and accurately compensated. As a consequence, the broadband phase matching can be thus achieved regardless of the mode-spacing frequencies. In this way, the mode spacing can be arbitrarily tuned without deteriorating the stability of the phase and power of the comb modes while the tuning can be performed with a very fast slope. In other words, it is capable of agile frequency tuning of the mode spacing. Especially, if a phase-continuous scan of the mode spacing is applied, the high-order comb modes will follow the fundamental scan with a multiplicated scan range.

These unique properties will be quite beneficial for applications where phase-continuous scan is urgently desired. In the following, such agile frequency comb is applied in several different application fields.

In the context of microwave photonics, the generation of high quality microwave signal has always been the primary issue. Thanks to the advantages of photonic technologies, microwave photonics is capable of generating and processing broadband

microwave signals, enabling functionalities that are difficult to realize in the electrical domain. Even though in this case, the generation and processing of broadband signals with high center frequencies is still the main challenge towards the ultimate aim for arbitrary waveform generation. In particular, the broadband chirped signals with arbitrary waveforms are of critical importance. With the proposed agile frequency comb, by simply extracting two high-order modes from the comb, the beat note between the two modes is able to be continuously swept if the mode spacing is scanned. Meanwhile, the scan will be naturally multiplied through the beating between the high-order comb modes. This way, it serves as a microwave photonic multiplier with minimum additional noise, facilitating the generation of arbitrary microwave waveforms with high center frequency and broad bandwidth.

For some application scenarios, a monochromic continuous-wave optical mode capable of phase-continuous tuning over a broad optical bandwidth while the phase and frequency can be precisely defined on demand is required rather than a frequency comb. Analogous to its electrical counterpart, such optical signal generator is referred to as optical single-frequency synthesizer, which has been regarded as a tremendously useful tool in many laser-based applications. In general, such optical single-frequency synthesizer is accomplished by referencing to the stabilized optical frequency comb. This has allowed a widely tunable laser to be tuned across a targeted spectral region with certain frequency stepping while the precision and accuracy is inherited from the reference comb. A heterodyne beating between the comb and the laser is detected and processed as an error signal to maintain the phase locking. However, once the laser is tuned one mode spacing, it has to reset the locking from mode to mode, leading to the breaking of the phase continuity. To deal with this discontinuity, instead of using a comb with fixed mode spacing as the reference, the comb mode itself can be tuned to serve as a tunable reference. This way, by coherently extracting and amplifying one designated comb mode, it can be straightforwardly used as a tunable monochromic optical mode. To this end, the proposed agile frequency comb is the perfect candidate for acting as such an elastically tunable reference. The demonstrated optical single-frequency synthesizer exhibits phase-continuous tunability with high coherence and frequency agility over a broad optical bandwidth.

Summary of related publication:

[1] **Weilin Xie**, Yi Dong*, Qian Zhou, Hongxiao Shi, Zongyang Xia, Fabien Bretenaker, Jie Qin, and Weisheng Hu, " Phase-continuous agile optical single-frequency synthesizer for long range FMCW reflectometry," (in Preparation).

We report on an optical single-frequency synthesizer that exhibits phase-continuous tunability with high agility and precision over a broad optical bandwidth. Instead of using a comb with fixed mode spacing, an agile frequency comb serves as a tunable reference, for which the mode spacing can be tuned in a phase-continuous manner with high agility while preserving stable phase and power of the comb modes. Successively, this unique tunability can be transferred to a continuous-wave (CW) laser in a coherent fashion adopting multi-loop composite phase locking with large loop bandwidth and high gain. This allows imprinting such phase-continuous tunability in connection with the precision, resolution, and coherence of the comb from any specified comb mode onto the CW laser. The characteristics in terms of agility, coherence, and precision are discussed together with the potential limitations.

[2] **Weilin Xie**, Qian Zhou, Fabien Bretenaker, Hongxiao Shi, Zongyang Xia, Yi Dong*, and Weisheng Hu, "Fourier transform-limited optical frequency-modulated continuous-wave interferometry over several tens of laser coherence lengths," ***Optics Letters***, vol. 41, no. 13, pp. 2962-2965, Jun. 2016.

We report on a versatile optical frequency-modulated continuous-wave interferometry technique that exploits wideband phase locking for generating highly coherent linear laser frequency chirps. This technique is based on an ultra-short delay-unbalanced interferometer, which leads to a large bandwidth, short lock time, and robust operation even in the absence of any isolation from environmental perturbations. In combination with a digital delay-matched phase error compensation, this permits the achievement of a range window about 60 times larger than the intrinsic laser coherence length with a 1.25 mm Fourier transform-limited spatial resolution. The demonstrated configuration can be easily applied to virtually any semiconductor laser. s

[3] **Weilin Xie**, Zongyang Xia, Qian Zhou, Hongxiao Shi, Yi Dong*, and Weisheng Hu, "Photonic generation of low phase noise arbitrary chirped microwave and sub-THz signals," ***Optics Express***, vol. 23, no. 14, pp. 18070-18079, Jul. 2015.

We present a photonic approach for generating low phase noise, arbitrary chirped microwave waveforms based on heterodyne beating between high order correlated comb lines extracted from frequency-agile optical frequency comb. Using the dual heterodyne phase transfer scheme, extrinsic phase noises induced by the separate optical paths are efficiently suppressed by 42-dB at the 1-Hz offset frequency. Linearly chirped microwave waveforms are achieved within 30-ms temporal duration, contributing to a large time-bandwidth product. The linearity measurement leads to less than 90 kHz RMS frequency error during the entire chirp duration, exhibiting excellent linearity for the microwave and sub-THz waveforms. The capability of generating arbitrary waveforms up to sub-THz band with flexible temporal duration, a long repetition period, broad bandwidth, and the large time-bandwidth product is investigated and discussed.

[4] **Weilin Xie**, Qian Zhou, Chao Zhang, Zongyang Xia, Hongxiao Shi, Yi Dong*, Lilin Yi, and Weisheng Hu, "Coherent comb generation with continuous sweep of repetition rate over one-octave," ***IEEE Photonics Technology Letters***, vol. 25, no. 24, pp. 2405-2407, Dec. 2013.

We proposed and demonstrated a coherent optical frequency comb generation with a broadband continuous sweep of repetition rate based on cascaded phase and intensity modulators. Broadband phase matching between electrical drive signals applied on the cascaded phase and intensity modulators are achieved by compensating propagation delay skew between the optical signal path and electrical signal path. Therefore, phase mismatch induced flatness deterioration is effectively suppressed. A flat-top 19-line optical frequency comb with repetition rate continuously sweeping over one-octave from 8.5 to 19 GHz is obtained, where the overall power deviation is<4dB.

Appendix II

Calculation of the 7-wave model

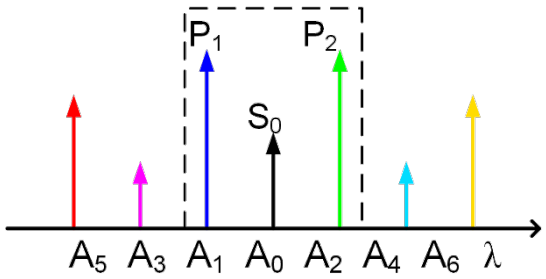

Fig. A.1 Illustration of 7-wave model.

(a) Experimental result of dual-pump degenerate PSA: considerable high-order waves are generated by underlying high-order FWM processes.

All the waves are co-polarized and co-propagating in a nonlinear medium. Starting from the NLSE with slowly varying envelopes of all the waves $A_{\mathrm{j}}(z) = \sqrt{P_{\mathrm{n}}}e^{i\varphi_{\mathrm{n}}}$, where P_n and φ_n hold for the power and phase of the waves, respectively. The parameters of the nonlinear medium are length L, attenutation coefficient α, nonlinear coefficient γ.

$$\begin{aligned}\frac{dA_0}{dz} = -\frac{\alpha}{2}A_0 + i\gamma\Bigg\{&\left[\left|A_0\right|^2 + 2\sum_{i=0,i\neq 0}^{6}\left|A_i\right|^2\right]A_0 + A_1^2A_3^*e^{-i\Delta\beta_{0311}z} + A_2^2A_4^*e^{-i\Delta\beta_{0422}z}\\ &+2A_1A_2A_0^*e^{-i\Delta\beta_{0012}z} + 2A_1A_6A_4^*e^{-i\Delta\beta_{0416}z} + 2A_1A_3A_5^*e^{-i\Delta\beta_{0513}z} + 2A_1A_4A_2^*e^{-i\Delta\beta_{0214}z}\\ &+2A_2A_5A_3^*e^{-i\Delta\beta_{0325}z} + 2A_2A_3A_1^*e^{i\Delta\beta_{2301}z} + 2A_2A_4A_6^*e^{i\Delta\beta_{2406}z} + 2A_4A_5A_1^*e^{i\Delta\beta_{4501}z}\\ &+2A_5A_6A_0^*e^{i\Delta\beta_{5600}z} + 2A_3A_4A_0^*e^{i\Delta\beta_{3400}z} + 2A_3A_6A_2^*e^{i\Delta\beta_{3602}z}\Bigg\}\end{aligned} \tag{8-1}$$

$$\frac{\partial A_1}{\partial z} = -\frac{\alpha}{2}A_1 + i\gamma\left\{\left[\left|A_1\right|^2 + 2\sum_{i=0,i\neq 1}^{6}\left|A_i\right|^2\right]A_1 + A_2^2A_6^*e^{i\Delta\beta_{2216}z} + A_0^2A_2^*e^{i\Delta\beta_{0012}z} + A_3^2A_5^*e^{i\Delta\beta_{3315}z}\right.$$
$$+2A_0A_2A_4^*e^{i\Delta\beta_{0214}z} + 2A_2A_5A_1^*e^{i\Delta\beta_{2511}z} + 2A_5A_6A_2^*e^{i\Delta\beta_{5612}z} + 2A_0A_5A_3^*e^{i\Delta\beta_{0513}z}$$
$$+2A_4A_5A_0^*e^{i\Delta\beta_{4501}z} + 2A_0A_4A_6^*e^{i\Delta\beta_{0416}z} + 2A_2A_3A_0^*e^{i\Delta\beta_{2301}z} + 2A_0A_3A_1^*e^{i\Delta\beta_{0311}z}$$
$$\left.+2A_3A_6A_4^*e^{i\Delta\beta_{3614}z} + 2A_3A_4A_2^*e^{i\Delta\beta_{3412}z}\right\} \quad (8\text{-}2)$$

$$\frac{dA_2}{dz} = -\frac{\alpha}{2}A_2 + i\gamma\left\{\left[\left|A_2\right|^2 + 2\sum_{i=0,i\neq 2}^{6}\left|A_i\right|^2\right]A_2 + A_1^2A_5^*e^{i\Delta\beta_{1125}z} + A_0^2A_1^*e^{i\Delta\beta_{0012}z} + A_4^2A_6^*e^{i\Delta\beta_{4426}z}\right.$$
$$+2A_0A_1A_3^*e^{i\Delta\beta_{0123}z} + 2A_1A_6A_2^*e^{i\Delta\beta_{1622}z} + 2A_1A_4A_0^*e^{i\Delta\beta_{1402}z} + 2A_0A_6A_4^*e^{i\Delta\beta_{0624}z}$$
$$+2A_0A_3A_5^*e^{i\Delta\beta_{0325}z} + 2A_0A_4A_2^*e^{i\Delta\beta_{0422}z} + 2A_3A_6A_0^*e^{i\Delta\beta_{3602}z} + 2A_5A_6A_1^*e^{i\Delta\beta_{5612}z}$$
$$\left.+2A_4A_5A_3^*e^{i\Delta\beta_{4523}z} + 2A_3A_4A_1^*e^{i\Delta\beta_{3412}z}\right\} \quad (8\text{-}3)$$

$$\frac{dA_3}{dz} = -\frac{\alpha}{2}A_3 + i\gamma\left\{\left[\left|A_3\right|^2 + 2\sum_{i=0,i\neq 3}^{6}\left|A_i\right|^2\right]A_3 + A_1^2A_0^*e^{i\Delta\beta_{1103}z} + A_0^2A_4^*e^{i\Delta\beta_{0034}z}\right.$$
$$+2A_1A_2A_4^*e^{i\Delta\beta_{1234}z} + 2A_0A_1A_2^*e^{i\Delta\beta_{0123}z} + 2A_1A_5A_3^*e^{i\Delta\beta_{1533}z} + 2A_1A_4A_6^*e^{i\Delta\beta_{1436}z}$$
$$+2A_5A_6A_4^*e^{i\Delta\beta_{5634}z} + 2A_4A_5A_2^*e^{i\Delta\beta_{4523}z} + 2A_0A_5A_1^*e^{i\Delta\beta_{0513}z} + 2A_2A_5A_0^*e^{i\Delta\beta_{2503}z}$$
$$\left.+2A_0A_2A_6^*e^{i\Delta\beta_{0236}z}\right\} \quad (8\text{-}4)$$

$$\frac{dA_4}{dz} = -\frac{\alpha}{2}A_4 + i\gamma\left\{\left[\left|A_4\right|^2 + 2\sum_{i=0,i\neq 4}^{6}\left|A_i\right|^2\right]A_4 + A_0^2A_3^*e^{i\Delta\beta_{0034}z} + A_2^2A_0^*e^{i\Delta\beta_{2204}z}\right.$$
$$+2A_1A_2A_3^*e^{i\Delta\beta_{1234}z} + 2A_0A_1A_5^*e^{i\Delta\beta_{0145}z} + 2A_1A_6A_0^*e^{i\Delta\beta_{1604}z} + 2A_0A_2A_1^*e^{i\Delta\beta_{0214}z}$$
$$+2A_2A_6A_4^*e^{i\Delta\beta_{2644}z} + 2A_2A_3A_5^*e^{i\Delta\beta_{2345}z} + 2A_0A_6A_2^*e^{i\Delta\beta_{0624}z} + 2A_5A_6A_3^*e^{i\Delta\beta_{5634}z}$$
$$\left.+2A_3A_6A_1^*e^{i\Delta\beta_{3614}z}\right\} \quad (8\text{-}5)$$

$$\frac{dA_5}{dz} = -\frac{\alpha}{2}A_5 + i\gamma\left\{\left[\left|A_5\right|^2 + 2\sum_{i=0,i\neq 5}^{6}\left|A_i\right|^2\right]A_5 + A_1^2A_2^*e^{i\Delta\beta_{1125}z} + A_0^2A_6^*e^{i\Delta\beta_{0056}z} + A_3^2A_1^*e^{i\Delta\beta_{3315}z}\right.$$
$$+2A_1A_2A_6^*e^{i\Delta\beta_{1256}z} + 2A_0A_1A_4^*e^{i\Delta\beta_{0145}z} + 2A_1A_3A_0^*e^{i\Delta\beta_{1305}z} + 2A_0A_3A_2^*e^{i\Delta\beta_{0325}z}$$
$$\left.+2A_2A_3A_4^*e^{i\Delta\beta_{2345}z} + 2A_3A_4A_6^*e^{i\Delta\beta_{3456}z}\right\} \quad (8\text{-}6)$$

$$\frac{dA_6}{dz} = -\frac{\alpha}{2}A_6 + i\gamma\left\{\left[\left|A_6\right|^2 + 2\sum_{i=0,i\neq 6}^{6}\left|A_i\right|^2\right]A_6 + A_2^2A_1^*e^{i\Delta\beta_{2216}z} + A_0^2A_5^*e^{i\Delta\beta_{0056}z} + A_4^2A_2^*e^{i\Delta\beta_{4426}z}\right.$$
$$+2A_1A_2A_5^*e^{i\Delta\beta_{1256}z} + 2A_1A_4A_3^*e^{i\Delta\beta_{1436}z} + 2A_0A_2A_3^*e^{i\Delta\beta_{0236}z} + 2A_3A_4A_5^*e^{i\Delta\beta_{3456}z}$$
$$\left.+2A_2A_4A_0^*e^{i\Delta\beta_{2406}z} + 2A_0A_4A_1^*e^{i\Delta\beta_{0416}z}\right\} \quad (8\text{-}7)$$

List of acronyms

Acronyms	Full name
ADC	Analog-to-Digital Converter
AOM	Acoustic-optic Modulator
APD	Avalanche Photo Diode
AQE	Amplitude Quantum Noise
ASE	Amplified Spontaneous Emission
ASK	Amplitude-shift Keying
BER	Bit Error Rate
BG	Bragg Grating
BPD	Balanced Photo-Detector
CW	Continuous-wave
DAQ	Digital Acquisition Card
DBR	Distributed Bragg Reflector
DD	Direct Detection
DFB	Distributed Feedback
DFB-FL	Distributed Feedback Fiber Laser
DSP	Digital Signal Processing
DSH	Delayed Self-Heterodyne/Homodyne
ECDL	External Cavity Diode Laser
EDFA	Erbium-Doped Fiber Amplifier
EOC	Electrical-to-optical Conversion

FBG	Fiber Bragg Grating
FET	Field-effect Transistor
FFT	Fast Fourier Transform
FMCW	Frequency-modulated Continuous-wave
FOPA	Fiber Optical Parametric Amplifier
FP	Fabry-Perot
FPF	Fabry-Perot Filter
FPGA	Field Programmable Gate Array
FWM	Four-wave Mixing
FUT	Fiber Under Test
FWHM	Full Width at Half Maximum
GVD	Group Velocity Dispersion
HNLF	Highly Nonlinear Fiber
ICT	Information Communication Technology
IM	Intensity Modulation
LIDAR	Light Detection and Ranging
LF	Loop Filter
LO	Local Oscillator
MZI	Mach-Zehnder Interferometry
MZM	Mach-Zehnder Modulator
NF	Noise Figure
OEC	Optical-to-electrical Conversion
OFC	Optical Frequency Comb
OPLL	Optical Phase-Locked Loop
OPO	Optical Parametric Oscillator

OSNR	Optical Signal-to-Noise Ratio
OVCO	Optical Voltage Controlled Oscillator
PBS	Polarization Beam Splitter
PC	Polarization Controller
PD	Photo-detector
PDH	Pound-Drever-Hall
PIA	Phase-insensitive Amplifier
PLL	Phase-locked Loop
PMD	Polarization Mode Dispersion
PMFC	Polarization Maintaining Fiber Coupler
PPLN	Periodically Poled Lithium Niobate
PSA	Phase-sensitive Amplifier
PSD	Power Spectral Density
PZT	Piezo-electric Transducer
RF	Radio Frequency
RIN	Relative Intensity Noise
RMS	Root Mean Square
SBS	Stimulated Brillouin Scattering
SCL	Semiconductor Laser
SE	Spectral Efficiency
SFDR	Spurious Free Dynamic Range
SFG	Sum Frequency Generation
SHG	Second Harmonic Generation
SL	Slave Laser
SNR	Signal-to-Noise Ratio
SOA	Semiconductor Optical Amplifier
SOP	State of Polarization
SPM	Self-phase Modulation

SRS	Stimulated Raman Scattering
SSB	Single Sideband
SSMF	Standard Single-Mode Fiber
TEC	Thermoelectric Cooling
TWM	Three-wave Mixing
VCO	Voltage Controlled Oscillator
VCSEL	Vertical Cavity Surface Emitting Laser
VOA	Variable Optical Attenuator
VLSI	Very Large Scale Integration
WDM	Wavelength-Division Multiplexing
XPM	Cross-phase Modulation
ZDF	Zero Dispersion Frequency
ZDW	Zero Dispersion Wavelength

List of symbols

t	Time
E	Optical field
ν	Optical frequency
ν_0	Center frequency, initial frequency
φ	Laser phase
φ_0	Initial laser phase
P	Optical power
c	Speed of light in vacuum
ω	Angular frequency
n	Reflective index
A	Slow-varying envelop of the optical field
$const$	Constant
f	Fourier frequency
A_{eff}	Effective mode area
γ	Nonlinear coefficient
α	Attenuation coefficient
β	Propagation constant
$\beta^{(n)}$	Nth order derivative of the propagation constant
$\Delta\beta$	Linear phase mismatch
λ_{ZDW}	Zero dispersion wavelength
$\Delta\lambda_{PPS}$	Pump-pump wavelength separation
$\delta\lambda_{OFS}$	Signal wavelength offset with respect to λ_{ZDW}
D_λ	Dispersion slope
z	Propagation length
θ	Relative phase
θ_0	Initial relative phase
κ	Total phase mismatch

g	Parametric gain
L_{eff}	Effective length

List of papers

Journal articles

[1] **Weilin Xie**, Aude Martin, Fabien Bretenaker, and Alfredo De Rossi*, "Characterization of linear and nonlinear properties of GaP Photonic crystal waveguide in continuous-wave regime," (in Preparation).

[2] **Weilin Xie**, Y. Dong*, Qian Zhou, Hongxiao Shi, Zongyang Xia, Fabien Bretenaker, Qin Jie, and Weisheng. Hu, " Phase-continuous agile optical single-frequency synthesizer for long range FMCW reflectometry," (in Preparation).

[3] **Weilin Xie***, Ihsan Fsaifes, Tarek Labidi, and Fabien Bretenaker, "Optimization of regenerative phase sensitive optical parametric amplifier for all-optical processing functionalities," ***Optics Express***, vol. 25, no. 11, pp. 12552-12565, May 2017.

[4] **Weilin Xie**, Qian Zhou, Fabien Bretenaker, Hongxiao Shi, Zongyang Xia, Yi Dong*, and Weisheng Hu, "Fourier transform-limited optical frequency-modulated continuous-wave interferometry over several tens of laser coherence lengths," ***Optics Letters***, vol. 41, no. 13, pp. 2962-2965, Jun. 2016.

[5] **Weilin Xie***, Ihsan Fsaifes, Tarek Labidi, and Fabien Bretenaker, "Investigation of degenerate dual-pump phase sensitive amplifier using multi-wave model," ***Optics Express***, vol. 23, no. 25, pp. 31896-31907, Dec. 2015.

[6] **Weilin Xie**, Zongyang Xia, Qian Zhou, Hongxiao Shi, Yi Dong*, and Weisheng Hu, "Photonic generation of low phase noise arbitrary chirped microwave and sub-THz signals," ***Optics Express***, vol. 23, no. 14, pp. 18070-18079, Jul. 2015.

[7] **Weilin Xie**, Qian Zhou, Chao Zhang, Zongyang Xia, Hongxiao Shi, Yi Dong*, Lilin Yi, and Weisheng Hu, "Coherent comb generation with continuous sweep of repetition rate over one-octave," ***IEEE Photonics Technology Letters***, vol. 25, no. 24, pp. 2405-2407, Dec. 2013.

[8] Y. Tong, D. Han, R. Chen, Z. Liu, **Weilin Xie**, and Y. Dong*, "Photonics-based coherent

wideband linear frequency modulation pulsed signal generation," ***Optics Letters***, vol. 26, no. 1, pp. 339-346, Jan. 2018.

[9] N. Deng, Z. Liu, X. Wang, T. Fu, **Weilin Xie**, and Y. Dong, "Distribution of a phase-stabilized 100.02 GHz millimeter-wave signal over a 160 km optical fiber with 4.1×10^{-17} instability," ***Optics Express***, vol. 26, no. 1, pp. 339-346, Jan. 2018.

[10] Yitian Tong, Qian Zhou, Damin Han, Baiyu Li, **Weilin Xie**, Zhangweiyi Liu, Jin Qin, Xiaocheng Wang, Yi Dong*, and Weisheng Hu, "Photonic generation of phase-stable and wideband chirped microwave signals based on phase-locked dual optical frequency combs," ***Optics Letters***, vol. 41, no. 16, pp. 3787-3790, Aug. 2016.

[11] Qian Zhou, Jin Qin, **Weilin Xie**, Zhangweiyi Liu, Yitian Tong, Yi Dong*, and Weisheng Hu, "Dynamic frequency-noise spectrum measurement for a frequency-swept DFB laser with short-delayed self-heterodyne method," ***Optics Express***, vol. 23, no. 22, pp. 29245-29257, Oct. 2015.

[12] Qin Jie, Qian Zhou, **Weilin Xie**, Yan Xu, Zhangweiyi Liu, Yitian Tong, Yi Dong*, and Weisheng Hu, "Coherence enhancement of a chirped DFB laser for FMCW reflectometry using a composite feedback loop," ***Optics Letters***, vol. 40, no. 19, pp. 4500-4503, Sep. 2015.

[13] Qian Zhou, Jie Qin, **Weilin Xie**, Zhangweiyi Liu, Yitian Tong, Yi Dong*, and Weisheng Hu, "Power-area method to precisely estimate laser linewidth from its frequency-noise spectrum," ***Applied Optics***, vol. 54, no. 28, pp. 8282-8289, Sep. 2015.

[14] Zongyang Xia, **Weilin Xie**, Dongning Sun, Hongxiao Shi, Yi Dong*, Weisheng Hu, "Photonic generation of linearly chirped millimeter-wave based on comb-spacing tunable optical frequency comb," ***Optical Engineering***, vol. 52, no. 12, pp. 126107, 2013.

[15] Qian Zhou, **Weilin Xie**, Zongyang Xia, Hongxiao Shi, Yi Dong*, and Weisheng Hu, "Compensation of phase error in optical frequency domain reflectometry using delay-matched sampling," ***Optical Engineering***, vol. 53, no. 7, 074103, Jul. 2014.

[16] Cheng Ma, Qin Zhou, Jie Qin, **Weilin Xie**, Yi Dong, and Weisheng Hu, "Fast spectrum analysis for an OFDR using the FFT and SCZT combination approach", ***IEEE Photonics Technology Letters***, vol. 28, no. 6, pp. 657-660, Mar. 2016.

[17] Dongning Sun, Yi Dong*, Hongxiao Shi, Zongyang Xia, Zhangweiyi Liu, Siwei Wang, **Weilin Xie**, and W. Hu, "Distribution of high-stability 100.04 GHz millimeter wave signal over 60 km optical fiber with fast phase-error-correcting capability," ***Optics Letters***, vol. 39, no. 10, pp. 2849-2852, May. 2014.

[18] Dongning Sun, Yi Dong*, Lilin Yi, Siwei Wang, Hongxiao Shi, Zongyang Xia, **Weilin Xie** and

Weisheng Hu, "Photonic generation of millimeter and terahertz waves with high phase stability," ***Optics Letters***, vol. 39, no. 6, pp. 1493-1496, Mar. 2014.

[19] Siwei Wang, Dongning Sun, Yi Dong*, **Weilin Xie**, Hongxiao Shi, Lilin Yi, Weisheng Hu, "Distribution of high stability 10-GHz local oscillator over 100-km optical fiber with accurate phase correction system," ***Optics Letters***, vol. 39, no. 4, pp. 888-891, Feb. 2014.

[20] Le Chang, Yi Dong*, Dongning Sun, Damin Zhang, **Weilin Xie** and Weisheng Hu, "Influence and suppression of coherent Rayleigh noise in fiber-optic-based phase-stabilized microwave-frequency transmission system (In Chinese)," ***Acta Optica Sinica***, vol. 32, no. 5, May. 2012.

Conference presentations

[1] **Weilin Xie**, Y. Dong, F. Bretenaker, H. Shi, Q. Zhou, Z. Xia, J. Qin, X. Lin, L. Zhang, and W. Hu, "Coherent single-mode extraction of agile frequency comb via phase-locking for broadband phase-continuous tuning," ***Asia Communications and Photonics Conference (ACP 2017)*** Guang Zhou, paper M3D3. 3.

[2] **Weilin Xie**, Y. Dong, F. Bretenaker, H. Shi, Q. Zhou, Z. Xia, J. Qin, L. Zhang, X. Lin, and W. Hu, "Efficient dynamic coherence transfer relying on offset locking using optical phase-locked loop," ***International Conference on Optical Instruments and Technology 2017 (OIT 2017)*** Beijing, paper OIT17-200-17.

[3] X. Tian, **Weilin Xie**, X. Wang, J. Qin, N. Deng, Y. Dong, and W. Hu, "Highly Linear Analog Photonic Link Based on Composite Optical Phase-Locked Loop," ***Optical Fiber Communication Conference (OFC 2017), OSA Technical Digest (online) (Optical Society of America, 2017)***, paper W2A.33.

[4] Q. Jie, Q. Zhou, **Weilin Xie**, Y. Dong, and W. Hu, "Linearization of broadband frequency sweep for temperature tuned DFB laser using an optoelectronic feedback loop," ***Asia Communications and Photonics Conference (ACP 2015)*** Hong Kong, ASu3I. 3.

[5] T. Fu, X. Wang, Z. Liu, N. Deng, **Weilin Xie**, and Y. Dong, "A highly precise fiber delay fluctuation measurement with a wide range," ***International Conference on Optical Instrument and Technology (OIT 2017)*** Beijing, paper OIT-200-41.

[6] Z. Zhu, H. Zhou, **Weilin Xie**, J. Qin, and Y. Dong, "10-Gb/s homodyne receiver based on Costas loop with enhanced dynamic performance," ***International Conference on Optical Communication and Networks (ICOCN 2017)*** Wuzhen, paper T7-O-06.

[7] H. Zhou, Z. Zhu, Weilin Xie, and Y. Dong, "Investigation of homodyne demodulation of RZ-BPSK signal based on an optical Costas loop," ***International Conference on Optical Instrument and Technology (OIT 2017)*** Beijing, paper OIT-200-47.

[8] H. Shi, Y. Dong, **Weilin Xie**, Q. Zhou, J. Qin, and W. Hu, "High-sensitivity 5Gb/s BPSK homodyne detection suing Costas loop," ***Asia Communications and Photonics Conference (ACP 2014)*** Shanghai, ATh4D. 6.

[9] D. Sun, Y. Dong, S. Wang, Z. Xia, **Weilin Xie**, H. Shi, L. Yi and W. Hu, "Photonic radio-frequency phase detector based on radio-frequency to intermediate-frequency phase mapping," ***Asia Communications and Photonics Conference (ACP 2013)*** Beijing, AF4A.7.

université PARIS-SACLAY | ÉCOLE DOCTORALE Ondes et Matière (EDOM)

Titre: Propriétés non-linéaires d'amplificateurs paramétriques à fibre optique sensibles à la phase pour le traitement du signal

Mots clés: Optique non-linéaire, mélange à quatre ondes, amplificateur sensible à la phase, photonique hyperfréquence

Résumé: La capacité et les performances des systèmes à fibres optiques et photoniques dépendent fortement du bruit et des non-linéarités des amplificateurs optiques. Dans ce contexte, les amplificateurs paramétriques à fibre optique (PS-FOPA), reposant sur le mélange à quatre ondes dans les fibres optiques, surpassent les amplificateurs conventionnels insensibles à la phase. En effet, leur sensibilité à la phase peut être exploitée pour l'amplification sans bruit et al compensation de la distortion non-linéaire. En conjonction avec leur large spectre de gain et d'autres fonctionnalités telles que la conversion de longueur d'onde, ils sont considérés comme des candidats prometteurs pour la prochaine génération d'amplificateurs optiques pour les communications et le traitement de signal tout optiques. Le PS-FOPA est classiquement décrit par les équations d'ondes couplées, dérivées de l'équation de Schrödinger non-linéaire qui ne contiennent que trois ou quatre ondes en interaction. Cependant, dans un cas plus général, l'apparition de fréquences supplementaires d'ordre plus élevé affectera inévitablement la sensibilité en phase.

L'objectif de cette thèse est d'étudier de manière approfondie les propriétés non-linéaires, en termes de gain et de sensibilité en phase d'un PS-FOPA dégénéré à double pompe pour différentes configurations. Une analyse numérique plus précise est obtenue en utilisant le modèle à 7 ondes qui incorpore les ondes supplémentaires issues de processus de mélange à quatre ondes d'ordre élevé. Ce modèle permet de donner une interprétation physique plus précise des interactions multi-ondes en fonction des conditions d'accord de phase, révélant les relations sous-jacentes entre la dispersion et la sensibilité de phase. De plus, la capacité de régénération simultanée de phase et d'amplitude d'un PS-FOPA basique est évaluée pour l'optimisation globale. Il permet d'exploiter pleinement la capacité potentielle d'un PS-FOPA de base agissant comme un bloc de construction fondamental des futures fonctionnalités tout optiques. L'approche basée sur ce modèle permet une optimisation orientée vers l'application et revêt une importance particulière pour la conception et l'optimisation de tels PS-FOPAs dans divers scénarios.

Title: Nonlinear Properties of Phase-sensitive Fiber-Optic Parametric Amplifiers for Signal Processing

Keywords: Nonlinear optics, Four-wave mixing, phase-sensitive amplifier, microwave photonics

Abstract: The capability and performance of the widely deployed fiber-optic and photonic systems strongly depend on the noise and nonlinearities of the optical amplifiers. In this context, phase-sensitive fiber-optic parametric amplifiers (PS-FOPAs), relying on four-wave mixing in silica optical fibers, outperforms conventional phase-insensitive amplifier thanks to their unique phase-sensitivity, which can be exploited for noiseless amplification and for the mitigation of the nonlinear impairment. In conjunction with the vast gain spectrum and other all-optical functionalities such as wavelength conversion, they have been regarded as a promising candidate for next-generation amplifiers towards all-optical communication and processing.
The PS-FOPA can be conventionally described by the fundamental coupled wave equations derived from the nonlinear Schrödinger equation that contains only three or four interacting waves. However, for a more general case, the emergence of high-order waves will inevitably affect the phase-sensitivity. Therefore, the objective of this thesis aims at the thorough investigation of the nonlinear properties in terms of the gain properties and the phase sensitivities with respect to different configurations for a dual-pump signal-idler degenerate PS-FOPA. The more accurate numerical analysis is obtained by using the 7-wave model that incorporates the first order high-order signals and idlers stemming from the high-order four-wave mixing processes. This model permits to assess a more precise physical interpretation of the multi-wave interactions based on the phase matching conditions, revealing the underlying relations between the dispersion and phase-sensitivity. Moreover, based on this model, the simultaneous phase and amplitude regenerative capability of a basic PS-FOPA is evaluated for the overall optimization. It allows fully exploiting the potential ability of a basic PS-FOPA acting as a fundamental building block of the future all-optical functionalities. The analysis approach permits application-oriented optimization and is of particular guiding significance for the design and the optimization of PS-FOPA in various scenarios.